The Pennsylvania State University

The Graduate School

Department of Aerospace Engineering

ENHANCEMENTS AND INVESTIGATION OF CAPABILITIES TO THE LANDING GEAR MODEL AND ACOUSTIC PREDICTION SOFTWARE

A Thesis in

Aerospace Engineering

by

Taylor Ries Marotta

Submitted in Partial Fulfillment
of the Requirements
for the Degree of

Master of Science

August 2011

The thesis of Taylor Ries Marotta was reviewed and approved* by the following:

Kenneth S. Brentner
Professor of Aerospace Engineering
Thesis Co-Advisor

Philip J. Morris
Boeing/ A.D. Welliver Professor of Aerospace Engineering
Thesis Co-Advisor

George A. Lesieatre
Professor of Aerospace Engineering
Deparment Head of Aerospace Engineering

*Signatures are on file in the Graduate School

ABSTRACT

The aerocoustic prediction program LGMAP has been enhanced and new comparisons have been made with experiments. The LGMAP method models landing gear with separate acoustic elements. These acoustic elements are assembled into groups that model specific assemblies of the landing gear such as the strut, wheel, and trailing edges. The upgrades to the program include corrections involving the cylinder acoustic element's scaling, non-dimensional lift and drag spectrums, and incident velocity vector. A new wheel model based on the Fink method was created in order to improve the directivity of the original LGMAP wheel model. This model differs from the Fink method, which models the landing gear's wheels as one bogey, because each individual wheel's location and size is specified by the user. A parameter has been created to model the flow effects the wheels induce on each other. The cylinder coefficients were recalibrated because of the changes made to the cylinder acoustic element. The calibration case was the QFF 6.3% scaled Boeing 777 main landing gear. For validation, landing gear models built by different users were compared and the importance of an appropriate and accurate model was discovered. Hoses and cables extremely close to large structures such as the oleo should not be represented in the LGMAP landing gear geometry in order to prevent an overprediction in high frequency noise. A blind test of LGMAP's capabilities was completed using an experimental case of a full scale Boeing 737 main landing gear. The Guo and Fink landing gear prediction methods, both included in NASA's ANOPP program, were compared against LGMAP's prediction method. The results from LGMAP produced underpredictions in high frequency noise and the directivity did match that from experimental data. The discrepancies between the experimental data and the LGMAP prediction could be the lack of resources that were used to build the landing gear geometry. The Guo method produces a more accurate prediction than LGMAP, but it still requires experimental data to complete its prediction.

LGMAP fared better against the Fink method because of LGMAP's strut prediction model. The capabilities of LGMAP as a noise source locator compared with experimental phased array measurements. The high fidelity features of the landing gear such as hoses and wires were dominant in both predicted and measured results. LGMAP's wheel model over predicts for all sideline observer cases. Based on the phased array measurements, an update of the wheel directivity model is advised.

TABLE OF CONTENTS

LIST OF FIGURES

LIST OF TABLES

LIST OF SYMBOLS

English

A	amplitude of normalized spectra
B	parameter defining normalized spectra
B_1	cylinder non-dimensional shedding function peak shedding variable
B_2	cylinder non-dimensional shedding function scaling variable
C	parameter defining normalized spectra
C'_d	coefficient of fluctuating drag
C'_l	coefficient of fluctuating lift
D	directivity function
D'	fluctuating drag
D_c	cylinder diameter
d	wheel diameter
e	first cylinder non-dimensional spectrum shape variable
F	spectrum shape function
F_{ND}	non-dimensional spectrum function
F_r	fluctuation force in the radiation direction
f	frequency, Hz
K	wave number
k	turbulent kinetic energy
L'	fluctuating lift
$\boldsymbol{l}$	cylinder length vector
M	freestream Mach number
M_r	Mach number in radiation direction
N_w	number of wheels per landing gear assembly
$\langle p^2 \rangle$	acoustic mean-squared pressure
p	second cylinder non-dimensional spectrum shape variable
p	acoustic pressure
r	distance from the source to the observer
S	Strouhal number
S_o	peak Strouhal number
U_0	free stream flow velocity
u_0	turbulent convection velocity
$\boldsymbol{V}$	freestream velocity vector
V_n	incident flow velocity

Greek

α	turbulent intesity
δ	turbulent boundary layer thickness
ε	trailing edge calibration variable
θ	polar angle
λ	wavelength
Π	acoustic power
ρ	atmospheric density
τ^*	Reynolds shear stress
ϕ	azimuthal angle

ω	angular frequency

Abbreviations

SPL	sound pressure level
OASPL	over-all sound pressure level

Superscripts/Subscripts

d	drag direction
e	emission direction
inc	incident value
l	lift direction
L	loading contribution to noise
M	Mach direction
n	normal direction
r	radiation direction
ret	retarded time
T	thickness contribution to noise
TE	trailing edge contribution to noise
∞	free stream value
$'$	perturbation quantity

Acknowledgements

The author would like to thank his advisors Dr. Kenneth Brentner and Dr. Philip Morris for the opportunity to work on this project and their continuous advice and guidance throughout his graduate studies.

This study was supported by The Boeing Company under sponsored research agreement contract no. 20006, with contract technical monitor Dr. Leon Brusniak. The author appreciates the helpfulness of Drs. Leon Brusniak, Yueping Guo, and Drew Wetzel of The Boeing Company.

The author would also like to thank The Pennsylvania State University Department of Aerospace Engineering for giving him the opportunity to study and earn his Bachelor and Master degrees. The faculty, staff, and fellow students have put in plenty of time to help him further his education and experience.

The author would finally like to thank his friends and family for their continuous support through both the good and tough times. All of this would be impossible without them.

Chapter 1

Introduction

The reduction of aircraft noise is a great concern for designers because major airports worldwide place restrictions on take-off and landing noise. Over time, engineers have successfully reduced the noise of engines, thus reducing noise during takeoff. When an aircraft is in a "dirty" configuration on approach, with high lift devices and landing gear deployed and with the engines throttled down, the largest contributor to noise is the airframe. The airframe noise is defined as the non-propulsive noise generated by the aircraft. Landing gear, flaps, and slats are the major sources of airframe noise. All three contribute similar levels of noise depending on the aircraft configuration so this requires engineers to design them with acoustics in mind. Flyover tests on aircraft during approach have made this apparent. Figure 1-1 presents a component buildup of the airframe noise from a Boeing 747, demonstrating the relative importance of landing gear noise.

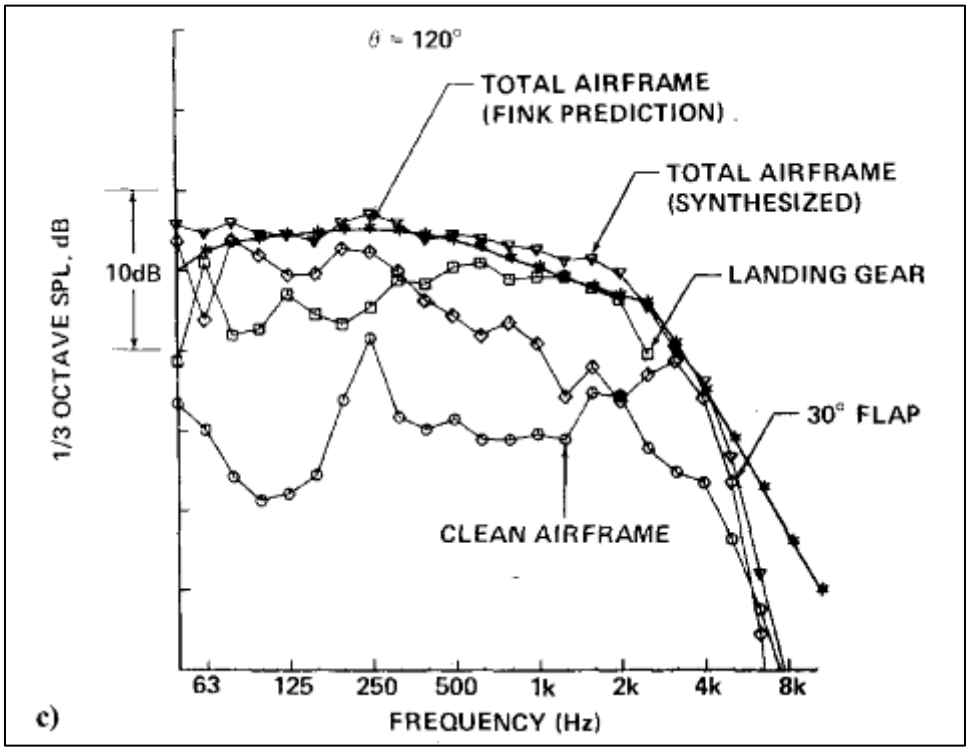

Figure 1-1. Airframe noise component buildup from a Boeing 747 flyover on approach at 199 knots. Prediction from the Fink Method is shown (Ref. 1).

Experimental research on landing gear noise produces accurate noise measurements, but this method takes a prohibitive amount of money and time. Uniquely identifying landing gear noise sources is very difficult to do experimentally. It requires either comparison of different configurations of the aircraft/model or the use of a phased array of microphones. For landing gear designers, this takes a toll on the resources required in order to reduce noise before production. What is needed is an accurate prediction method that can quickly estimate landing gear noise.

An aircraft landing gear is made up of wheels, support struts, hydraulic devices, hoses, and other complex parts (see Figure 1-2 for an example). The struts system, which includes the entire landing gear, except the bogie and doors, are bluff bodies that can include sharp edges and protruding objects. The complexity of the strut system makes noise prediction of the landing gear

especially difficult. The source of a landing gear's high frequency noise component, the most annoying to the human ear, is made up of the smaller parts such as the hydraulic hoses, electrical wires, and axle and brake assembly (Ref. 2). In order to create a quieter landing gear system, the designer will require a prediction method that will accurately estimate the high frequency noise.

Figure 1-2. Close up of a Boeing 777 main landing gear (Ref. 3).

1.1 The Current Tools for Landing Gear Prediction

Currently, there are three common landing gear prediction methods available in the United States: NASA's Fink Method, Boeing Corporation's Guo method, and Penn State University's LGMAP (Refs. 4, 5). Both Fink and Guo methods are now part of NASA's Aircraft Noise Prediction Program (ANOPP) and have been compared and assessed with wind tunnel experimental data (Refs. 6, 7).

NASA's ANOPP software package originally only incorporated the Fink method developed for the Federal Aviation Administration by United Technologies Corp. for airframe noise calculations (Ref. 8). Fink (Ref. 9) published his empirical noise prediction method in 1977 using experimental data and flight tests with two and four wheel landing gear models attached to gliders. For these glider tests, a Braunschweig Akaflieg SB-10 was selected for its "aerodynamically clean" characteristics (Ref. 10). The directivity measurements were used to shape non-dimensional directivity functions used in the method. Only two physical dimensions of the landing gear are used (the tire diameter and strut length), making the prediction very simple to use. However, this method also has been shown to under predict noise at high frequencies when compared with other methods, especially for landing gear with extensive hoses and wires. This can be observed in Figure 1-3 where a Boeing 737 main landing gear noise prediction made by the Fink method is compared with a Guo prediction method. The Guo prediction method is accurate at high frequency ranges for this case. Another deficiency of the Fink method is the strut noise directivity. As one can see in Figure 1-4, the strut does not produce noise directly below the aircraft. This is due to an oversimplification of a landing gear's strut geometry, which is modeled as an isolated cylinder. Though an isolated cylinder does not produces significant noise for observer locations along its axis (Ref. 11), a landing gear's strut system often contains

horizontal supports and other irregularities, which can produce noise in a direction along the strut's axis.

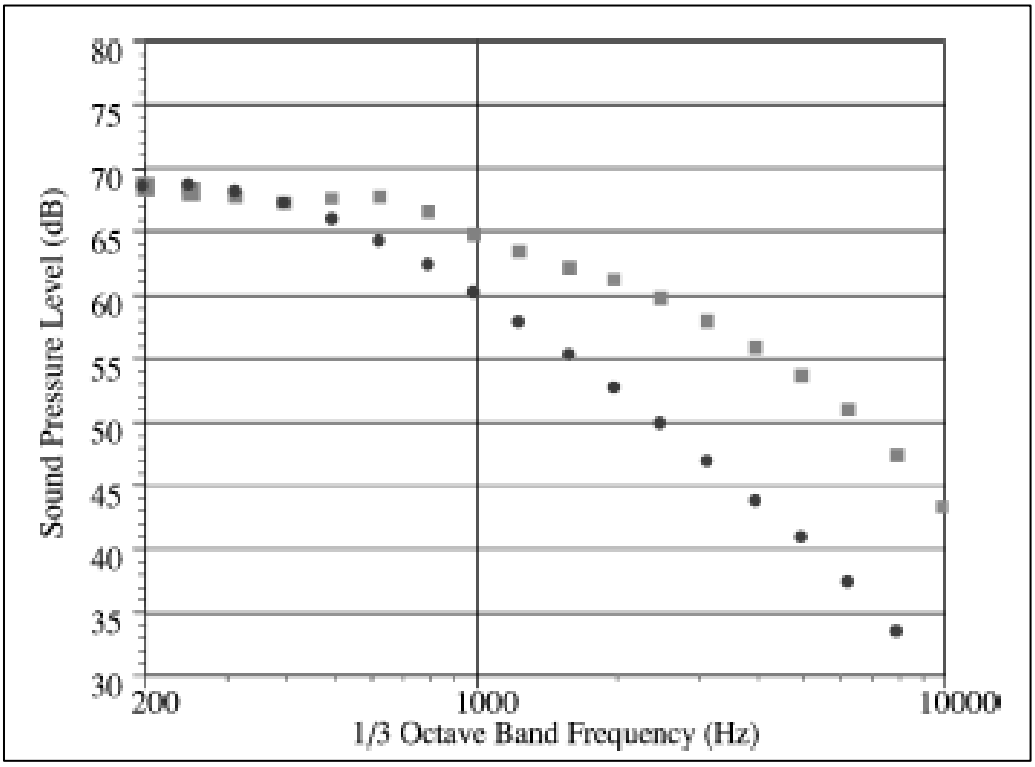

Figure 1-3. Spectrum comparison of Fink's Model (circles) and Guo Model (squares). The noise prediction is of a Boeing 737 at an overhead location at $M = 0.24$ (Ref. 6).

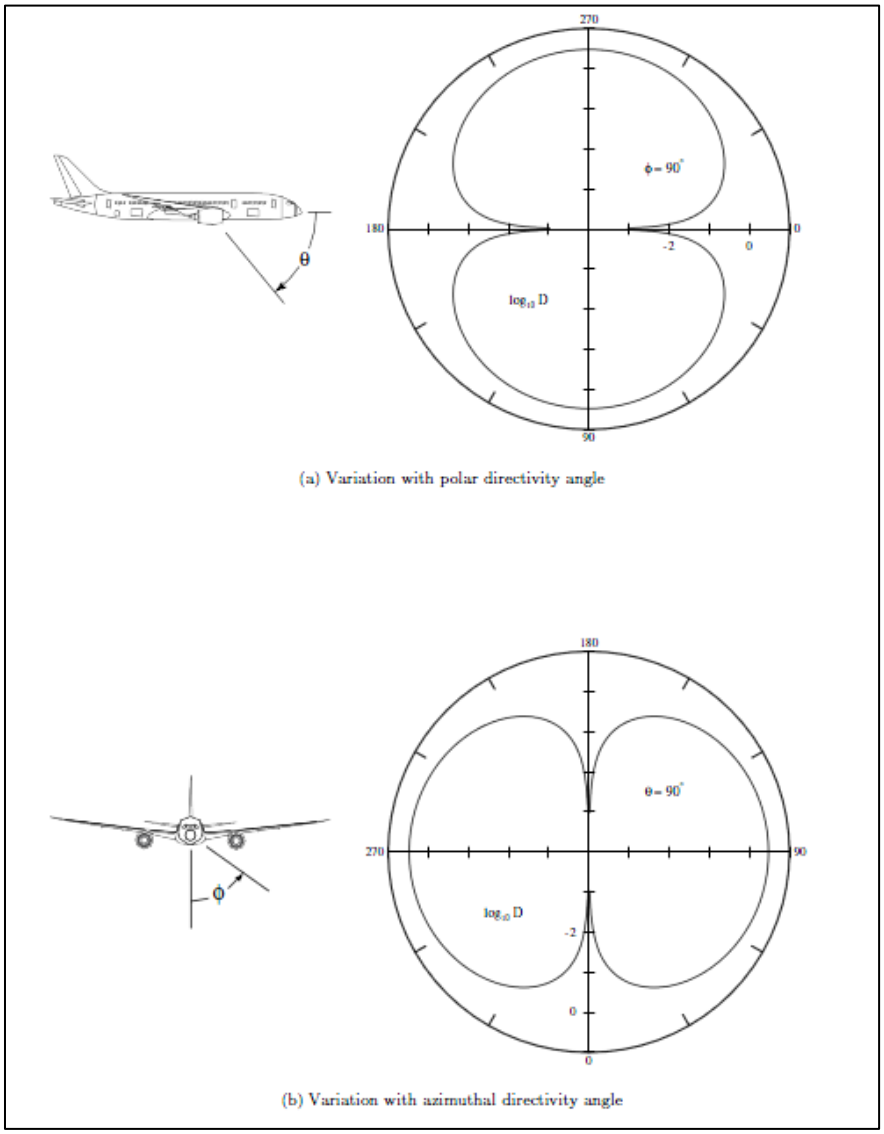

Figure 1-4. Directivity Level for landing gear strut noise for the Fink Method (Ref. 12).

Boeing Corporation's Guo method of landing gear noise prediction separates the landing gear components into three categories: wheels, main struts, and small details (Ref. 13). Developed by Dr. Yueping Guo, the method takes the surface area of each the categories and uses several empirically defined constants to build the noise prediction in terms of a narrow band spectrum. The results from this method produce better predictions for high frequency noise than the Fink method (Figure 1-3) (Ref. 6). In order to predict landing gear noise accurately, extensive

knowledge of the landing gear's geometry is required. Unlike mid frequency main strut and low frequency wheel noise sources, the high frequency noise source geometry is estimated using a complexity factor. The factor is a function of gross weight, total length of all main struts, and number of wheels. One parameter required in this method, the flow energy conversion efficiency parameter, is currently determined by matching predictions with experimental measurements (Ref. 7). It should be noted that this prediction method does not apply to scaled landing gear models since the method does not follow Strouhal scaling (Ref. 7).

1.2 Thesis Overview

The object of the present thesis' research is to further develop the landing gear noise prediction method, LGMAP, and document and assess its capabilities as a landing gear acoustic prediction method. The thesis is organized to first give the reader a quick but informative overview of the prediction method used by LGMAP before the changes discussed in this thesis are applied. This includes any equations used by acoustic elements that are required in order to understand the improvements made to LGMAP. All changes to the code and method along with their effects on past and future predictions are discussed. It was discovered that LGMAP's original wheel model produces incorrect directivity, so a new model, based on the Fink method wheel model, was developed and is discussed and verified. After calibration, LGMAPs current capabilities are demonstrated. Focus is placed on the capabilities of the method's high frequency predictions and on any unique methods users can employ toward creating a LGMAP landing gear geometry. Also, the noise of three different landing gears is predicted and discussed in this thesis: Boeing 777 main gear, Gulfstream 550 nose gear, and Boeing 737 main gear. For each of

these landing gear cases, experimental results and predicted results from other methods are compared with LGMAP.

Chapter 2

Description of LGMAP's Prediction Scheme

The Landing Gear Model and Prediction (LGMAP) is a physics based empirical landing gear noise prediction scheme (Ref. 4). The landing gear prediction is built from several elements from LGMAP's acoustic element toolbox. The toolbox is made up of three distinct acoustic elements: the cylinder acoustic element, the trailing edge acoustic element, and the reflective surface element. The cylinder acoustic elements are the building blocks for the strut and wheel assemblies that make up the landing gear geometry. For the strut system, the user inputs the size and location of each strut member and the program represents each member with several correlated isolated cylinder acoustic elements. The wheel of the original scheme is made of an assembly of acoustic cylinder elements as visualized in Figure 2-1. The program also allows approximate scattering and shielding calculations for the cylinder acoustic elements. The trailing edges of wings or doors are represented with a trailing edge acoustic element. The reflective surface element can be placed in any location by the user and reflects noise from the other acoustic elements. Unlike the cylinder and trailing edge acoustic elements, the reflective surface does not generate noise itself.

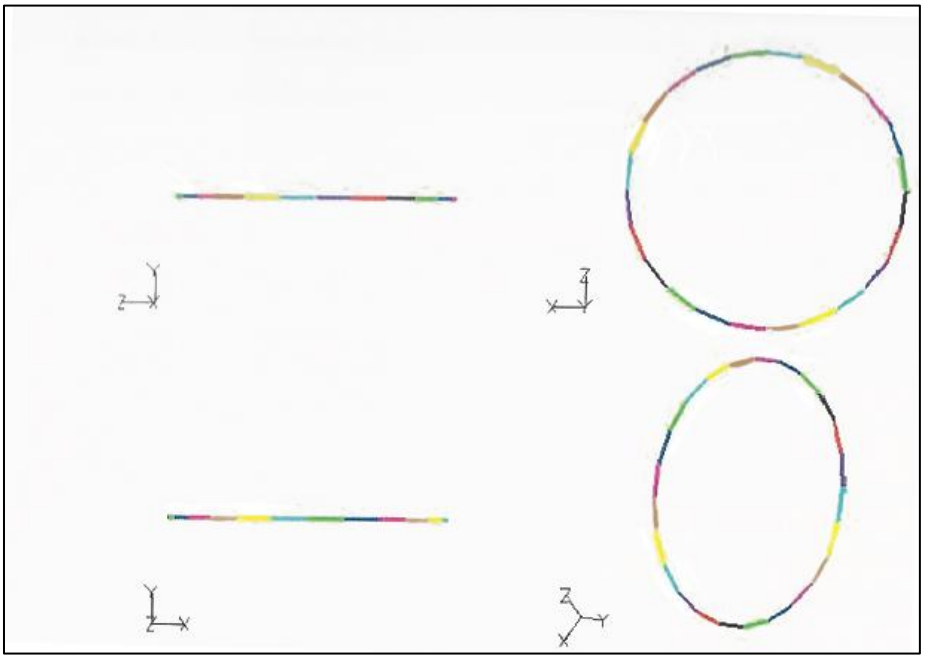

Figure 2-1. Different views of the original LGMAP wheel model. Each cylinder acoustic element in the figure is represented as a different color. This illustrates how the original LGMAP wheel assembly is modeled using many cylinder acoustic elements (Ref. 5).

LGMAP uses a coordinate system that is different from other prediction methods discussed in this thesis. These prediction methods (Fink and Guo) are part of NASA's ANOPP noise prediction program. Both the LGMAP and ANOPP coordinate system are defined in Figure 2-2 and Figure 2-3.

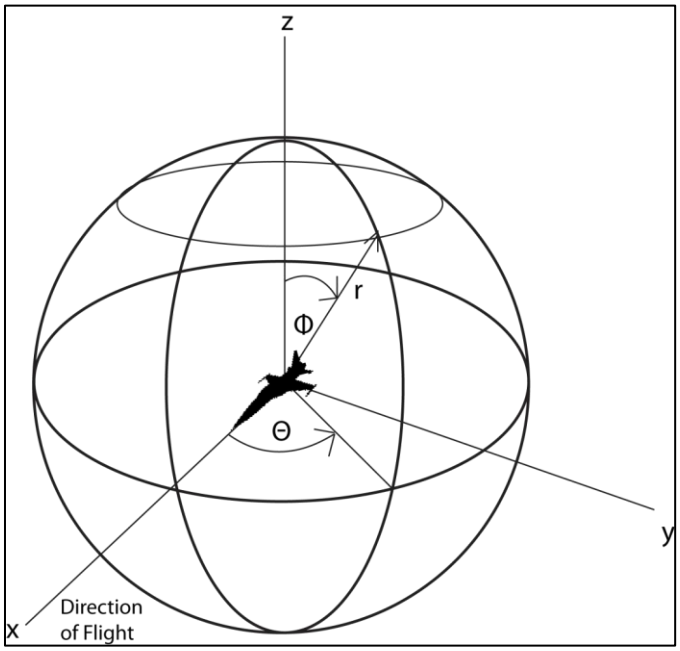

Figure 2-2. LGMAP Coordinate System

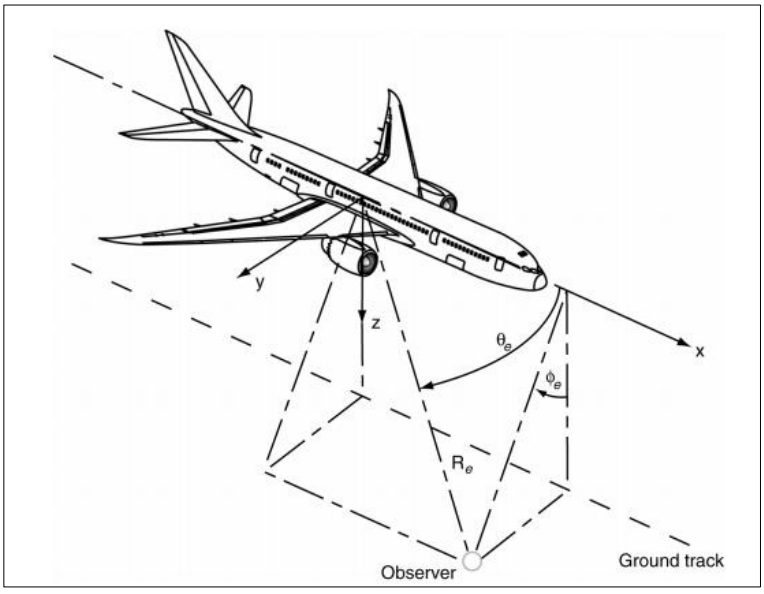

Figure 2-3. ANOPP Coordinate System (Ref. 7).

2.1 Cylinder Acoustic Element

The cylinder acoustic element is the basic building block for both strut and wheel assemblies in LGMAP. Though the cylinders contain assembly specific coefficients, the noise calculations for the wheel assembly and strut assembly are the same. The only other difference between each assembly is how the cylinders are arranged. For the strut assembly, the user specifies the location and size of each cylinder acoustic element that would best represent the strut of the landing gear in question. The wheel assembly includes more automation. The user only determines the location, diameter, and treadwidth of the wheel. LGMAP arranges several cylinder acoustic elements (the amount is set by the user) in a ring with the diameter of the ring as the wheel diameter and the cylinder diameter as the treadwidth. The coefficients used in the noise calculation for the wheel assembly are determined by the number of wheels specified in the landing gear geometry and the location of the cylinder acoustic element in relation to other cylinder acoustic elements in that assembly.

For a cylinder acoustic element, the unsteady loading is the primary source of noise generation (Ref. 14). These loads are modeled using a non-dimensional loading spectrum. The fluctuating lift and drag forces are defined by the normal component of the local flow velocity. The peak shedding frequency, lift coefficient, and drag coefficient are calibrated with experimental cases so that the cylinder produces noise similar to a strut. The wheel specific cylinder's coefficients are modeled to match the Fink method wheel model. The shedding frequency is determined by Equation 2-1 with D being the characteristic length of the cylinder. For LGMAP, the non-dimensional loading spectrum and the amplitude of the load are shown in Equation 2-2 through Equation 2-4 and Equations 2-5 through Equation 2-6 respectively (Ref. 4).

$$S = \frac{fD_c}{V_n} \tag{2-1}$$

$$F_{ND}(S) = B_2 S^{e-1}(B_1 + S^p)^{-e} \tag{2-2}$$

$$B_1 = -S_0^p \left(\frac{e(1-\rho)-1}{e-1} \right) \tag{2-3}$$

$$B_2 = \left[\int_S S^{e-1}(B_1 + S^p)^{-e} \right]^{-1} \tag{2-4}$$

$$L'(S) = \frac{1}{2}\rho V_n^2 D C_l' F_{ND}(2S) \tag{2-5}$$

$$D'(S) = \frac{1}{2}\rho V_n^2 D C_d' F_{ND}(S) \tag{2-6}$$

Values of the numerous coefficients for those equations were determined through calibration using experimental acoustic wind tunnel noise measurements. The final coefficients determined by Dr. Lopes are shown in Table 2-1. Cylinder coefficients for a wheel in a six-wheel assembly are determined by the location of the cylinder in relation to the entire wheel.

Table 2-1. Original LGMAP Coefficients determined through calibration

	e	p	S_0	C_l'	C_d'
Cylinder Acoustic Element For Strut Assembly	2.5	2.15	0.22	0.17	0.034
Cylinder Acoustic Element For Two or Four-Wheel Assembly	2.0	1.5	0.18	0.32	0.17
Cylinder Acoustic Element For Front and Rear Six-Wheel Assembly	2.0	1.5	0.18	0.255	0.11
Cylinder Acoustic Element For Top and Bottom Six-Wheel Assembly	1.75	1.6	0.25	0.184	0.08

The fluctuating loads generated by the acoustic cylinder elements are converted into sound at an observer by using modified version of Farassat's Formulation 1A of the Ffowcs William and Hawkings equation (15; 16), shown in Equation 2-7.

$$4\pi p'_L(x,t) = \frac{1}{c}\int_{f=0}\left[\frac{\dot{F}_r}{r|1-M_r|^2}\right]_{ret} dS + \int_{f=0}\left[\frac{F_r - F_M}{r^2|1-M_r|^2}\right]_{ret} dS + \frac{1}{c}\int_{f=0}\left[\frac{F_r\left(r\dot{M}_r + cM_r - cM^2\right)}{r^2|1-M_r|^3}\right]_{ret} dS \tag{2-7}$$

This equation was simplified and converted from the time domain to the frequency domain for LGMAP by Dr. Leonard Lopes (Ref. 4). The cylinder acoustic elements are assumed to be isolated and unaffected by each other. So the components are added incoherently i.e., the acoustic signals are added on a pressure squared basis. This simplified, frequency domain version is shown in Equation 2-8.

$$p'^2_L(f) = \sum_{cyl}\frac{F_r^2 D^2 l^2}{16}\left[\frac{(1-M_r)^2 + r^2\kappa^2}{r^4|1-M_r|^4}\right] \tag{2-8}$$

2.2 Trailing Edge Acoustic Element

The trailing edge element in LGMAP applies a simplified version of the Ffowcs William and Hall trailing edge equation (Ref. 17), shown in Equation 2-9 and Equation 2-10 respectively.

$$4\pi p^*_{TE}(r,\theta,\phi;\omega) = \frac{2^{5/2}e^{i\left(\frac{1}{4}\pi - kr\right)}}{r\pi^{1/2}} k^{1/2}\sin^{1/2}\phi\cos\frac{\theta}{2}\tau^*\delta^{-3/2}V \tag{2-9}$$

$$4\pi p^*_{TE}(r,\theta,\phi;\omega) = \frac{2^{5/2}e^{i\left(\frac{1}{4}\pi - kr\right)}}{r\pi^{1/2}} k^{1/2}\sin^{1/2}\phi\cos\frac{\theta}{2}\tau^*\delta^{-3/2}\varepsilon l^3 \tag{2-10}$$

The volume of the turbulent source region, *V*, is estimated to be the cube of the turbulent mixing length, *l*, times the trailing edge calibration constant, ε, of order O(1). The Reynolds shear stress term (Equation 2-11), τ^*, is modeled using the turbulence intensity, α, and a spectrum function which is shown in Equation 2-12 through Equation 2-14.

$$F(S) = B_2(10S)^{e-1}[B_1 + (10S)^p]^{-e} \tag{2-11}$$

$$B_1 = -S_0^p\left(\frac{e(1-p)-1}{e-1}\right) \tag{2-12}$$

$$B_2 = [S^{e-1}(B_1 + S^p)^{-e}]^{-1} \tag{2-13}$$

The turbulence intensity, along with the turbulent mixing length and the trailing edge calibration constant are entered by the user. This requires the user to find these variables through mean flow calculations or wake estimates. Previously, these values were found using CFD calculations of the landing gear and resultant prediction produced favorable results (Ref. 4).

The next chapter summarizes the enhancements made to the LGMAP method and the reasons that made the changes necessary. These changes forced a recalibration of the cylinder acoustic elements and the recalibration process is described as well.

Chapter 3

Improvements and Enhancements to LGMAP

The goal of this thesis is to validate the prediction capabilities of LGMAP and document the how to effectively use this recently developed tool. Several prediction cases were created to be compared with experimental data and other predictions. The predictions resulted in questions about the capabilities of the method, especially the directivity.

One of the first landing gear cases investigated was of Gulfstream nose landing gear. Source localization maps using a phased array method (Figure 3-1) of the Gulfstream G550 were made available (18) and were compared with LGMAP's own predictions (Figure 3-2). The Gulfstream experimental case is described further in Section 4.3.2. The original LGMAP prediction is shown in the figure as a "flattened" spherical observer grid based on the LGMAP spherical coordinate system shown in Figure 2-2. The wheel is by far the dominant source of noise of the landing gear. The strut assembly, including the main oleo, does not make significant contributions to total predicted noise. The source localization maps contradict the LGMAP prediction and show that the strut produces a significant portion of the landing gear noise. This brings into doubt LGMAP's capability as a noise prediction scheme, especially since it had shown promise in early testing (Ref. 4).

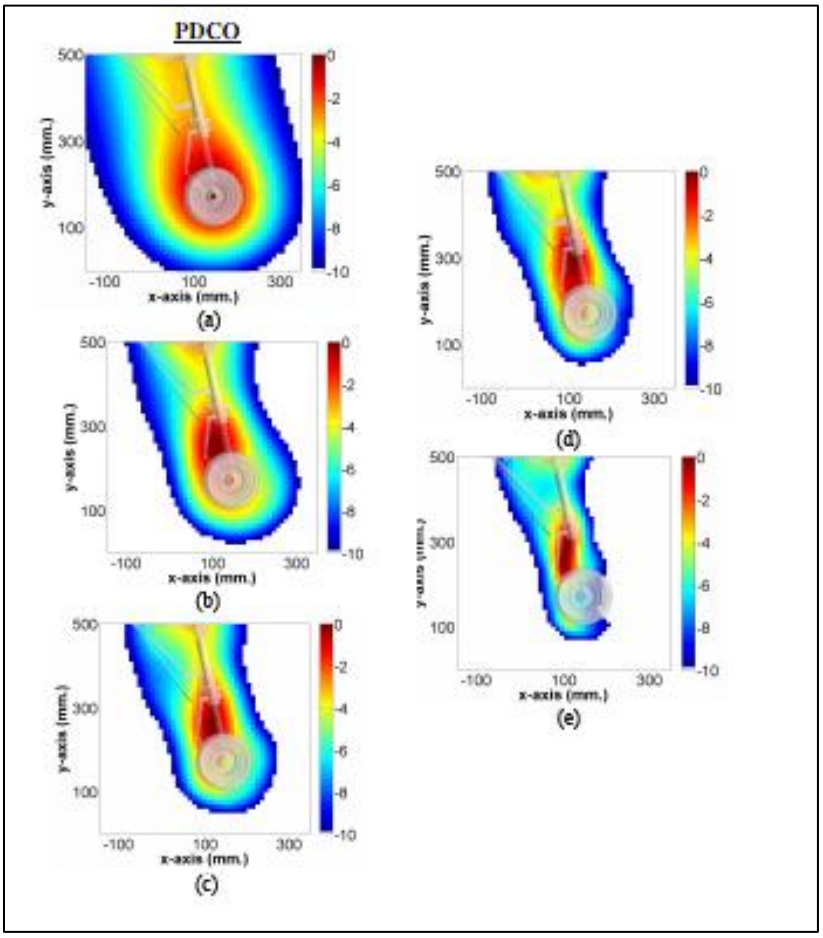

Figure 3-1. Noise source localization maps of 25% scaled Gulfstream G550 nose landing gear at frequencies (a) f=1.25kH, (b) f=2.5kH, (c) f=4kH, (d) f=5kH, (e) 8 f=kHz. Levels are in normalized dB (Ref. 19).

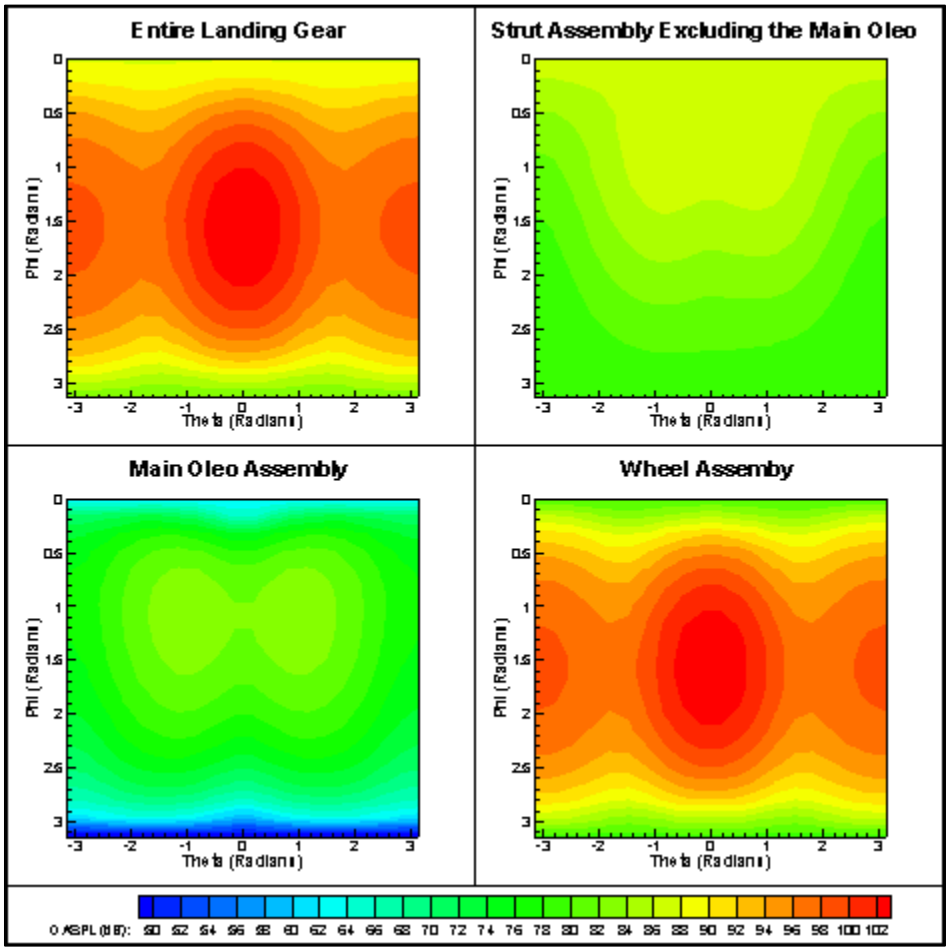

Figure 3-2. Component LGMAP prediction over a spherical observer grid. Observer radius is 1 meter.

LGMAP's wheel assembly directivity is also a concern. Having a dipole shape, the maximum OASPL is found at the front and rear of the wheel. The Fink method used in ANOPP, which had been a trusted, albeit simplistic, landing gear prediction method, shows just the opposite (Figure 3-3). This is troubling because the LGMAP wheel acoustic element was originally calibrated with the Fink method wheel element. The cylinder acoustic elements that make up the wheel assembly had been adjusted in order to match more closely with experimental results, but this was done only for cases with six wheels and observer locations directly below the aircraft. In hindsight, two observer positions are not sufficient to accurately characterize the

directivity calculation. Also this adjustment still retained the directivity of the one, two, and four wheel bogeys. An updated or completely new wheel element was required for accurate sideline and flyover predictions.

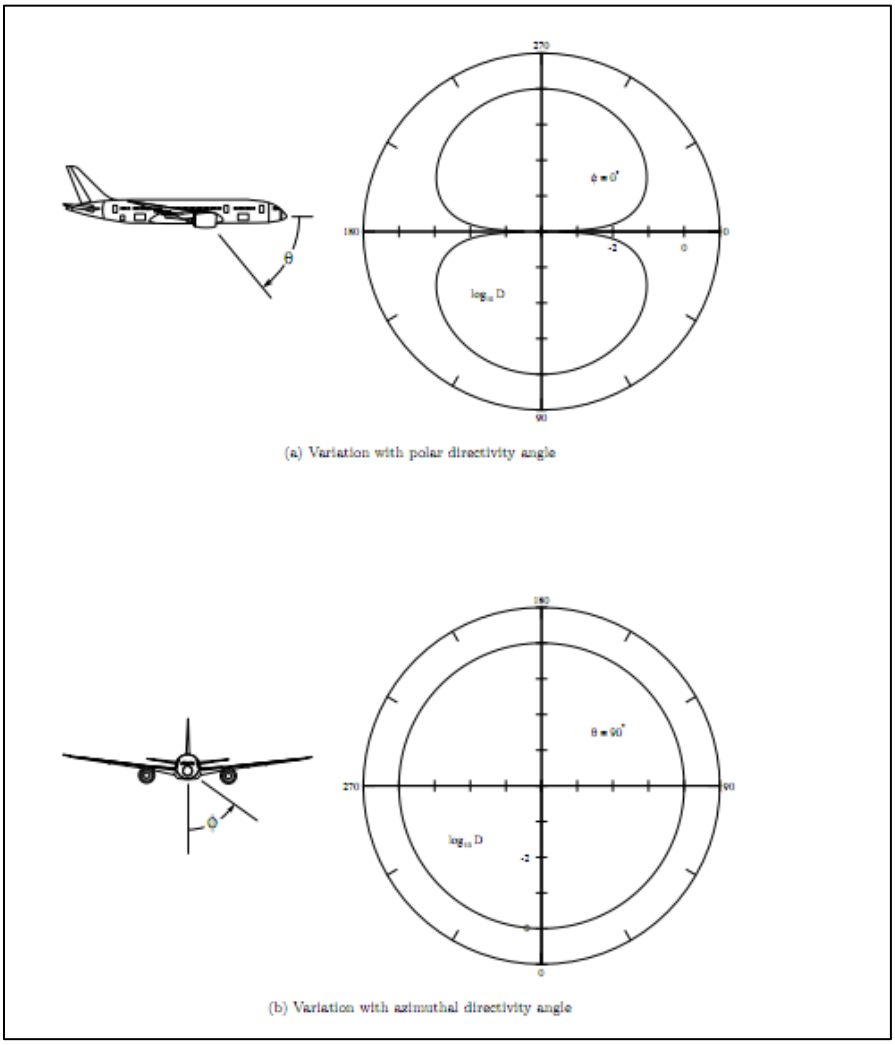

Figure 3-3. ANOPP Fink method directivity level for landing gear wheel noise (12).

Due to discrepancies between LGMAP's predictions and the experimental measurements for the Gulfstream G550, a repetition of LGMAP's previous validation tests was performed. The current frequency based LGMAP version at that time had several components calibrated using the original time based LGMAP software. The most completely described data set used in those

calibrations was of the Boeing 757 main landing gear. These test cases were compared with the ANOPP Fink Method in order to calibrate the wheel components (Figure 3-4).

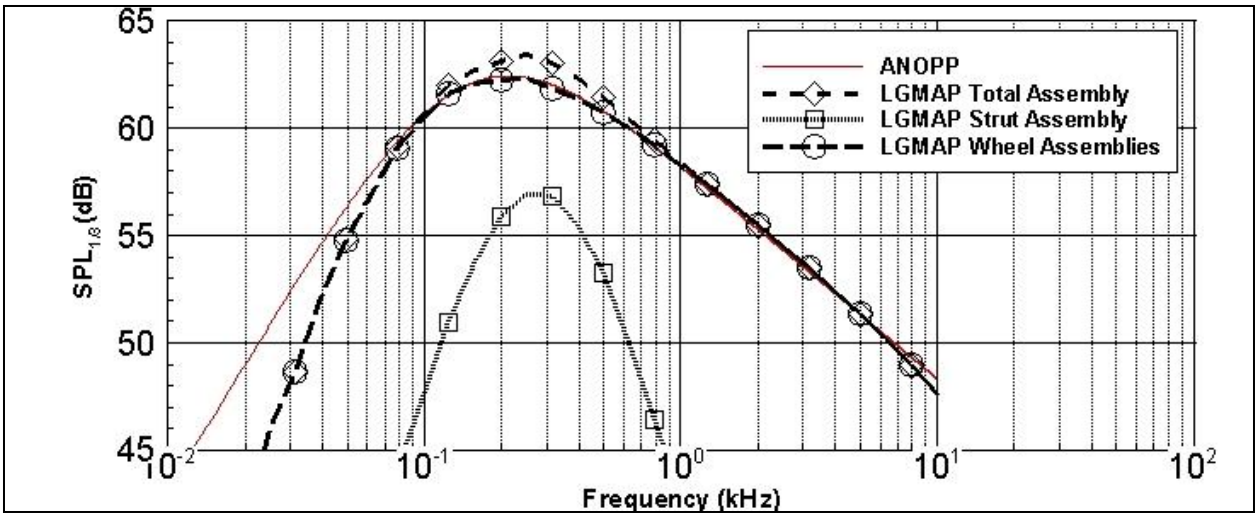

Figure 3-4. Third Octave sound pressure levels versus Frequency for a full scaled Boeing 757 main landing using time-based LGMAP. The observer is located 45^0 down from the foward velocity vector. The forward velocity is 0.2 Mach and the atmospheric conditions are at sealevel (5).

Using the same conditions, geometry, and observer location, the Boeing 757 case was predicted using the current frequency based LGMAP (Figure 3-5), but it was unable to reproduce the previous results. Both the strut and wheel component third-octave levels were unacceptably high and needed to be re-evaluated in order for LGMAP to predict accurate sound pressure levels.

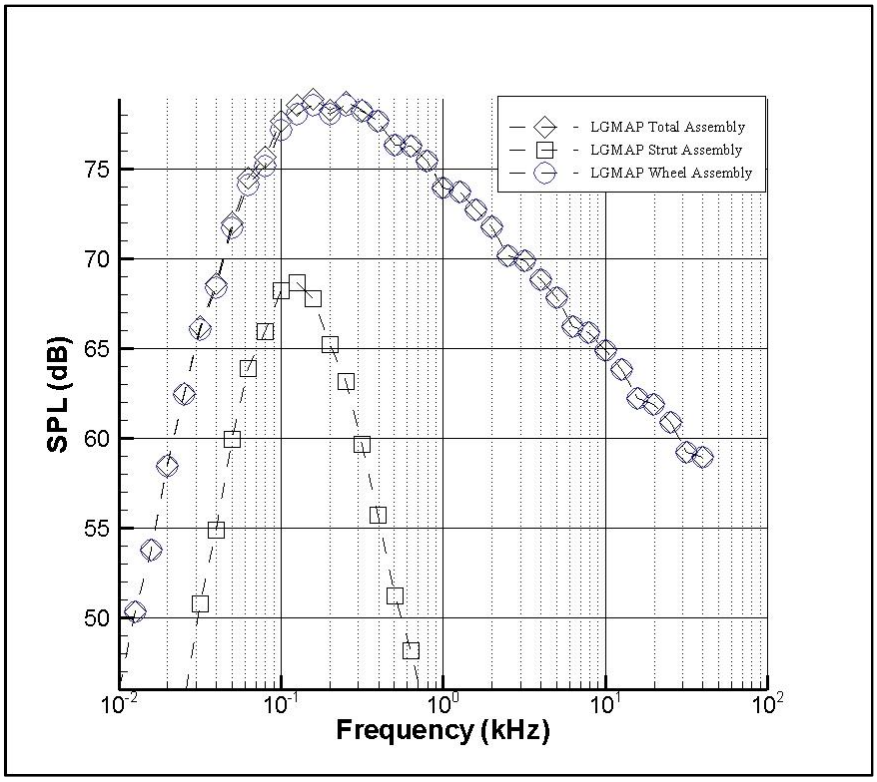

Figure 3-5. Third Octave sound pressure levels versus Frequency for a full scaled Boeing 757 main landing using frequency-based LGMAP. The observer is located 45^0 down from the forward velocity vector. The forward velocity is 0.2 Mach and the atmospheric conditions are at sea level.

3.1 Cylinder Scaling

Early in LGMAP's development, it was not shown that cylinder acoustic elements scale correctly with Strouhal number. Cylinders with the same ratio of observer distance to cylinder size (length and diameter) and the same observer directivity should scale exactly with SPL and Strouhal number. This property is fundamental in aeroacoustics. After investigation of the current LGMAP version at that time, this property was not present in LGMAP's prediction

(Figure 3-6). Although the shape of the spectrum remains the same, the amplitude increases along with cylinder size. This leads to under predictions for small cylinder objects in the landing gear geometry such as hydraulic hoses, which primarily effects high frequency noise.

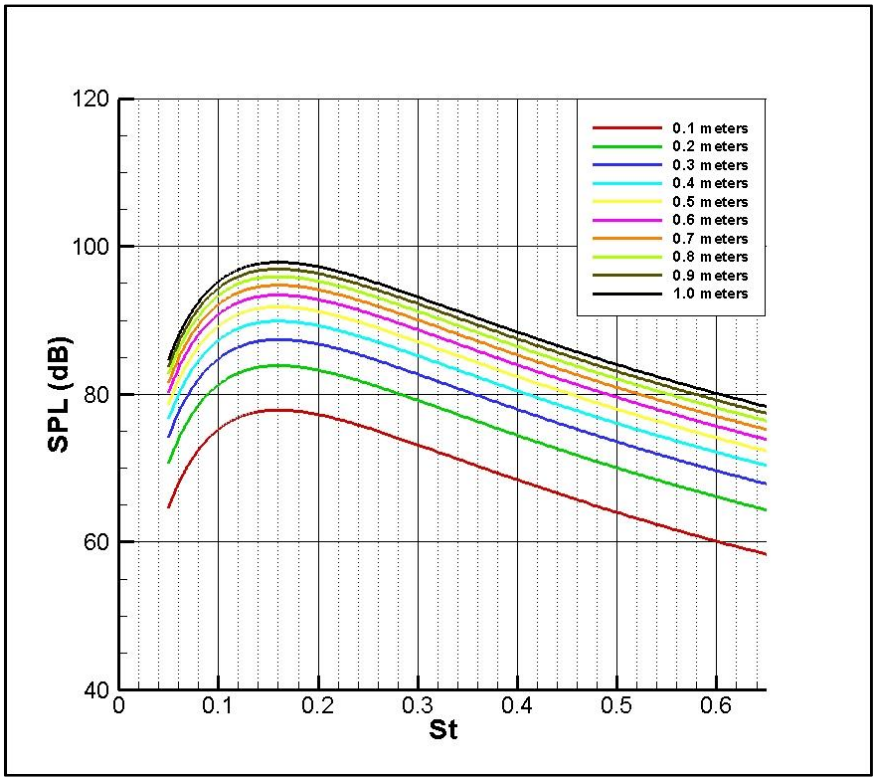

Figure 3-6. Original LGMAP SPL levels of scaled single isolated cylinders per Strouhal number. Observer locations are scaled as well. The flow velocity is Mach 0.2 and the atmospheric conditions remain constant for all cases. The legend is organized by cylinder diameter. Observer distance is located 128 diameters from the center of the cylinder at an angle of 90^0 from the velocity vector.

Investigation of the code revealed that the problem was in the modified Farassat's Formulation 1A (Equation 2-7). The equation was miscoded and required an update. The isolated cylinder cases were predicted again with the update and the results produced the expected result (Figure 3-7). This update, along with others, necessitated a new updated calibration of the cylinder acoustic elements.

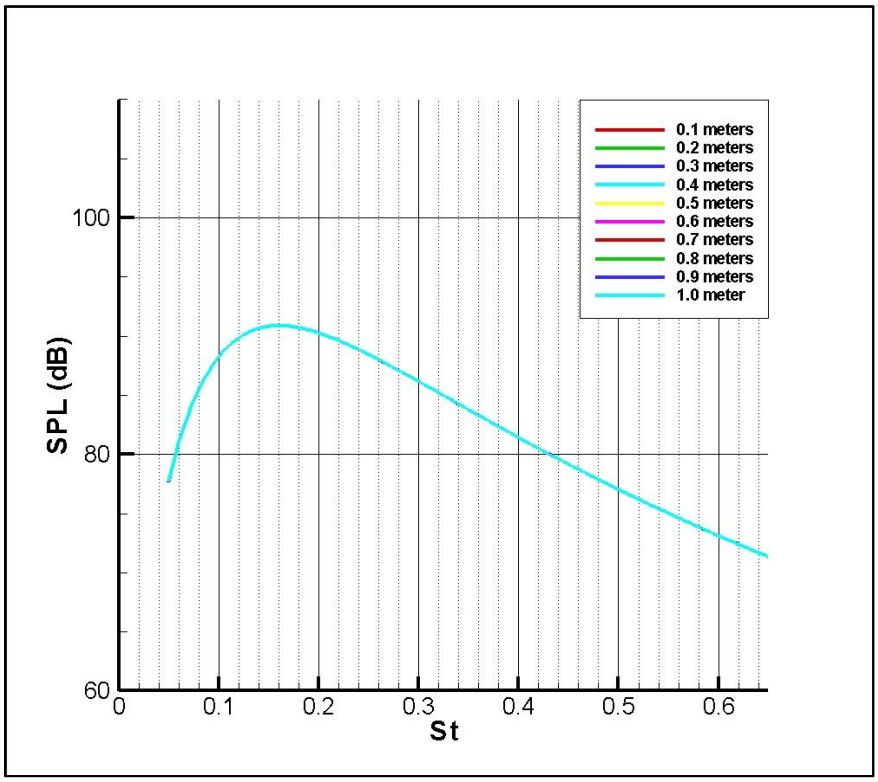

Figure 3-7. Corrected LGMAP SPL levels of scaled single isolated cylinders per Strouhal number. Observer locations are scaled as well. The flow velocity is Mach 0.2 and the atmospheric conditions remain constant for all cases. The legend is organized by cylinder diameter. Observer distance is located 128 diameters from the center of the cylinder at an angle of 90^0 from the velocity vector. The cylinder lift and drag coefficients were no calibrated when these results were taken.

In order to determine the implications of this error, a case ran by Dr. Lopes was revisited with the updated code. The case chosen was of a 6.3% scaled Boeing 777 main landing gear with a single observer. This was chosen because the landing gear geometry consisted of small cylinders that represented hydraulic hoses. The results (Figure 3-8), after recalibration of the cylinder, show an over prediction of high frequency noise. This result draws into question the accuracy of LGMAP predictions made before this update. Since LGMAP cylinders were calibrated using experimental data from a 6.3% scaled Boeing 777 main landing gear model (4), full scale predictions would be grossly underpredicted in the entire frequency range. Due to this

error, the rest of LGMAP's code regarding the cylinder acoustic element was tested for other potentially erroneous results.

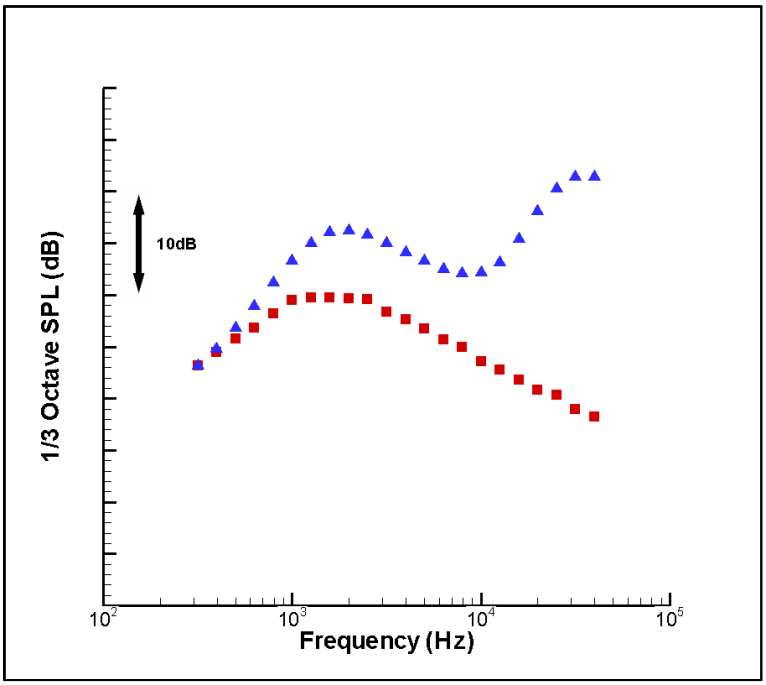

Figure 3-8. LGMAP 1/3 octave SPL levels of a 6.3% scaled Boeing 777 port side main landing gear. The observer is located 0.222 meters below, 1.5055 meters starboard, and 0.079760 meters forward of the landing gear. The red squares are the original LGMAP prediction and the blue triangles are the corrected LGMAP prediction.

3.2 Non-dimensional Cylinder Spectrum

The investigation of LGMAP's code related to the cylinder model revealed the non-dimensional spectrum (Equation 1.2), which gives the "shape" of the cylinder's noise spectrum, was erroneous for the unsteady drag force prediction (Figure 3-9). The error was found to be in the Strouhal number calculation in the case of the drag.

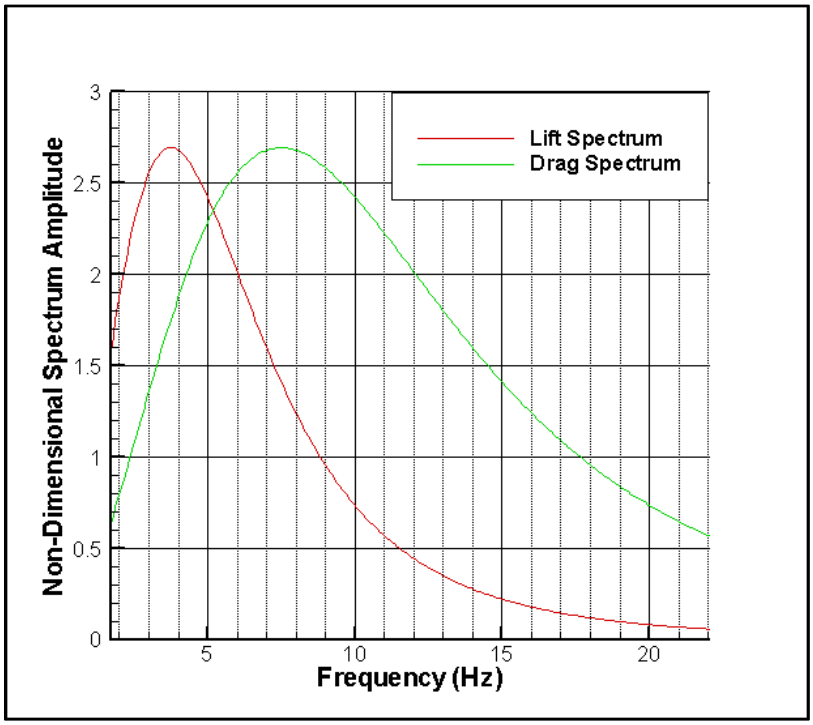

Figure 3-9. Correct non-dimensional lift spectrum and incorrect non-dimensional drag spectrum for a cylinder produced by uncorrected version of LGMAP.

The Karman vortices, shed when flow passes over a cylinder, alternate in direction and this alternation creates unsteady lift. Because the forces in the drag direction are the same for each vortex compared to the alternating direction of the lift forces, the frequency of the unsteady drag force is twice that of the lift. The nature of the error found in LGMAP was that the amplitude of the alternating drag forces was specified erroneously. But since the drag coefficient is calibrated, any predictions would be unaffected. The calibrated drag coefficient would be incorrect though.

3.3 Incident Velocity Vector

In LGMAP, only flow perpendicular to the length of the cylinder is used in noise calculation as discussed in Section 2.1. This flow is known as the incident flow velocity, V_n. It assumed that flow along the length of the cylinder does not have a significant effect on the noise produced. LGMAP was not properly computing the perpendicular flow, (Equation 3-1).

$$V_n = \|\mathbf{V}\| - \frac{|\hat{\mathbf{l}} \cdot \mathbf{V}|}{\|\mathbf{l}\|} \tag{3-1}$$

A correct equation was determined and is shown in Equation 3-2 with ***l*** defined as the length vector of the cylinder.

$$V_n = \sqrt{\|\mathbf{V}\|^2 - \left(\mathbf{V} \cdot \frac{\hat{\mathbf{l}}}{\|\mathbf{l}\|}\right)^2} \tag{3-2}$$

3.3 New LGMAP Wheel Model

As discussed in Section 2.1, LGMAP originally used a ring of cylinder acoustic elements to model a landing gear wheel. The wheel's lift and drag coefficients and peak Strouhal frequencies found in the cylinder's loading calculations are different than those for the strut cylinder. Dr. Lopes first calibrated LGMAP's wheels using the ANOPP Fink method for predicting landing gear noise and later he used experimental data for calibration (Ref. 4). It has been found that the directivity of the previous LGMAP wheel model (Figure 3-10) was very different to that used by Fink (Figure 3-11).

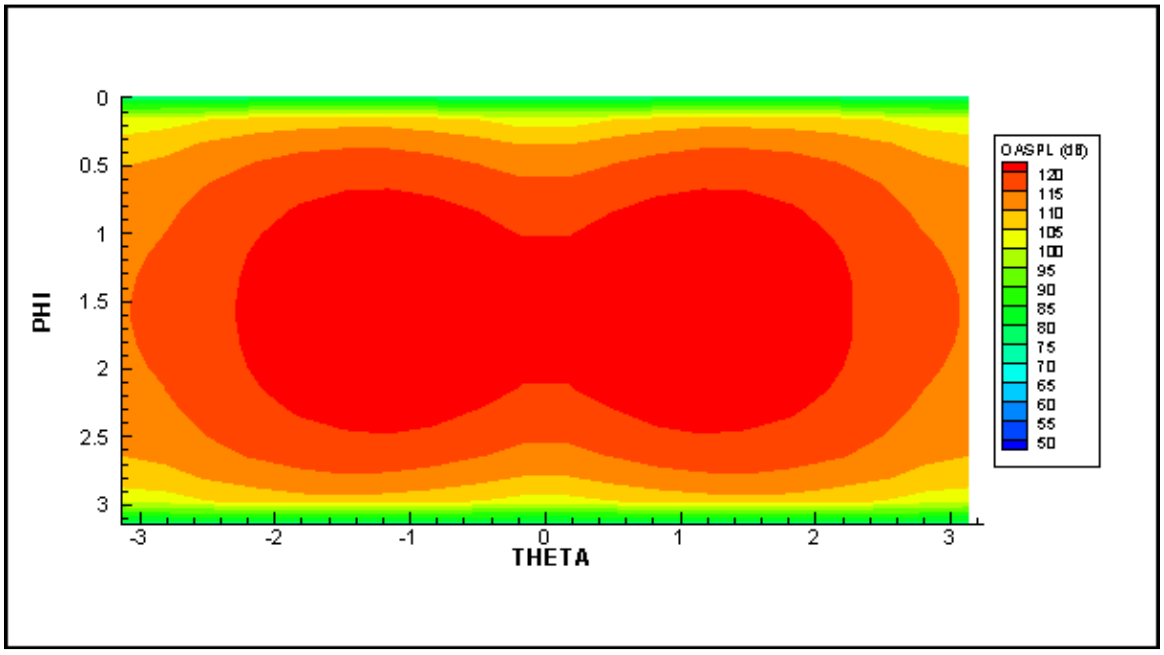

Figure 3-10. OASPL over a spherical observer grid with a radius of 170 meters. The noise source is the Boeing 757 Wheels (four wheels) modeled by LGMAP's original wheel acoustic element.

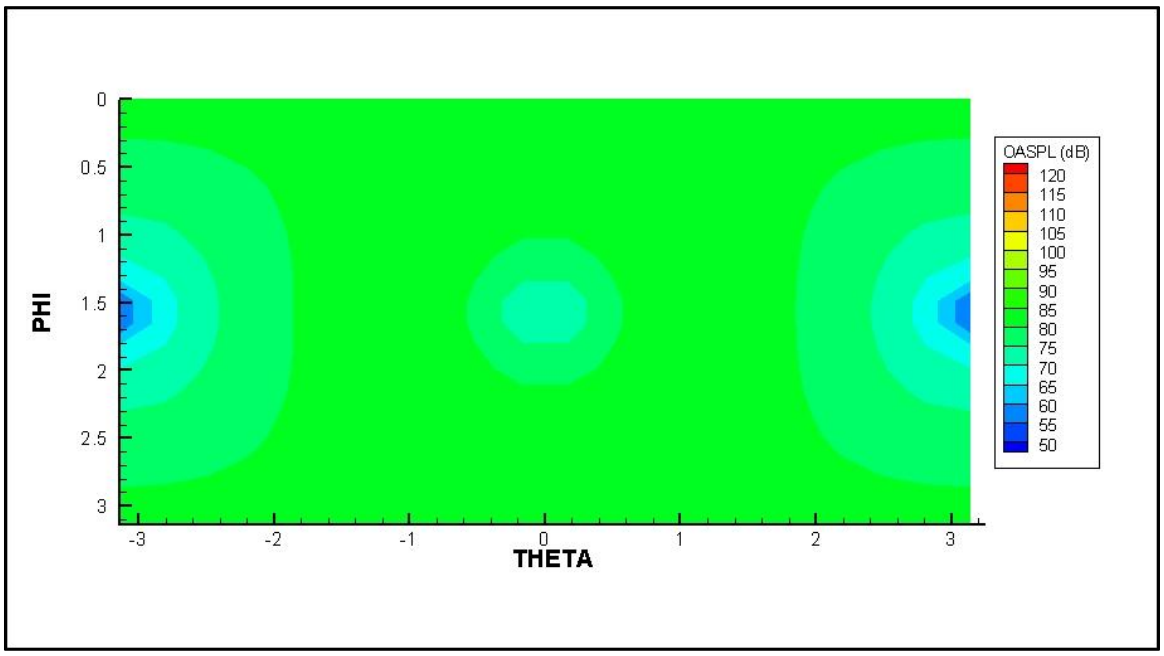

Figure 3-11. OASPL over a spherical observer grid with a radius of 170 meters. The noise source is the Boeing 757 wheels (four wheels) modeled by ANOPP's wheel model.

A ring of cylinders acoustic elements is unable to produce noise directivity similar to Fink's without changing the noise from every individual cylinder element. This would defeat the usefulness of using cylinders to predict wheel noise in LGMAP. Since Fink's model is still the only source to simply model the wheel noise individually, it was decided to base a new LGMAP wheel model on the Fink prediction method.

3.3.1 The ANOPP Based Wheel

The new ANOPP based wheel model (ABWheel) is a single Fink method wheel, for which the user can specify the dimensions and location. The most important difference between the two wheel models is that the LGMAP wheel bogey is comprised of several individual ABWheels, whereas the ANOPP Fink method wheel contains the entire landing gear's wheel bogey. LGMAP's shielding and scattering capabilities are applied to the model as well, with the wheel represented as an isolated cylinder. Like LGMAP, ANOPP sums strut and wheel noise on a pressure squared basis (Equation 3-3).

$$\langle p^2 \rangle = \frac{\rho c \Pi}{4\pi {R_e}^2} \frac{D(\theta \ , \phi \ ) F(S_t)}{(1 - M \cos\theta \ )^4} \tag{3-3}$$

The method calculates the acoustic power, Π, using Equation 3-4, where $K=4.349x10^4$ for one or two-wheel landing gear and $K=3.414x10^4$ for a four-wheel landing gear.

$$\Pi_{wheel} = KM^6 N_w d^2 \tag{3-4}$$

The directivity, *D*, and the spectrum function, *F*, for a landing gear's wheels are calculated using Equation 3-5 and Equation 3-6 respectively (Ref. 12).

$$D(\theta, \phi) = \frac{3}{2}\sin^2\theta \tag{3-5}$$

$$F(S) = A\frac{S^n}{(B + CS^m)^q} \tag{3-6}$$

ANOPP outputs SPL in the third octave pressure squared basis. Hence, the ANOPP model is not directly compatible with LGMAP and the wheel equation cannot be inserted directly into LGMAP because the program adds the noise from different sources using a narrow band spectrum pressure squared. To make the ANOPP model compatible with LGMAP, the constant *n* is reduced by one and the amplitude of normalized spectra, *A*, is changed from 13.59 to 0.085 so that the pressure squared reflects the narrow band spectrum.

For a one wheeled landing gear, the ABWheel and ANOPP match perfectly as a single ABWheel is essentially an ANOPP wheel source. As seen in the spherical observer contours shown in Figure 3-12 and Figure 3-13, two isolated ABWheels produce very similar results to an identical ANOPP source. The OASPL agreement for four and six wheel bogeys is noticeably less (Figure 3-14 through Figure 3-17). Although ANOPP is not designed to model six wheels, it has been shown that it compares reasonably with experimental data (Ref. 7).

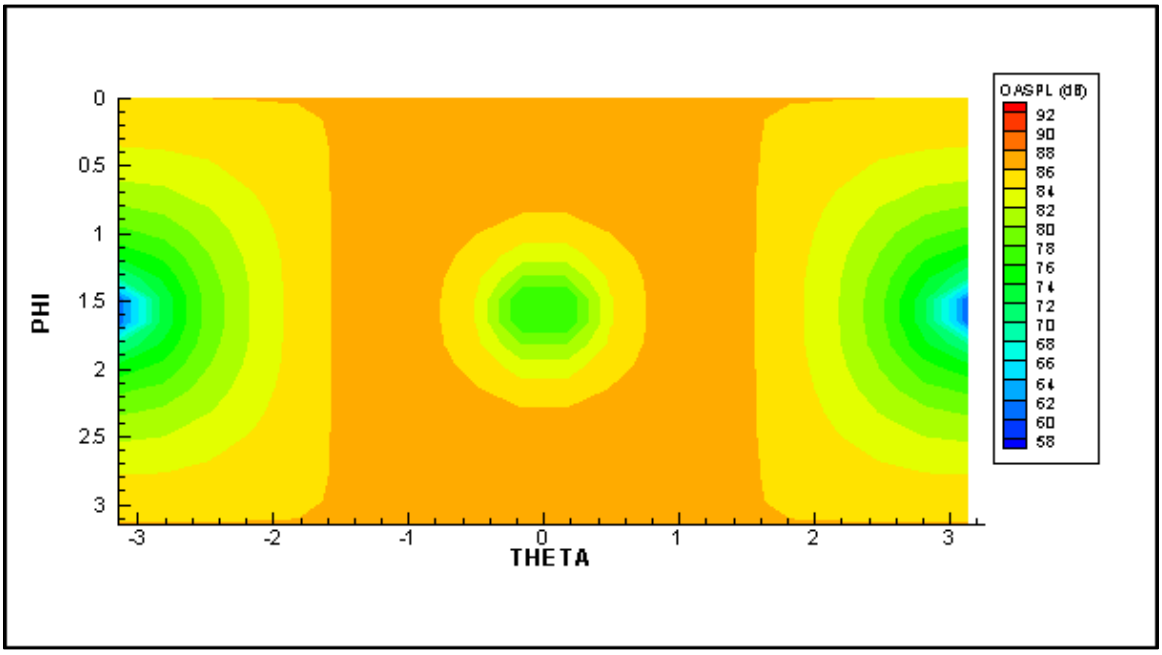

Figure 3-12. OASPL over a spherical observer grid with a radius of 170 meters. The noise source is the GS550 nose gear's two wheels modeled using ANOPP.

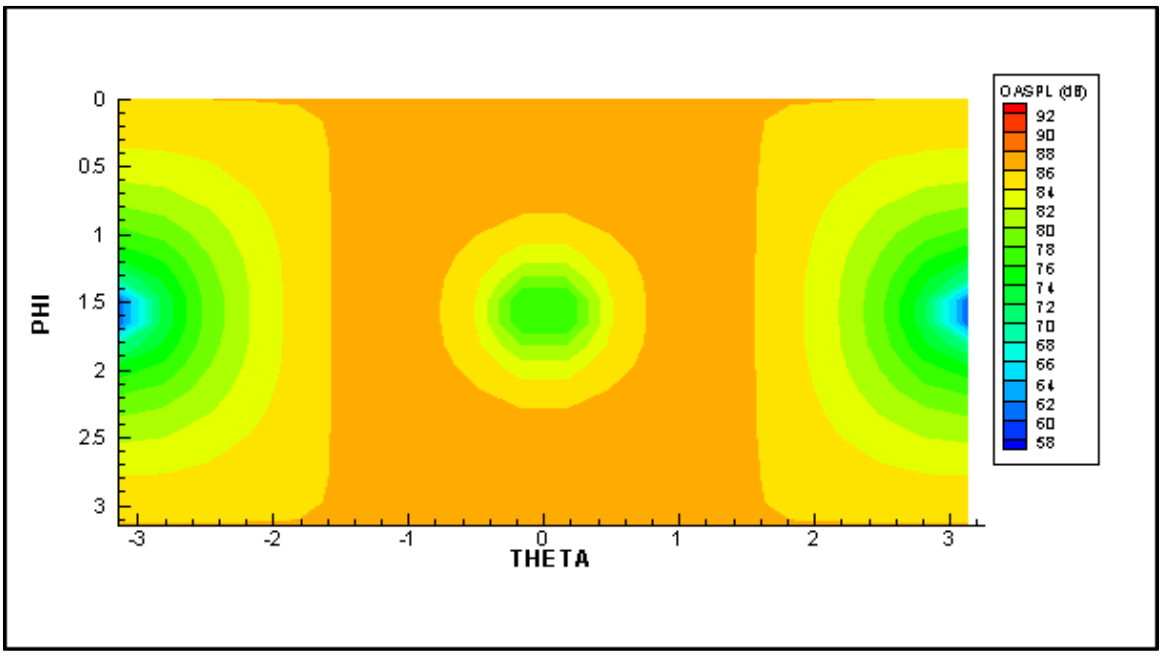

Figure 3-13. OASPL over a spherical observer grid with a radius of 170 meters. The noise source is the GS550 nose gear's two wheels modeled using the ABWheel model.

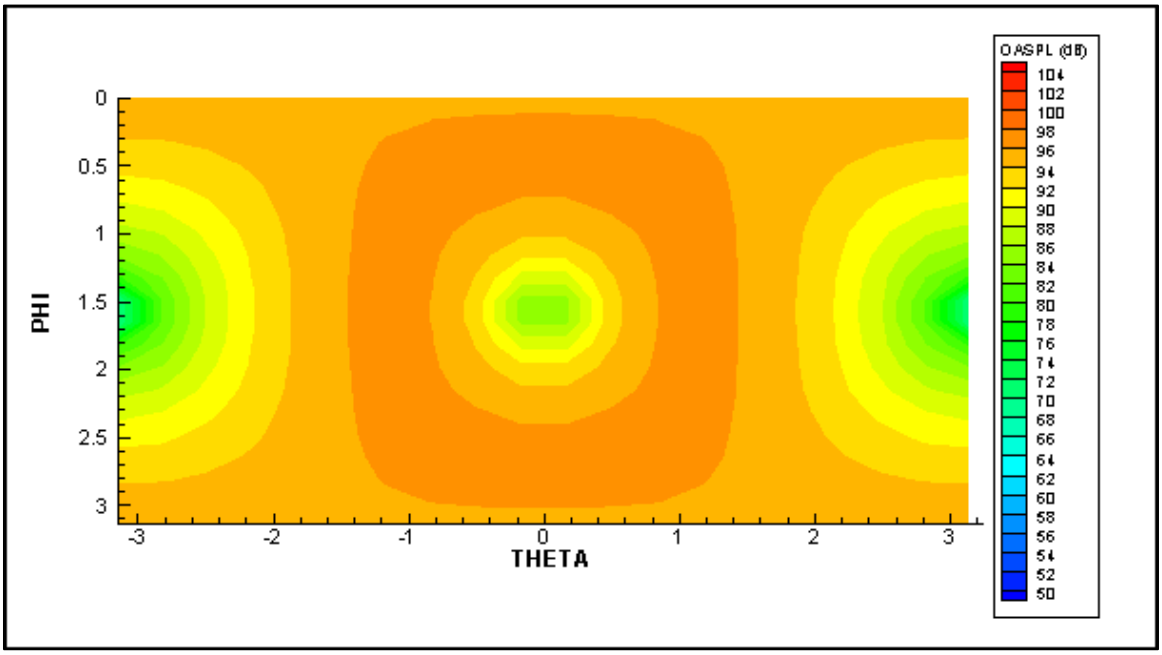

Figure 3-14. Wheels of the Boeing 757 (Four Wheels) OASPL directivity using the ANOPP wheel model. Observer distance is 170 meters and free stream Mach number is 0.20.

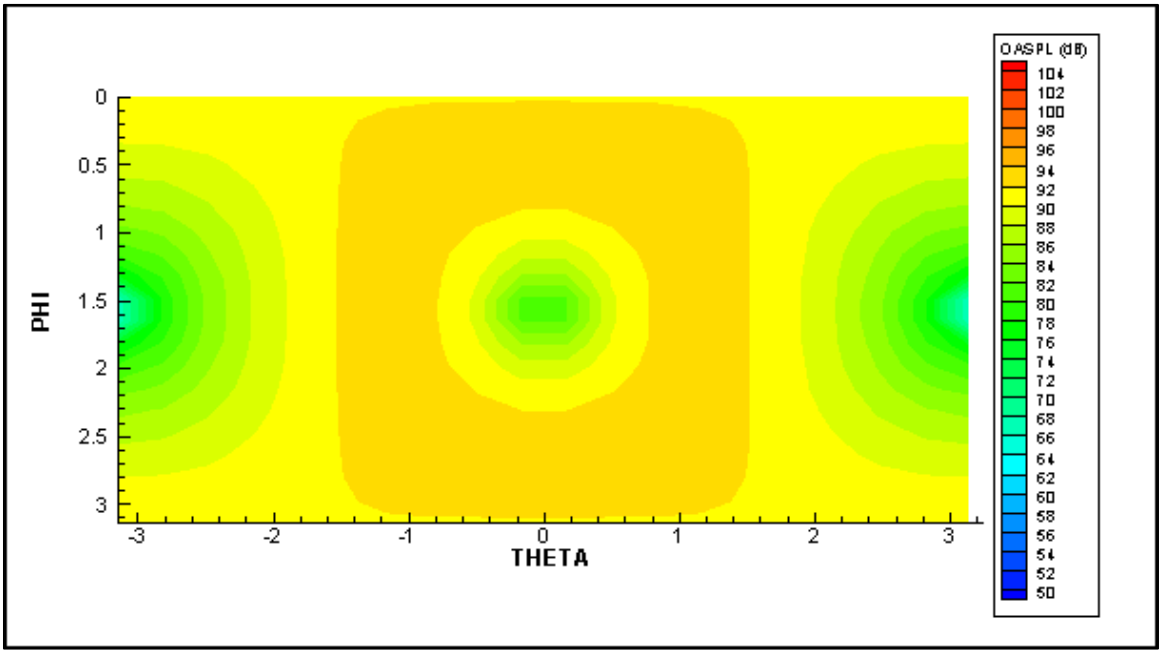

Figure 3-15. Wheels of the Boeing 757 (Four Wheels) OASPL directivity using an original ABWheel model. Observer distance is 170 meters and free stream Mach number is 0.20.

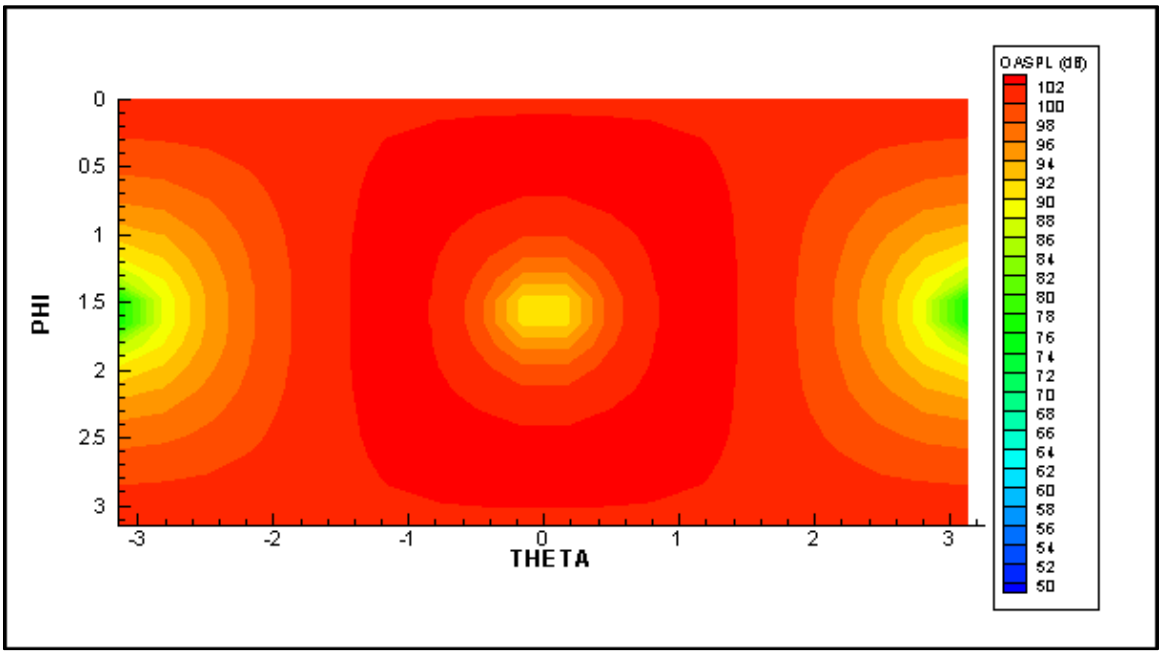

Figure 3-16. OASPL over a spherical observer grid with a radius of 170 meters. The noise source is the Boeing 777 main gear's six wheels modeled using ANOPP.

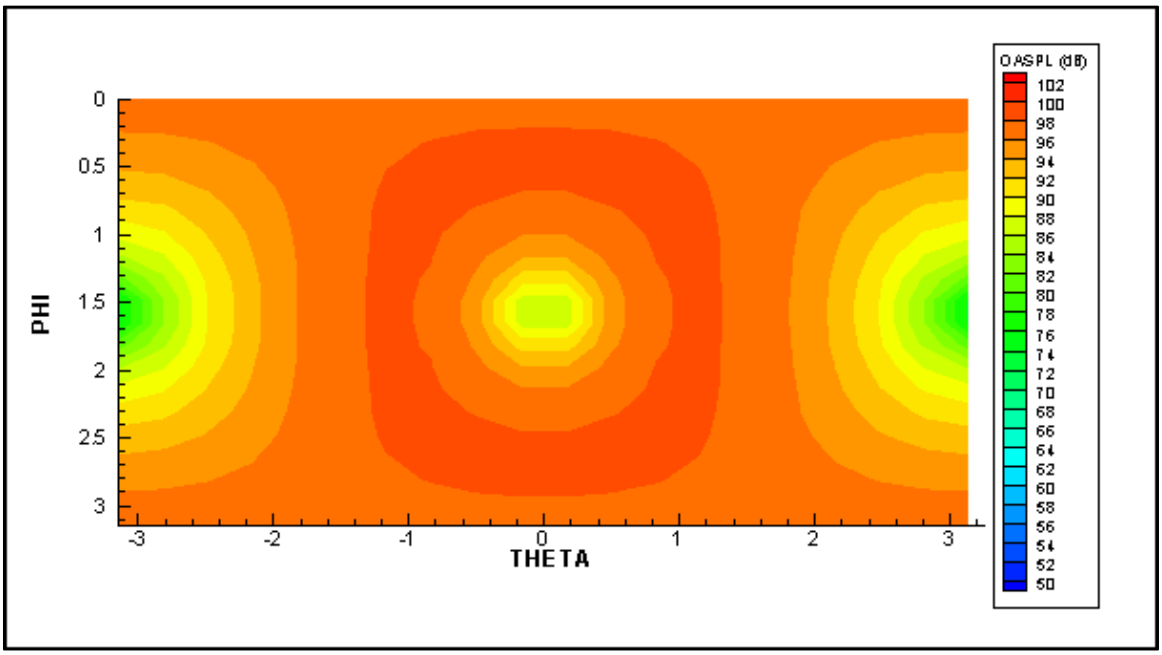

Figure 3-17. OASPL over a spherical observer grid with a radius of 170 meters. The noise source is the Boeing 777 main gear's six wheels modeled using the ANOPP Based Wheel model.

3.3.2 The "In Wake" Parameter

The four and six wheel ABWheels do not compare as well with the ANOPP model because the Fink method uses different constants in the spectrum and acoustic power equations (12). The reason for this is that the flow over any rear wheel is affected by wheels ahead of it. For the sake of simplicity, LGMAP has an option for the ABWheel, "inwake', that will specify that it is in the wake of another wheel. If this is the case, the ABWheel alters the spectrum and acoustic power equations' constants. As a starting point, the Fink method constants of a four wheel landing gear were used. The spectrum equation constants had to be modified for a narrowband spectrum in the same way as a one to two wheel landing gear. To do this, the constant *A* is changed from 0.0577 to 0.00037. Surprisingly, the ANOPP constants work very well (Figure 3-18 and Figure 3-19). The differences are small enough that it was decided to continue using the ANOPP constants.

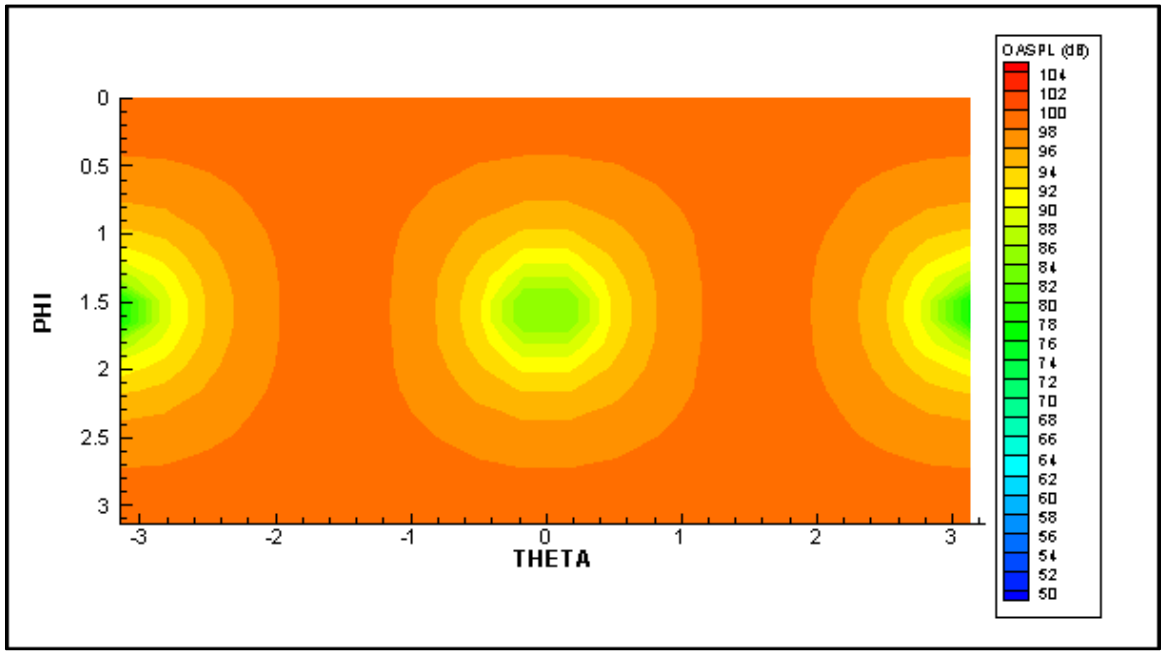

Figure 3-18. Wheels of the Boeing 757 (Four Wheels) OASPL directivity using the AB wheel model with additional "in wake" calculations. Observer distance is 170 meters and free stream Mach number is 0.20.

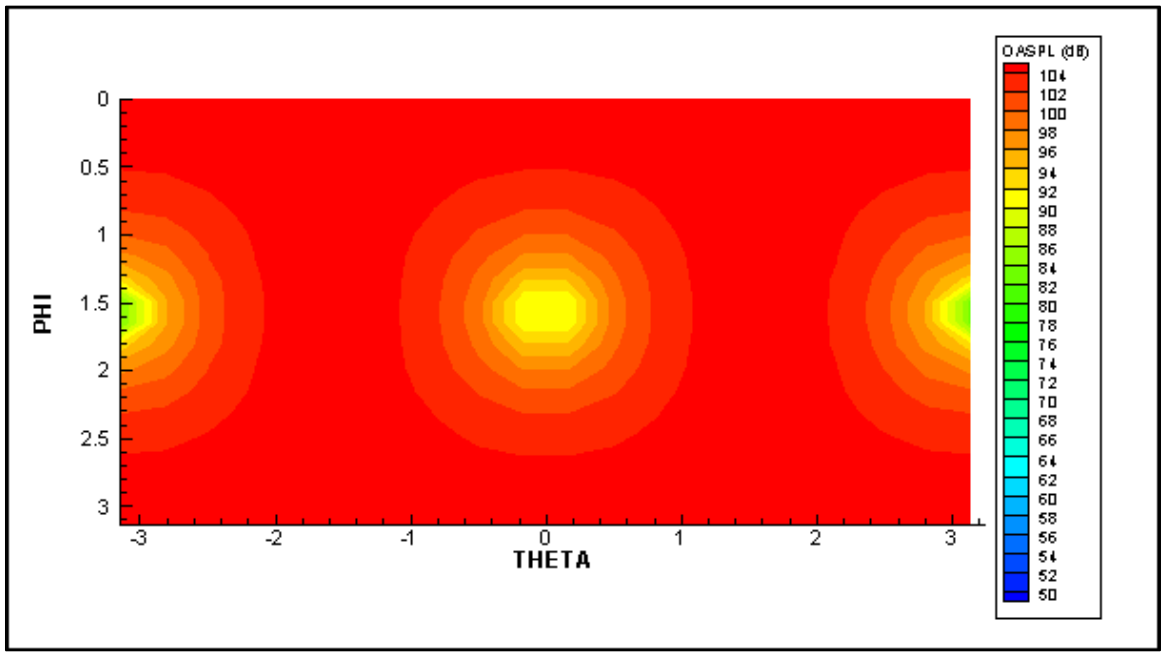

Figure 3-19. Wheels of the Boeing 777 (Six Wheels) OASPL directivity using the AB wheel model with additional "in wake" calculations. Observer distance is 170 meters and free stream Mach number is 0.20.

3.4 Cylinder Calibration

Because LGMAP required extensive changes to the cylinder noise calculations, the lift and drag coefficients of the unsteady forces required recalibration. Directivity predictions of an isolated cylinder by Cox, Brentner, and Rumsey (Ref. 11) were used for calibration (Figure 3-20). This calibration was only preliminary as a strut component of a landing gear will not have the exact properties of a circular cylinder, but it is still very useful. The directivity of a strut would match fairly well with the cylinder and this is also an opportunity to confirm the directivity of LGMAP predictions after the updates. The fluctuating coefficients of lift and drag were set to match the OASPL results from Cox, Brentner, and Rumsey (Figure 3-21) for an isolated cylinder under turbulent flow. The ratio between these coefficients remained after further calibrations to preserve the directivity.

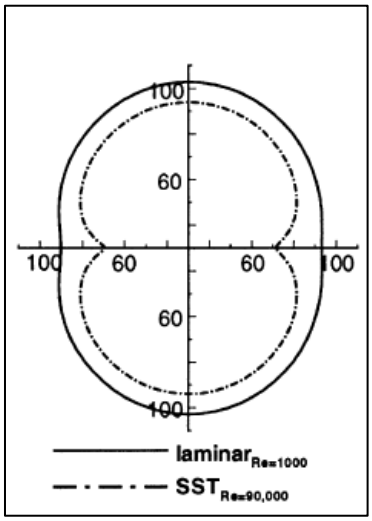

Figure 3-20. Predicted OASPL directivity pattern of a circular cylinder from Cox, Brentner, and Rumsey for $M = 0.2$. Flow is traveling from right to left. Axes units are decibels (dB, re:20 Pa) in overall sound pressure level. Observer is located 128 diameters from the cylinder. The cylinders length is 26.3 diameters (Ref. 11).

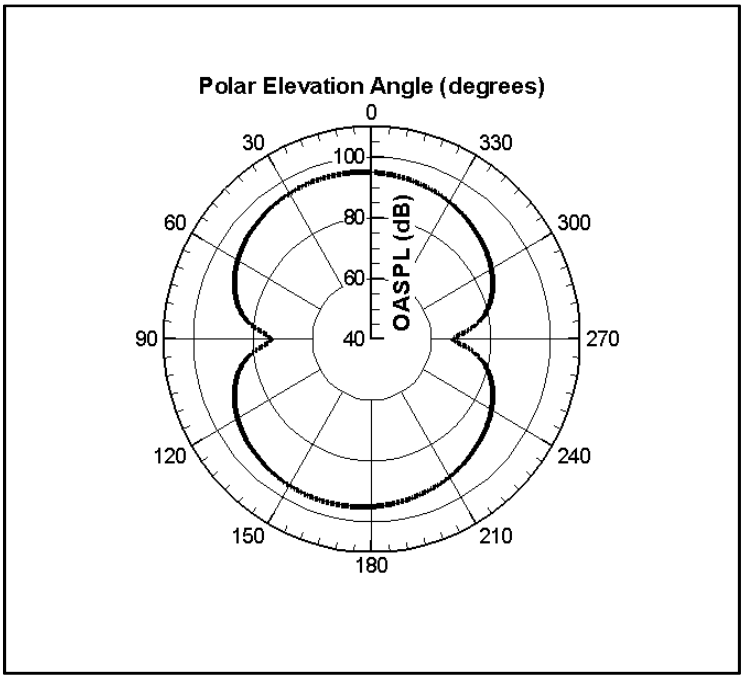

Figure 3-21. LGMAP OASPL directivity patterns of a circular cylinder for M = 0.2. Flow is traveling from right to left. Axes units are decibels (dB, re:20^{1}Pa) in overall sound pressure levels. Observer is located 128 diameters from the cylinder. The cylinders length is 26.3 diameters. Dr. Lopes' equation for F_r^2 is used to solve for sound pressure levels.

The shape of the cylinder acoustic element's spectrum was mostly unchanged. The broadband nature that was to mimic a strut, remained unchanged, and the peak Strouhal number should not have to change either, even with the scaling issue of the cylinder acoustic element. To confirm this, the same experimental data used to calibrate the directivity were also used to find the peak Strouhal number (Figure 3-22). As expected, the peak Strouhal number remained unchanged. The calibrated coefficients can be compared with the originals in Table 3-1.

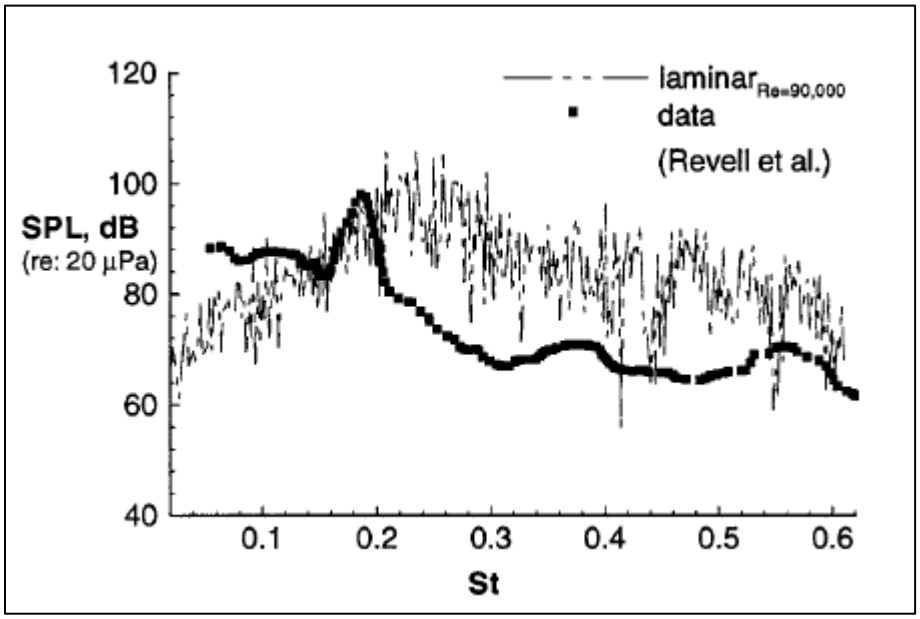

Figure 3-22. Experimental spectrum measurements of the isolated cylinder used to calibrate the initial peak Strouhal number for the cylinder acoustic element. The Microphone is located 128 cylinder diameters away from the mid-span of the cylinder and at a 90^{O} angle to the freestream flow. The laminar predicted data shown in this figure was not used for LGMAP calibration (Ref. 11).

Table 3-1. Cylinder acoustic element coefficients calibrated with experimental data of an isolated cylinder

	e	p	S_0	C_l'	C_d'
Original Calibration	2.5	2.15	0.22	0.17	0.034
Calibrated to Isolated Cylinder	2.5	2.15	0.22	0.01	7.50E-5

First, the calibrations were made by checking the initially polar directivity results and spectrum results with the experimental measurements. The peak Strouhal number would be adjusted first, if it was not already at 0.22. The spectrum shape of the cylinder acoustic element was unaffected by LGMAP's upgrades, so the non-dimensional spectrum shape variables *e* and *p* were unchanged. Next, the lift and drag coefficients were incrementally changed until the predictions matched the experimental results. The ideal coefficients could be calculated analytically, but the effort to do so was time consuming. By knowing the non-dimensional

spectrum of both the drag and lift, it would take many calculations to work backward from the OASPL. The process of changing the coefficients would have to be repeated for the entire landing gear strut. The complexity of the cylinder acoustic element arrangement that makes up the strut assembly makes solving for the coefficients analytically infeasible.

These original calibrations are made to predict noise of an isolated cylinder, not a landing gear strut, so further calibration is required. With the ABWheel model in place, the strut cylinders can be calibrated accurately with experimental results. Research has shown that the ANOPP Fink method compares well with a 6.3% scaled Boeing 777 main landing gear model experiment performed at the NASA Langley Quiet Flow Facility (QFF) (Ref. 7). The geometry model used in the calibration can be viewed in Figure 3-23 and further detail on the experimental case is provided in detail in Chapter 4. Table A-1in Appendix lists the contents of the entire LGMAP landing gear geometry. Because the ABWheel produces essentially that same noise as ANOPP, this experimental case is used to calibrate the strut cylinders. It should be noted that the ANOPP Fink strut does not produce noise directly below the landing gear which is not the case with LGMAP. A cylinder or a landing gear strut that is not perpendicular to the horizon will produce noise directly below the landing gear. The Fink method wheel model includes the entire landing gear bogey, so the landing gear's truck is not included in the strut prediction. Also, there have been wind tunnel tests on the Boeing 777 main landing gear that show changes to the truck do not affect the resultant noise by any large degree (Ref. 20). With this information, it is assumed that trucks from different landing gear do not vary significantly from each other.

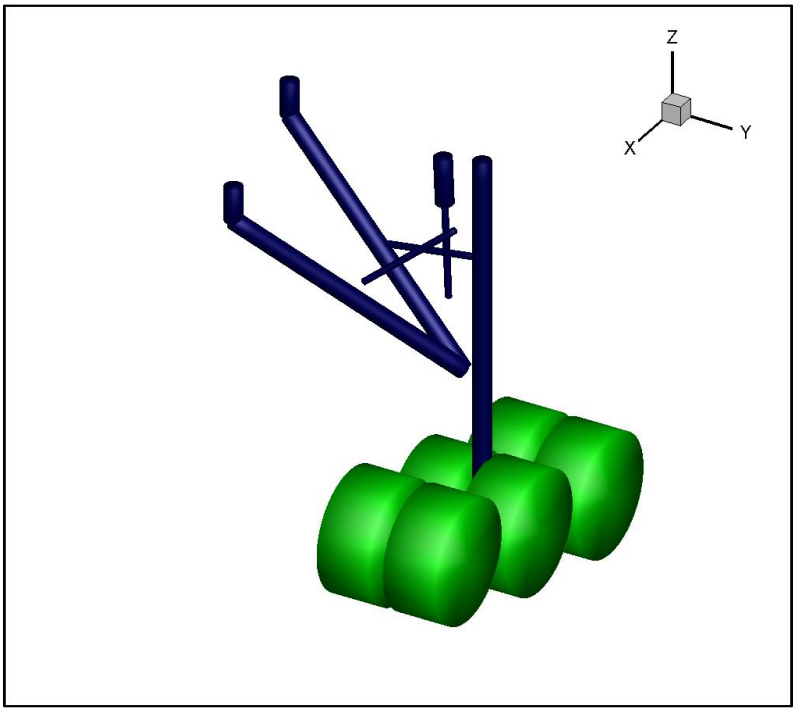

Figure 3-23. LGMAP landing geometry of the 6.3% scaled Boeing 777 main landing gear. The ABwheels acoustic elements are presented in green and the cylinder acoustic elements that comprise the strut assembly is shown in blue.

To begin the calibration, the single observer spectrum results from the experiment were gathered. Two observer locations were available: one is located directly below the model and th other has the polar ANOPP coordinates $\theta_e = 59.3°$, $\phi_e = 51.7°$. Initial predictions were made using the coefficients calibrated to the isolated cylinder. These predictions showed the strut was overpredicting the low frequency noise. The peak Strouhal number and fluctuating drag and lift coefficients were adjusted incrementally until the predictions from both observer locations matched fairly well with the experimental data. There was little effort made to match high frequency noise since the hoses and wires are not included in the LGMAP calibration geometry model. This calibration is for main oleos, support struts, and other large members of a landing gear's strut system. It was unknown if very small parts required different cylinder coefficients or not.

Experimental data of a 6.3% scaled Boeing 777 main landing performed at the NASA Langley QFF provides contour maps at several third octave frequencies (Ref. 20). These results are very useful as they were used to calibrate the directivity, amplitude, and peak Strouhal frequency of the strut cylinder further. Small changes to the coefficients were made to closer match these experimental measurements. The ABwheel produces a majority of the predicted noise and was not adjusted for these calibrations. This limited the ability to match the noise at some observer locations. The resultant calibrated cylinder coefficient can be compared with older versions in Table 3-2.

Table 3-2. Cylinder acoustic element coefficients calibrated with experimental data of QFF 6.3 scaled Boeing 777 main landing gear.

	e	p	S_0	C_l'	C_d'
Calibrated to Isolated Cylinder	2.5	2.15	0.22	0.01	7.50E-5
Calibrated to 6.3% Scaled Boeing 777	2.5	2.15	0.33	2.25E-3	1.69E-5

The directivity of the LGMAP prediction now compares very well with the experiment. Single point observer locations were also analyzed and the LGMAP prediction is close to the experimental and ANOPP predictions (Figure 3-24 through Figure 3-28). The coordinate system used for these figures follows those used in the experiment as seen in Figure 3-29. Notice that the strut noise is much higher in the LGMAP prediction than from ANOPP when the observer is directly below the landing gear. Also the LGMAP prediction's peak Strouhal number is closer to the experimental data than ANOPP. This experimental data was used in the calibration of the previous version of LGMAP, but the directivity did not match as accurately as the new version (Figure 3-30).

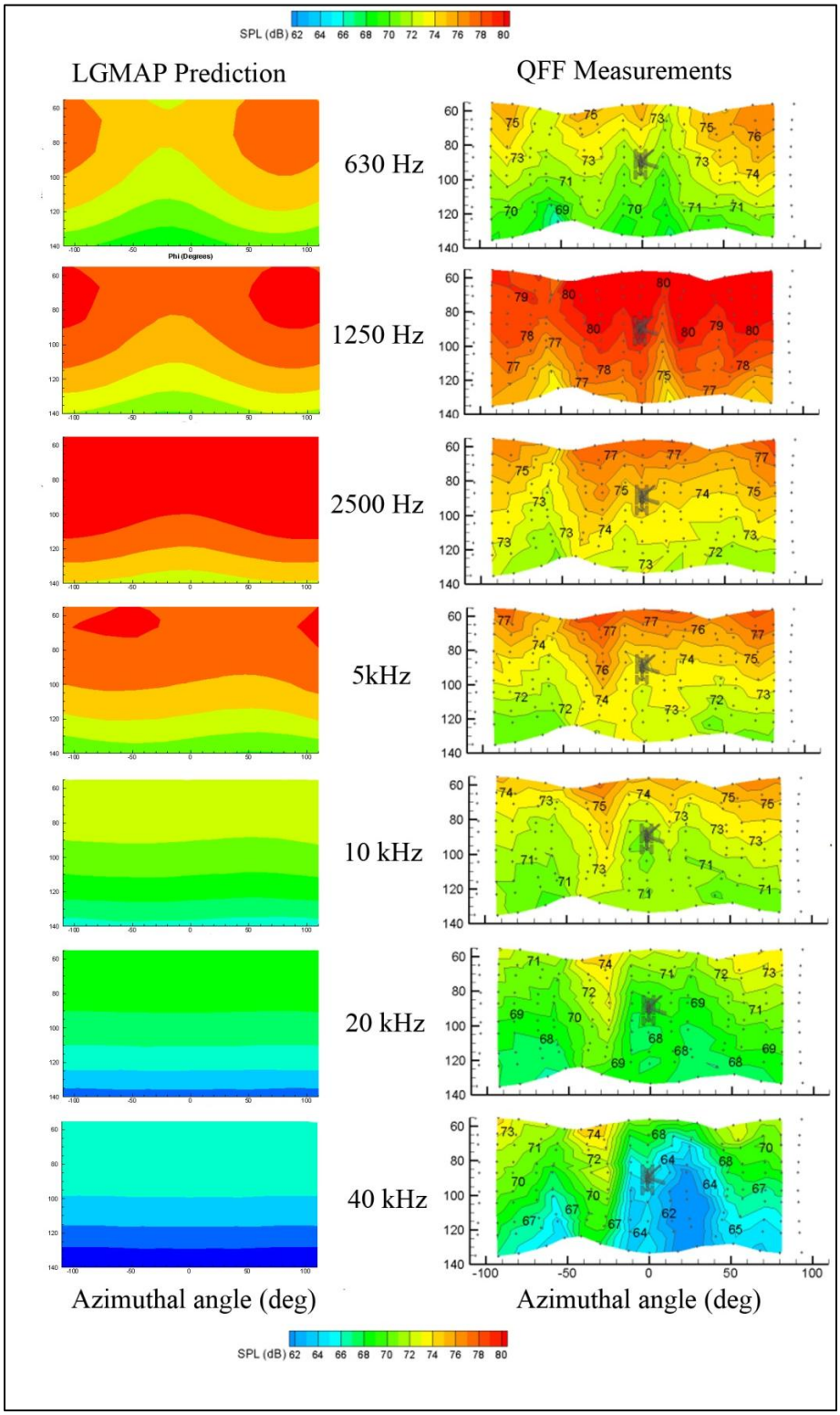

Figure 3-24. Directivity plot of current version of LGMAP predicted noise to measurements from the QFF experiment (Ref. 20). The coordinate system is in the ANOPP form.

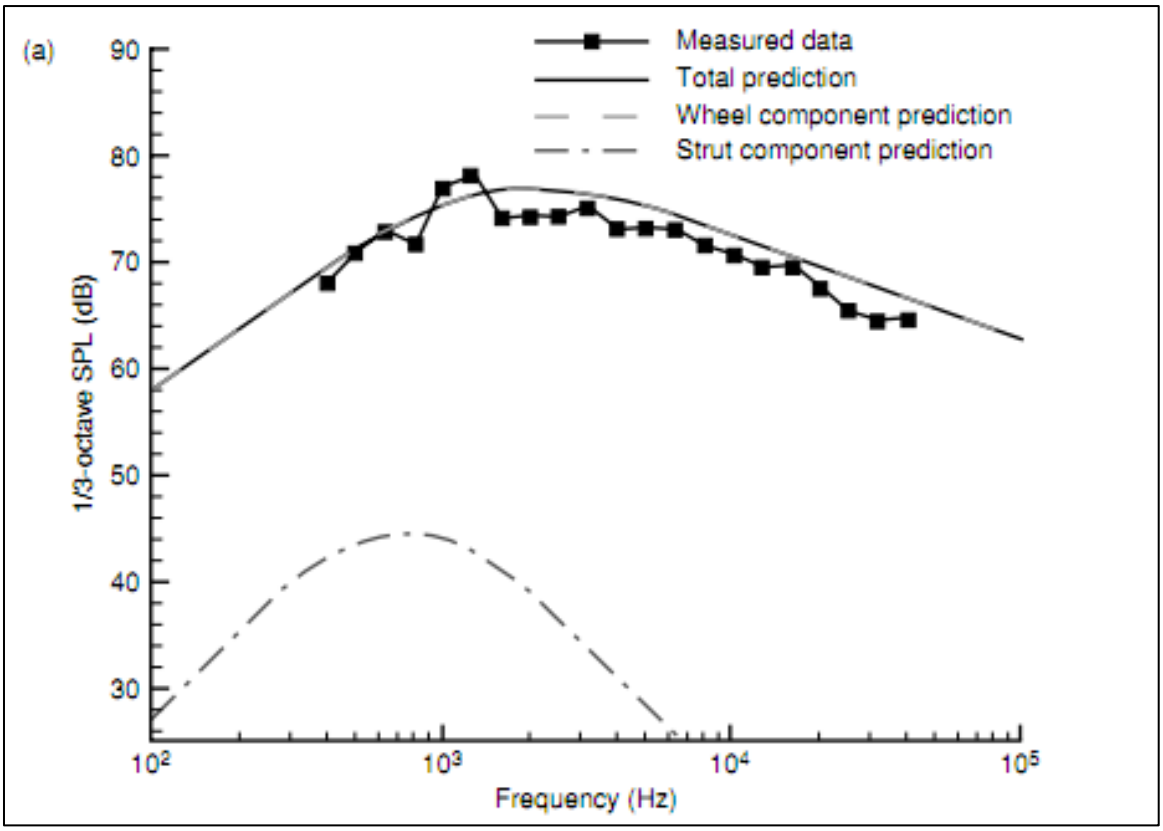

Figure 3-25. ANOPP Fink method predictions for the total and component spectra of a 6.3% scaled Boeing 777 main landing gear compared with measured data. Observer position is at $\boldsymbol{\theta_e = 87.1°}$, $\boldsymbol{\phi_e = 1.0°}$ in ANOPP coordinates (Ref. 7).

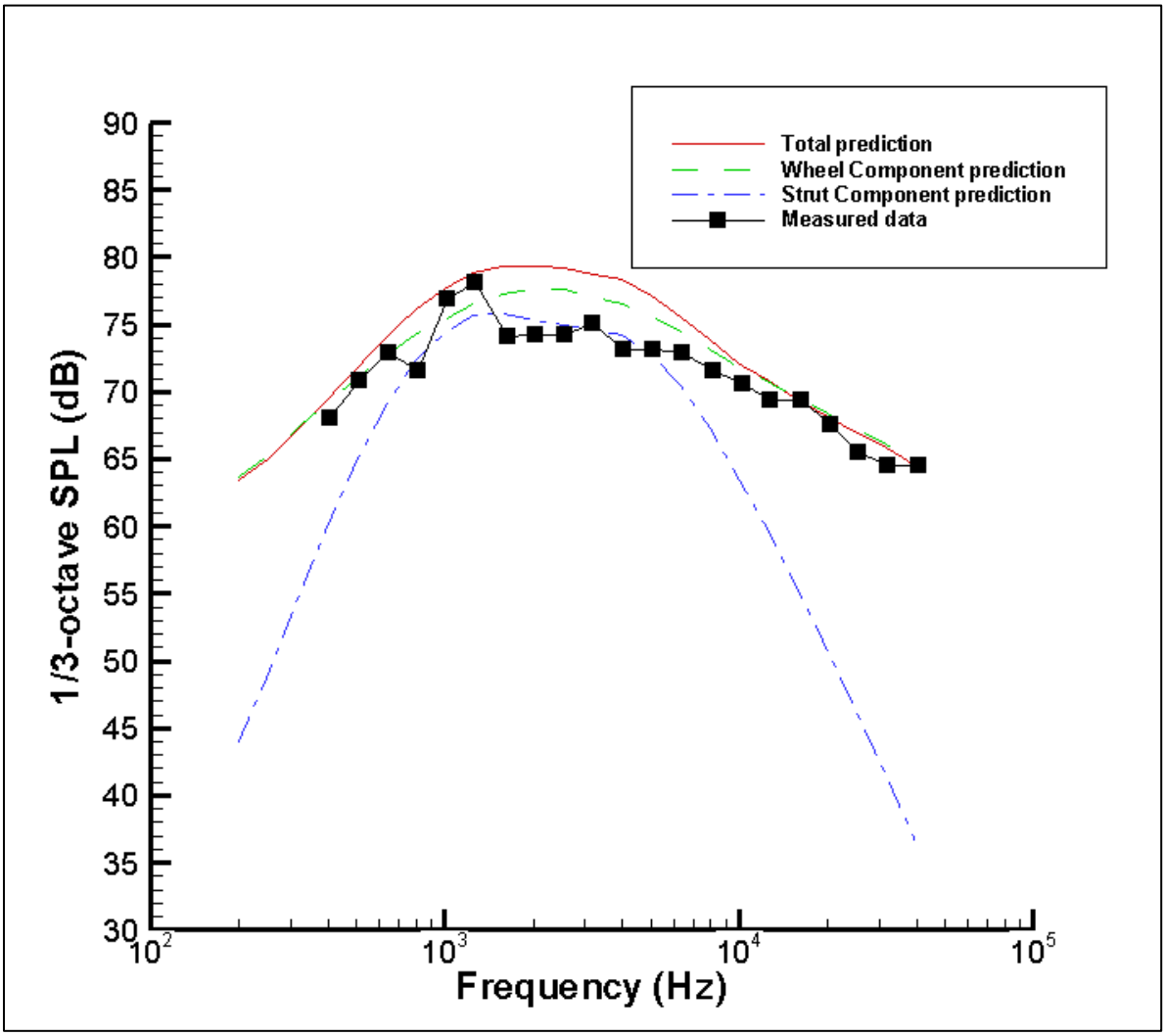

Figure 3-26. LGMAP predictions for the total and component spectra of a 6.3% scaled Boeing 777 main landing gear compared with measured data. Observer position is at $\boldsymbol{\theta_e = 87.1°}$, $\boldsymbol{\phi_e = 1.0°}$ in ANOPP coordinates.

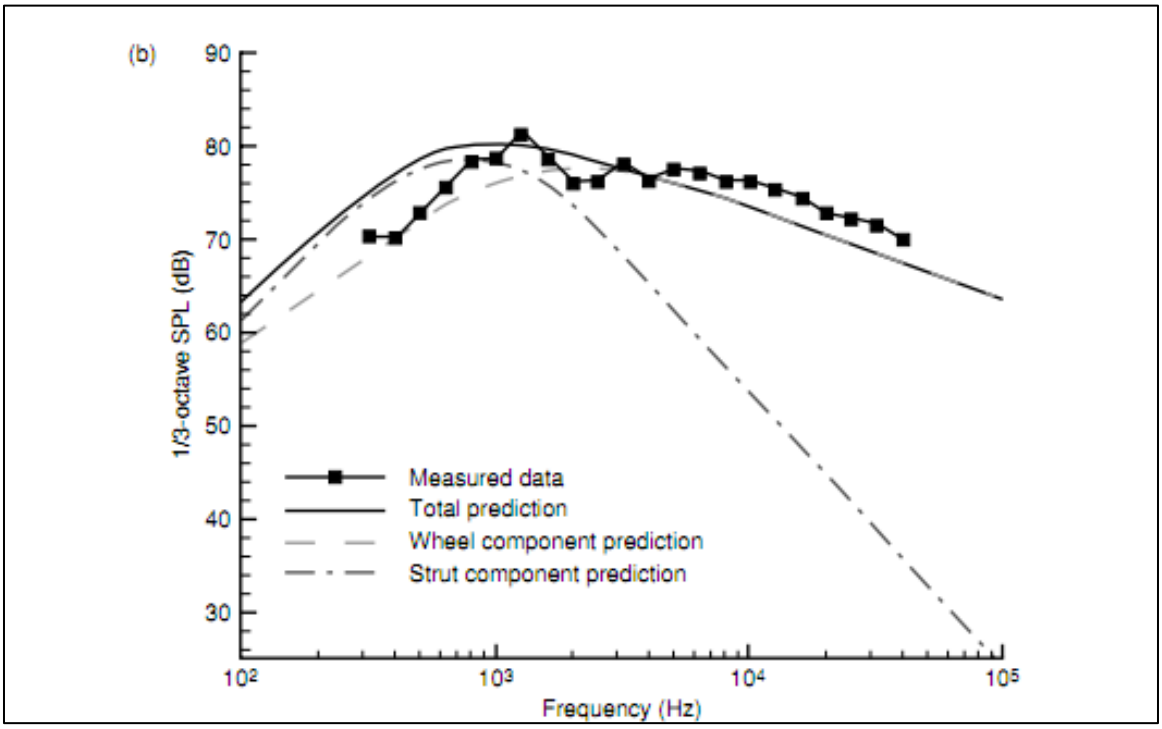

Figure 3-27. ANOPP Fink method predictions for the total and component spectra of a 6.3% scaled Boeing 777 main landing gear compared with measured. Observer position is at $\boldsymbol{\theta_e} = \mathbf{59.3}°$, $\boldsymbol{\phi_e} = \mathbf{51.7}°$ in ANOPP coordinates (Ref. 7).

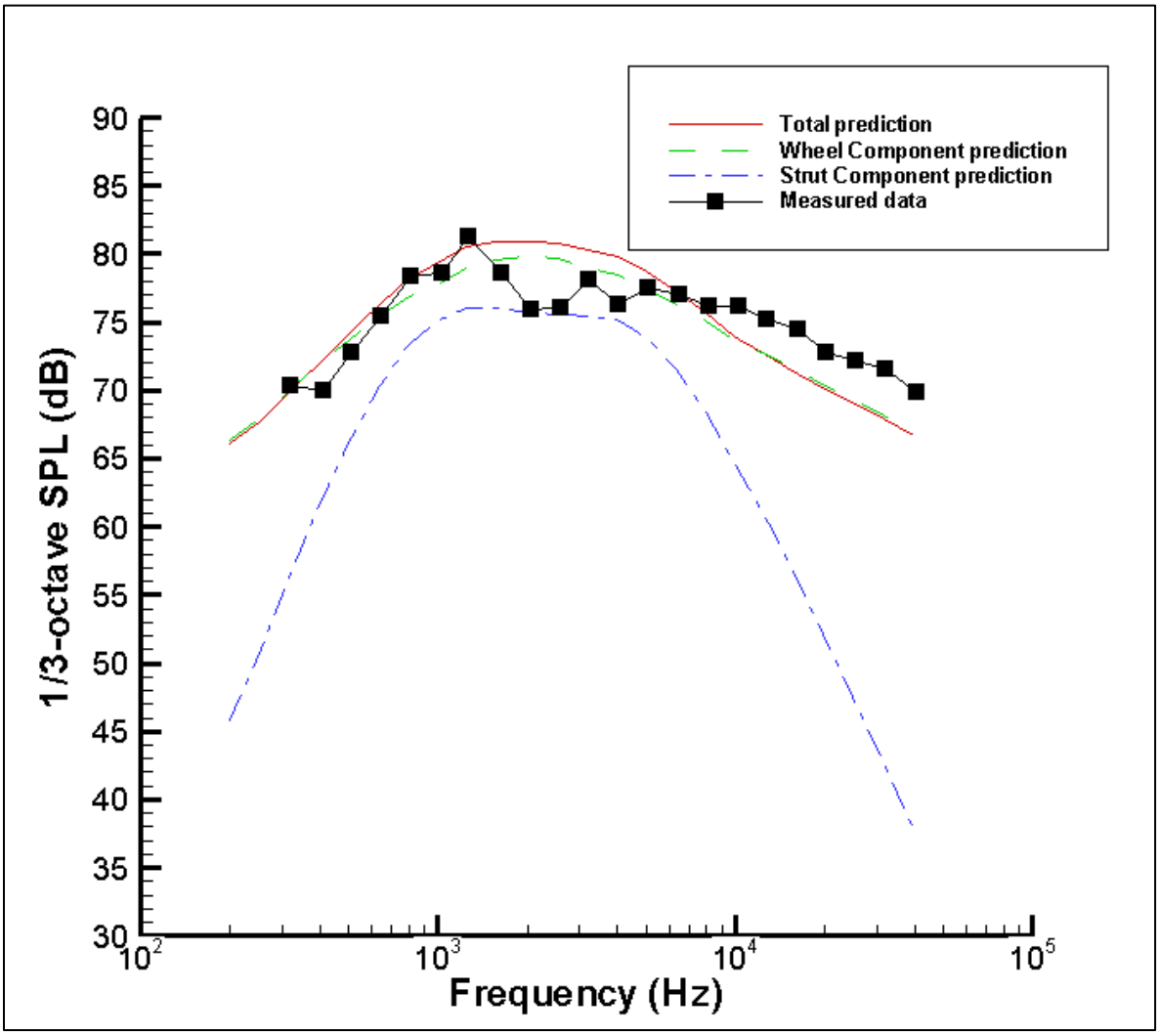

Figure 3-28. LGMAP predictions for the total and component spectra of a 6.3% scaled Boeing 777 main landing gear compared with measured data. Observer position is at $\boldsymbol{\theta_e = 59.3°}$, $\boldsymbol{\phi_e = 51.7°}$ in ANOPP coordinates.

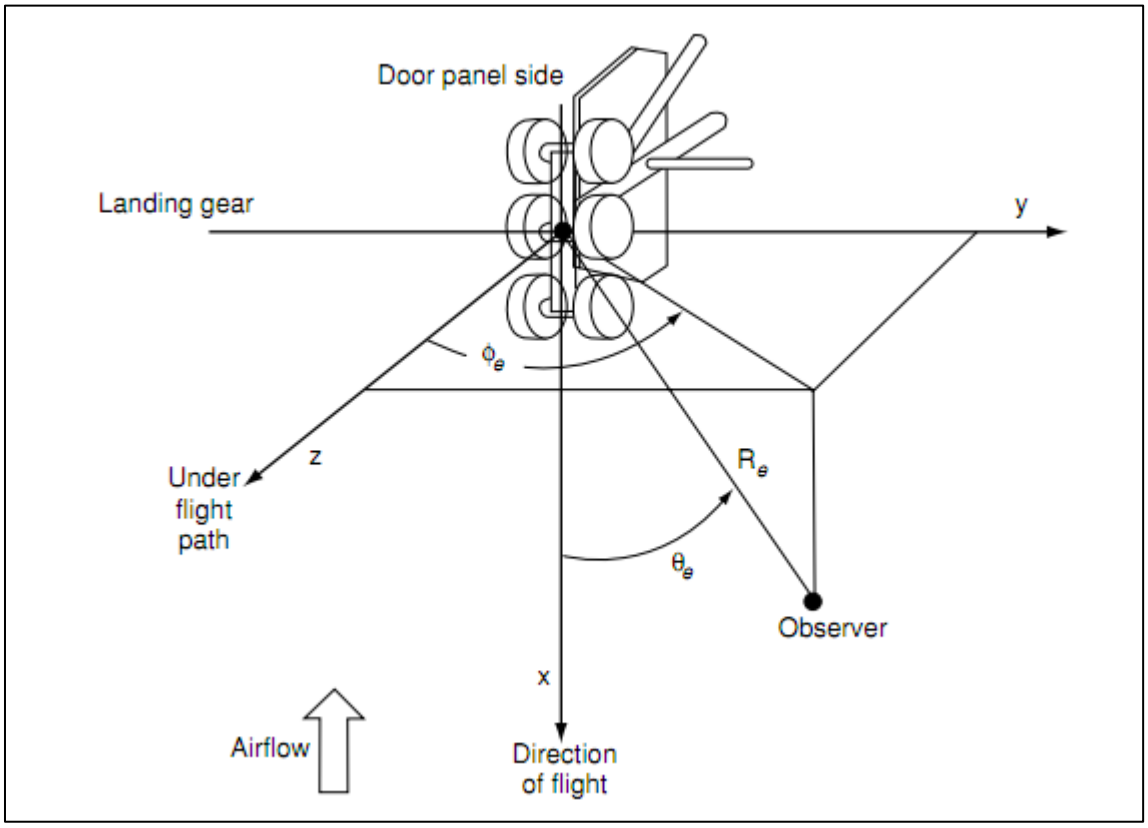

Figure 3-29. Quiet Flow Facility coordinate system for 6.3% scaled Boeing 777 main landing gear (Ref. 20).

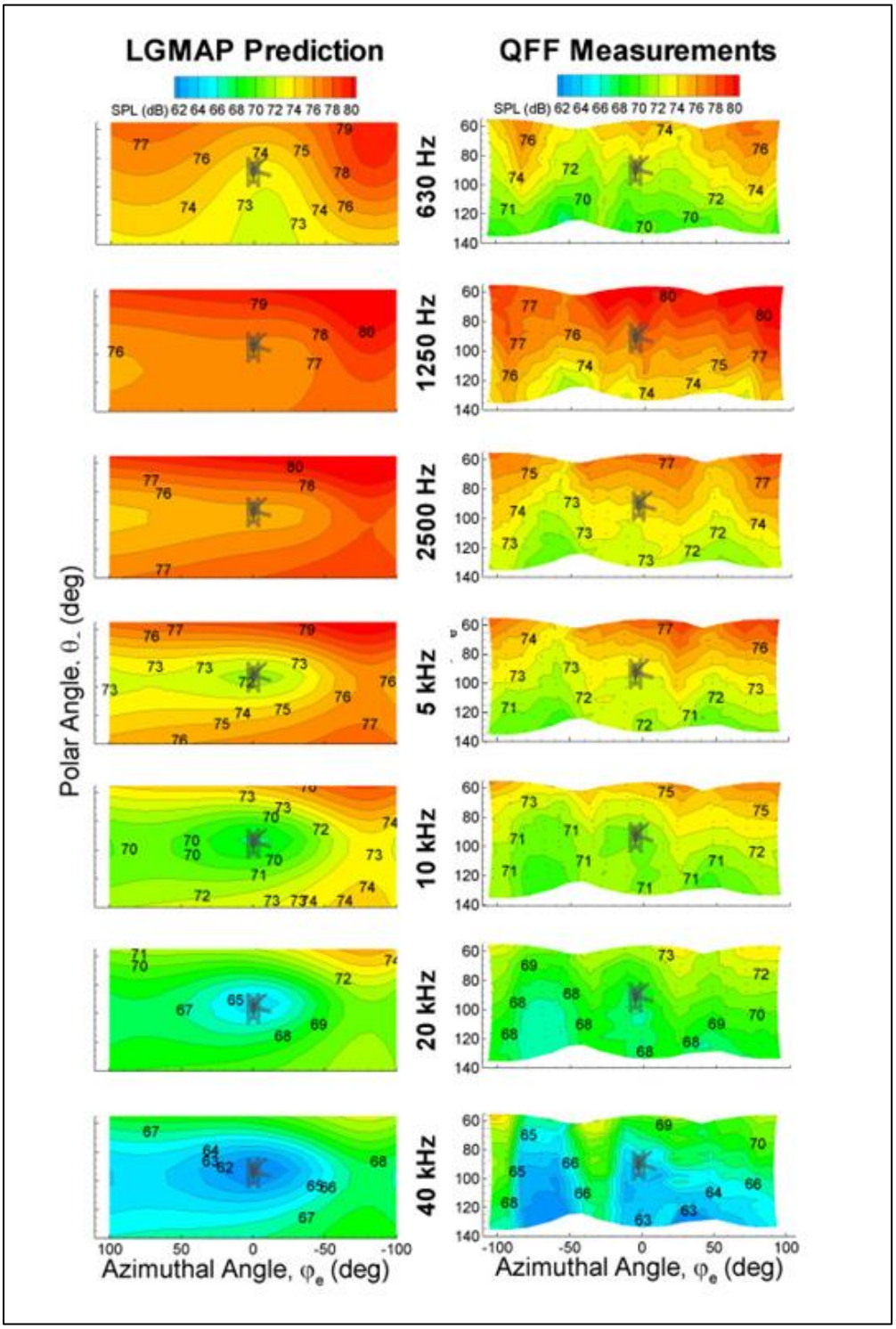

Figure 3-30. Comparison of directivity plot of previous version LGMAP predicted noise and measurements from the QFF experiment. The coordinate system is in the ANOPP form (Ref. 4).

The LGMAP geometry model used for these strut calibrations was constructed by Dr. Leonard Lopes using measurements available to him. This geometry model was rebuilt for reasons discussed in Section 4.1 and the modification that affects the calibration is to the main oleo. For this geometry model, which is presented in Figure 3-31 and Table A-2, measurements from the actual 6.3% scaled wind tunnel model were used whenever possible and the new LGMAP model is considered a better representation than the older one. The cylinder diameters, especially for the oleo, are the correct size. The new diameter sizes change the peak frequency and amplitude of the strut noise prediction. A low fidelity version of the geometry was used calibrated the cylinder coefficients again. The single point observer spectrums are shown in Figure 3-32 and Figure 3-33 and the new coefficients in Table 3-3.

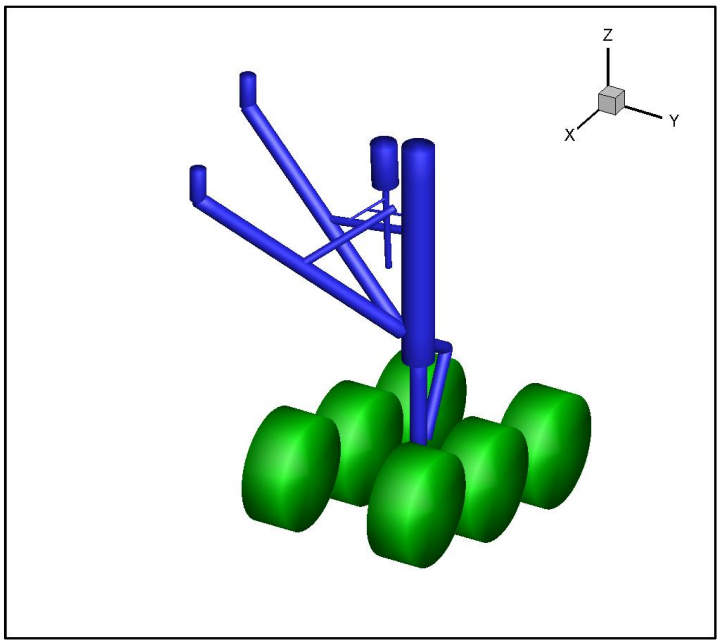

Figure 3-31. Revision of 6.3% scaled Boeing 777 main landing gear. The ABwheel acoustic elements and cylinder acoustic elements are in green and blue respectively.

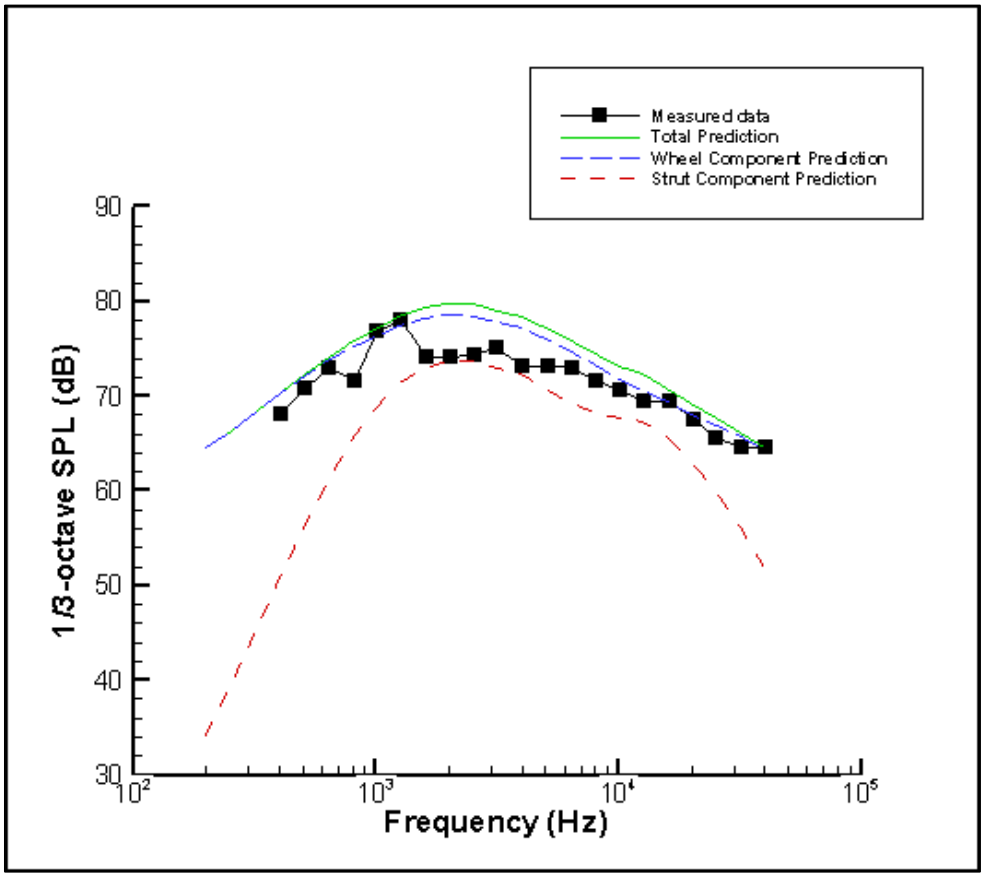

Figure 3-32. LGMAP predictions with recalibrated cylinder coefficients for the total and component spectra of a 6.3% scaled Boeing 777 main landing gear with an updated geometry model compared along with measured data. Observer position is at $\boldsymbol{\theta_e = 87.1°}$, $\boldsymbol{\phi_e = 1.0°}$ in ANOPP coordinates.

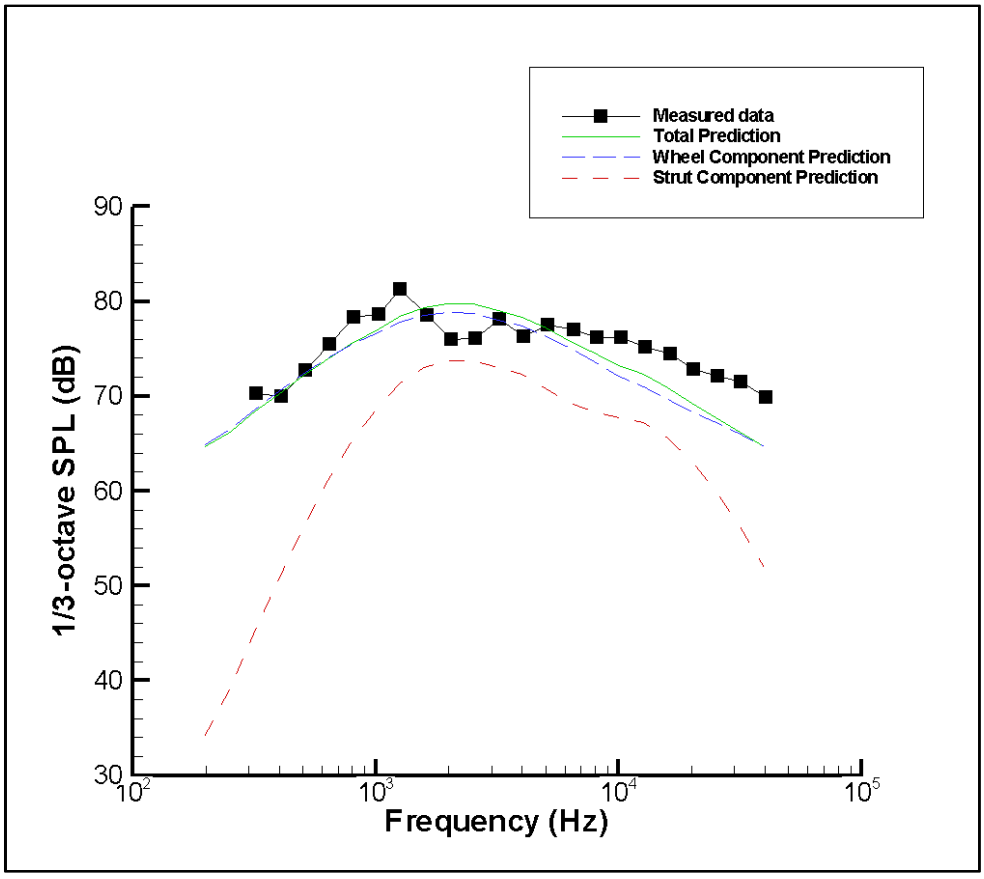

Figure 3-33. LGMAP predictions with recalibrated cylinder coefficients for the total and component spectra of a 6.3% scaled Boeing 777 main landing gear with an updated geometry model compared along with measured data. Observer position is at $\boldsymbol{\theta_e = 59.3°}$, $\boldsymbol{\phi_e = 51.7°}$ in ANOPP coordinates.

Table 3-3. Cylinder acoustic element coefficients calibrated with experimental data of QFF 6.3 scaled Boeing 777 main landing gear employing the new model and comparing to the old model.

	e	p	S_0	C_l'	C_d'
Original Calibration to 6.3% Scaled Boeing 777	2.5	2.15	0.33	2.25E3	1.69E-5
Updated Calibration to 6.3% Scaled Boeing 777	2.5	2.15	0.44	1.80E3	1.35E-5

Now with these enhancements completed, a thorough assessment of LGMAP capabilities could be made. This was the final time LGMAP was calibrated. For future predictions, the

cylinder coefficients remained unchanged. The next chapter compares and analyzes LGMAP predictions with experimental measurements and predictions from other methods.

Chapter 4

Demonstration and Analysis of LGMAP's Capabilities

With the calibration of LGMAP's cylinder acoustic element and new ABwheel acoustic element complete, the validation of the method's prediction capabilities resumed. It is important, especially with the numerous changes to the method, that a thorough analysis is completed. LGMAP is evaluated using three different sets of experimental measurements and two other landing gear noise prediction methods. This chapter is separated into three sections specified by different aspects of the validation. The first compares the LGMAP landing gear geometries built by different users and the resulting noise predictions. This explores the importance of well crafted landing gear geometry representation. The next section details a LGMAP prediction and compares it with other prediction methods along with experimental data. This prediction is blind in the sense that it did not involve the calibration data and the geometry was not altered after any comparisons with the other results were made. The final section investigates the capability of LGMAP map as a tool to identify specific noise sources of a landing gear. Different components of the landing gear are isolated and the results are compared with phased array measurements.

4.1 Geometry Creation Technique Study

Prior to this work, the use of LGMAP has been limited to its creator. Since the representation of strut members as cylinders brings many geometry approximations, especially regarding the cylinder diameter, geometries created by different users may not compare and the resultant noise prediction could be unacceptably different. LGMAP is intended to be used by

many users, so it is imperative that possible different geometry techniques be investigated and studied. The geometry for the 6.3% Boeing 777 main landing gear was chosen for this test because it is the most detailed landing gear geometry available. It contains a complex assortment of hydraulic hoses, cables, and wires along with several horizontal struts which allows many landing gear design features to compare with.

4.1.1 Description of 6.3% Scaled Boeing 777Main Landing Gear Experiment

At NASA Langley's Quiet Flow Facility wind tunnel (QFF), a highly detailed 6.3%-scaled Boeing 777 main landing gear (Figure 4-1) was studied extensively using a 41-microphone directional array system positioned at many different observer angles (Ref. 20). The goal of these experiments was to provide a database of both individual microphone and Deconvolution Approach for the Mapping of Acoustic Sources (DAMAS) derived measurements for validation of landing gear noise prediction models.

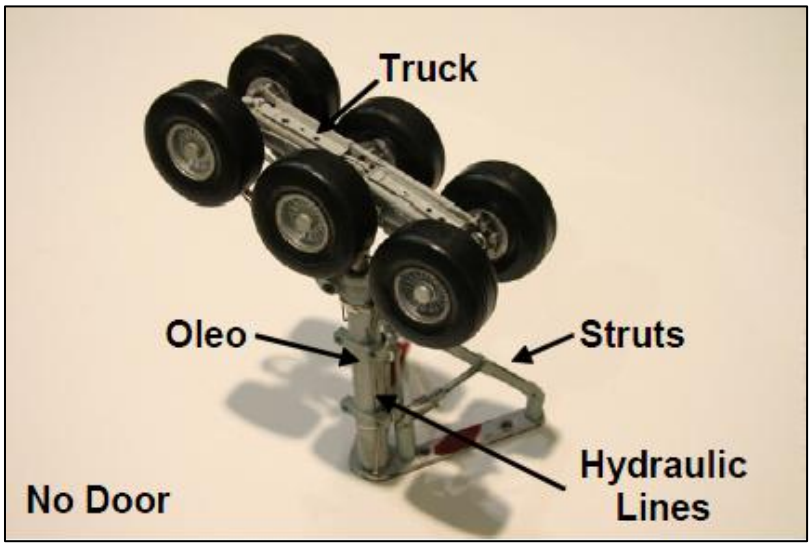

Figure 4-1. 6.3% scaled Boeing main landing gear tested at QFF. This model is the baseline without the landing gear door. This configuration was used when possible when compared with LGMAP (Ref. 20).

The scaled model is very detailed in order to represent the complexity of the actual landing gear faithfully and thus the resultant noise. Electrical wiring and pressure tubing was used to model hydraulic lines and cables (Figure 4-2). The diameter of the electrical wiring and pressure tubes are three times larger than the actual landing gear parts they represent. This aspect is important when modeling the LGMAP landing gear geometry because the diameter affects the amplitude and peak frequency of the noise. Four different configurations of the model were evaluated experimentally, so the effectiveness of different noise treatment could be investigated. Only the baseline and the baseline without the door are used for LGMAP's validation. The baseline without the landing gear door is a favorable model to compare predictions with since LGMAP lacks a door acoustic model. However, data was only available in contour plots at limited 1/3 octave frequency bands. A single point observer 1/3 octave spectrum that was compared with LGMAP comes from the baseline model.

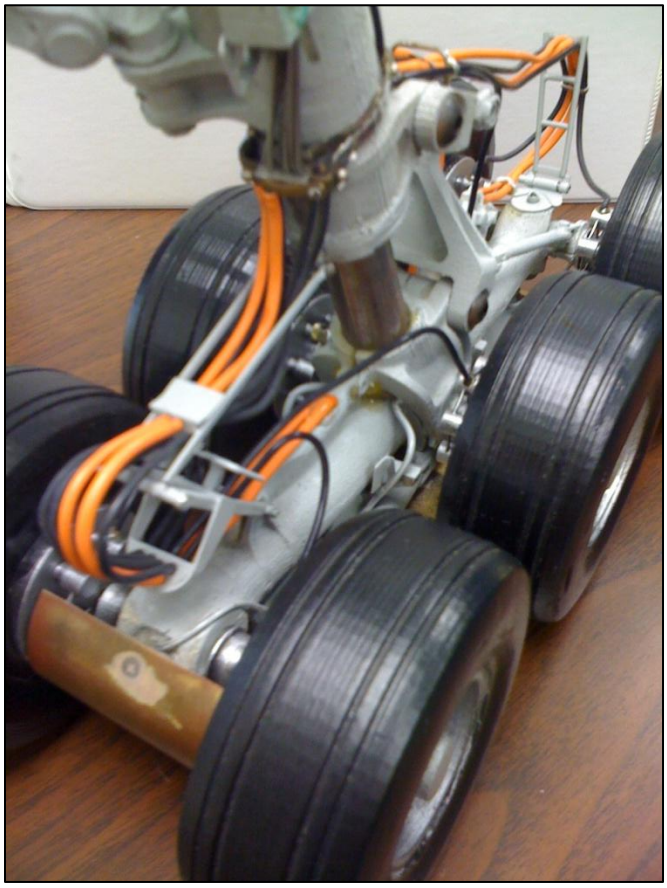

Figure 4-2. Detail of the 6.3% scaled model's electrical wiring used to represent hydraulic lines.

4.1.2 LGMAP Calibration Case Landing Gear Geometry

A high fidelity geometry created by Dr. Lopes (Figure 4-3) was made using available reference data. He did not have the scaled model available to him, so he had to make do with references for the real landing gear. As presented in Figure 4-3, there are three distinct features of his landing gear geometry: the wheel, strut assembly, and the hydraulic hoses and cables, which include the supports for the hoses and cables. Originally, the truck and brake assemblies were included, but with the inclusion of the ABWheel, these componentes are already included in the wheel prediction. In fact, if added, the truck and brakes (Figure 4-4) would have a detrimental effect to the total strut noise prediction (Figure 4-5). The truck has little impact on

the noise, but the brakes themselves do. They produce almost as much noise as the rest of the strut assembly.

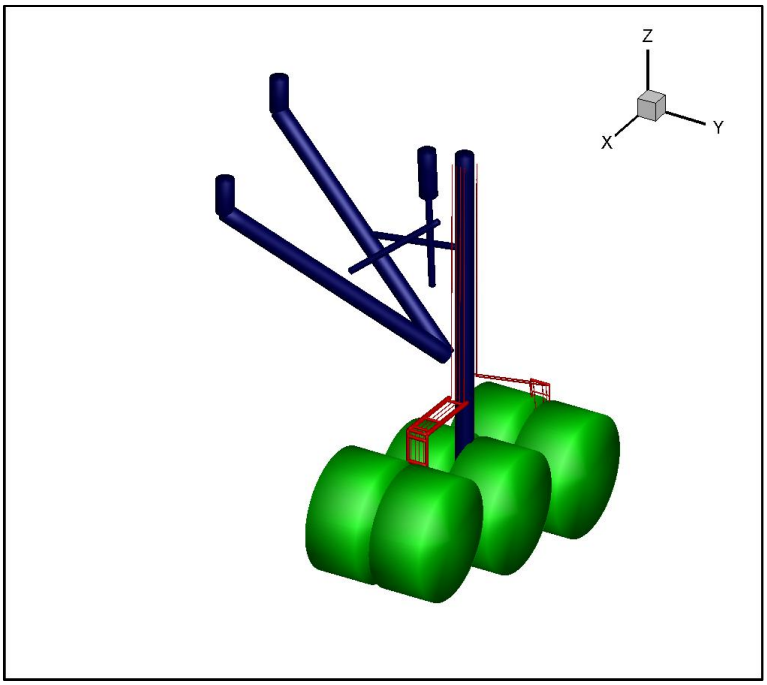

Figure 4-3. The high fidelity LGMAP geometry representation of the 6.3% scaled Boeing 777 main landing gear by Dr. Leonard Lopes. The ABwheels, struts, and high frequency components, which include the hydraulic hoses, lines, and cables, are presented in green, blue, and red respectively. Note the small cylinder acoustic elements representing cables and hoses along the main oleo.

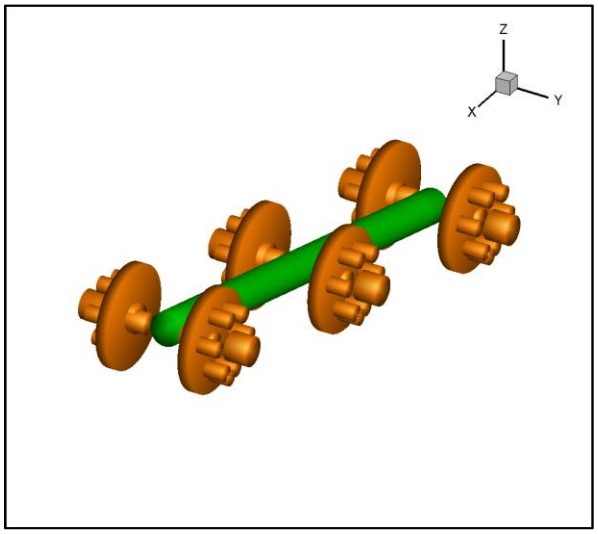

Figure 4-4. LGMAP landing gear geometry of the truck (green) and brakes (orange). The ABwheel includes these features in its prediction.

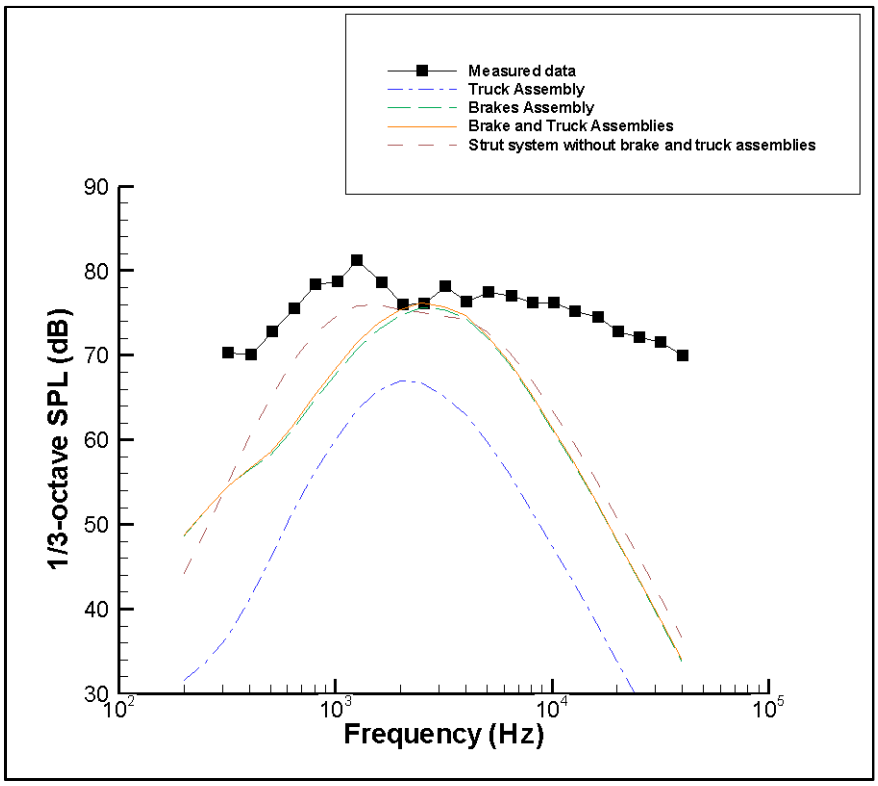

Figure 4-5. Prediction breakdown featuring the truck and brakes components. Observer position is at $\boldsymbol{\theta_e = 59.3°}$, $\boldsymbol{\phi_e = 51.7°}$ in ANOPP coordinates. When included, the brake and truck assemblies have a contributing noise addition to the strut system prediction. Including these features with the ABWheel has a negative effect on the noise prediction.

When redesigning the LGMAP geometry from scratch, the goal was to represent the scaled model, not the full scale production landing gear. Images of the scaled model, such as Figure 4-2, information from research articles (Ref. 21), and references of the real life landing gear when need, such as Figure 4-6, were used in collaboration to produce a new geometry. The pixel counting software DataThief (Ref. 22) was used to produce landing gear geometry coordinates from the images. Certain features, such as the wheels, were used as scaled references so that the dimensions of other landing features could be determined.

Figure 4-6. Boeing 777 main landing gear at touchdown. The image was used within conjunction of other resources to produce a LGMAP geometry of the 6.3% scaled model (Ref. 23).

Representing the smaller details such as the hoses and cables proved to be a challenge. Having the hoses and cables bend accurately is very important. A cylinder acoustic element that is perpendicular to the flow produces significantly more noise than one which is parallel. Also

unlike the original model, the hoses and cables along the oleo were not included. Physically, these are flush with the oleo and the flow around them is greatly influenced by the much larger oleo. Any sound that they do produce would also be shielded by the oleo. In the new model, those physical components are considered part of the main oleo. If these particular hoses and cables were included, they would be treated as small diameter long isolated cylinders producing large amounts of high frequency noise by the LGMAP method.

The new LGMAP model, as presented in Figure 4-7, differs visually from the original. The most noticeable differences are the diameter of the main oleo, size and location of the hydraulic hoses and cables, addition of the torsion arm, and the location of the wheels. The support strut remained unchanged, except for the addition of the locking hydraulics. Both geometry coordinates can be found in Appendix as Tables A-3 and A-4.

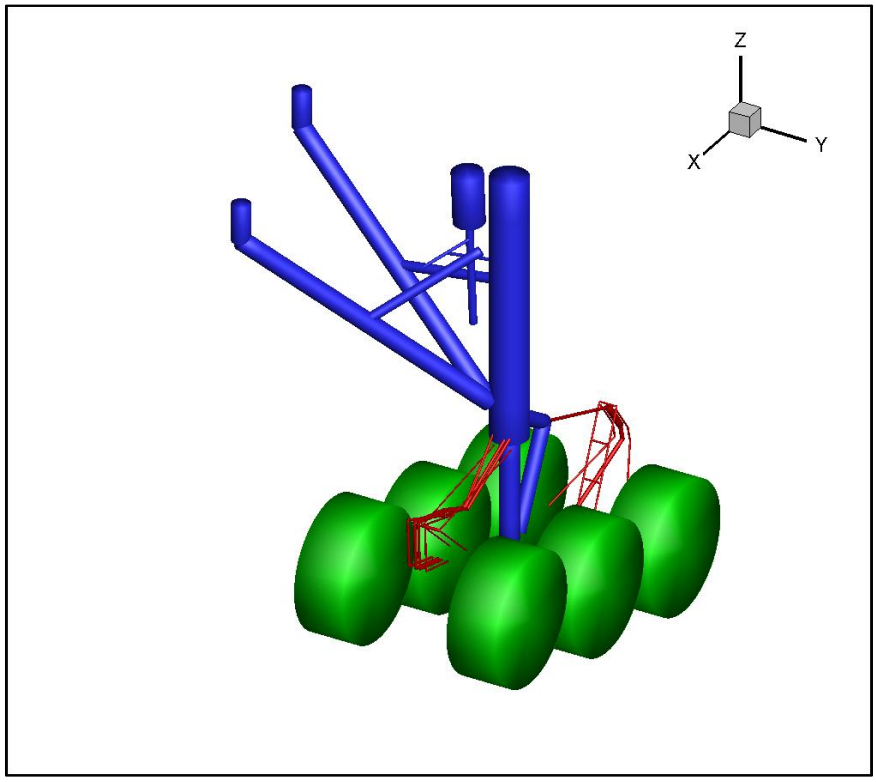

Figure 4-7. The revision of the high fidelity LGMAP geometry representation of the 6.3% scaled Boeing 777 main landing. The ABwheels, struts, and high frequency components, which include the hydraulic hoses, lines, and cables, are presented in green, blue, and red respectively.

4.1.3 Preliminary Analysis of Original Results

Before the two geometries are compared, a detailed look at the older model is conducted, since the high fidelity version was not investigated with the updated LGMAP method. With cylinder scaling corrected, it was presumed and demonstrated (Figure 3-8) that the original predictions greatly over predict the noise in the high frequency range. Further analysis shows that the source of this over prediction is the hoses and cables along the oleo (Figure 4-8). The addition of the oleo wires accounts of about a 10 dB increase at its peak. It is the single largest noise source of the entire landing gear features. The LGMAP representation is inaccurate in this model because of the flow and shielding interaction between these hoses and cables and the oleo.

In the future, it is imperative that interactions such as these be considered in the LGMAP geometry creation process.

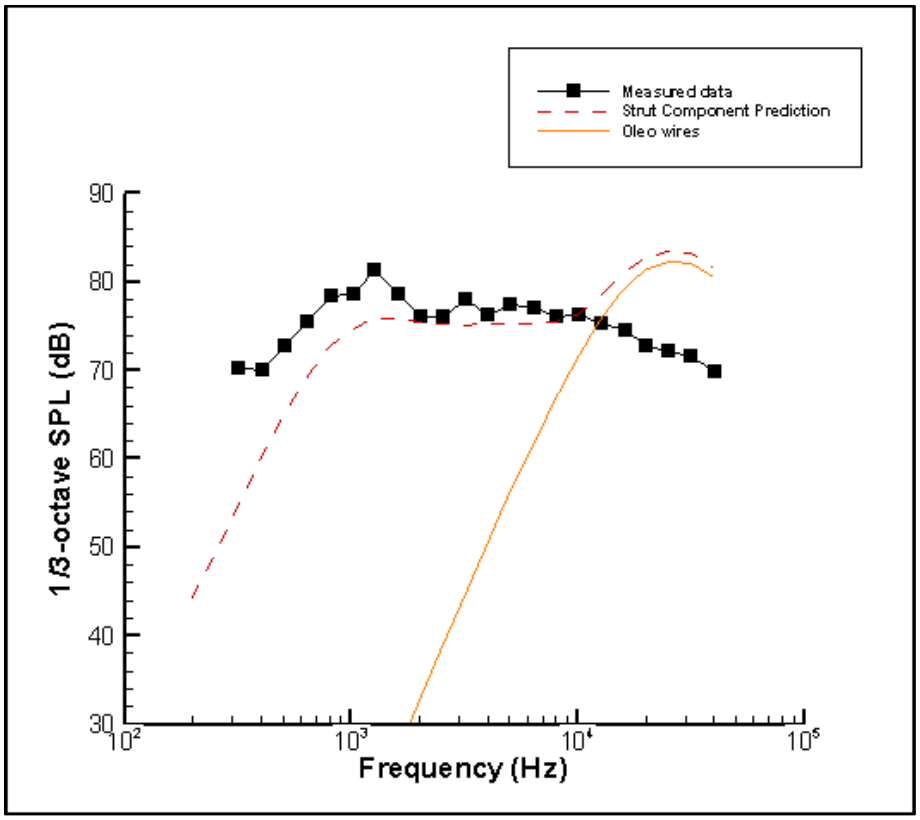

Figure 4-8. 6.3% scaled Boeing 777 main landing gear prediction featuring high fidelity component adjacent to the main oleo and its effect on the total strut component noise. Observer position is at $\boldsymbol{\theta_e = 59.3°}$, $\boldsymbol{\phi_e = 51.7°}$ in ANOPP coordinates.

4.1.4 Comparison of the Two Geometry Results

When comparing the results of the two detailed landing gear geometries (Figure 4-9 and Figure 4-10), the newer model is much more accurate in both mid and high frequency ranges. The prediction with the observer close to the location which is directly below the model (Figure

4-10), overpredicts the noise when both models are used. The larger diameter cables and wires, along with the lack of acoustic cylinders representing the cables and wires along the oleo, have a large impact in the high frequency noise prediction. This shows the importance of having an accurate reference when creating the landing gear geometry. Images of the 6.3% scaled model and detail of the size of the components that help build the geometry model also produce a better noise prediction.

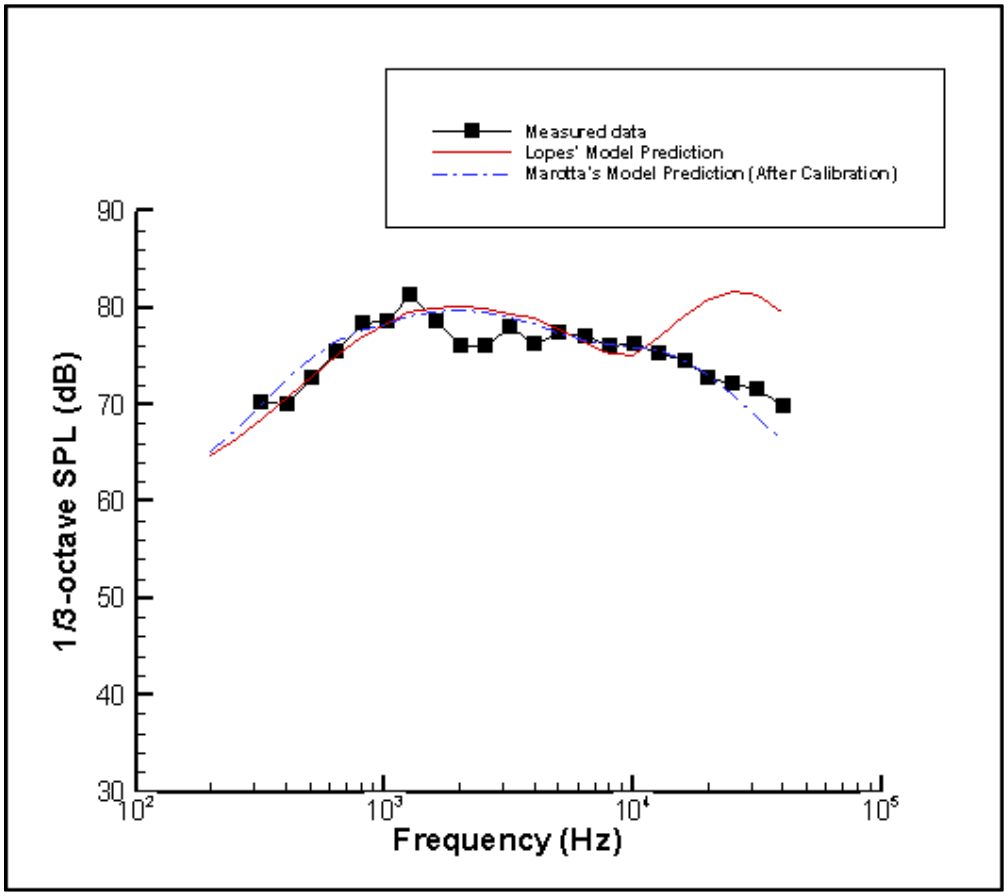

Figure 4-9. LGMAP predictions of a 6.3% scaled Boeing 777 main landing gear with an updated geometry model compared with Lope's model along with measured data. Observer position is at $\boldsymbol{\theta_e = 59.3°}$, $\boldsymbol{\phi_e = 51.7°}$ in ANOPP coordinates.

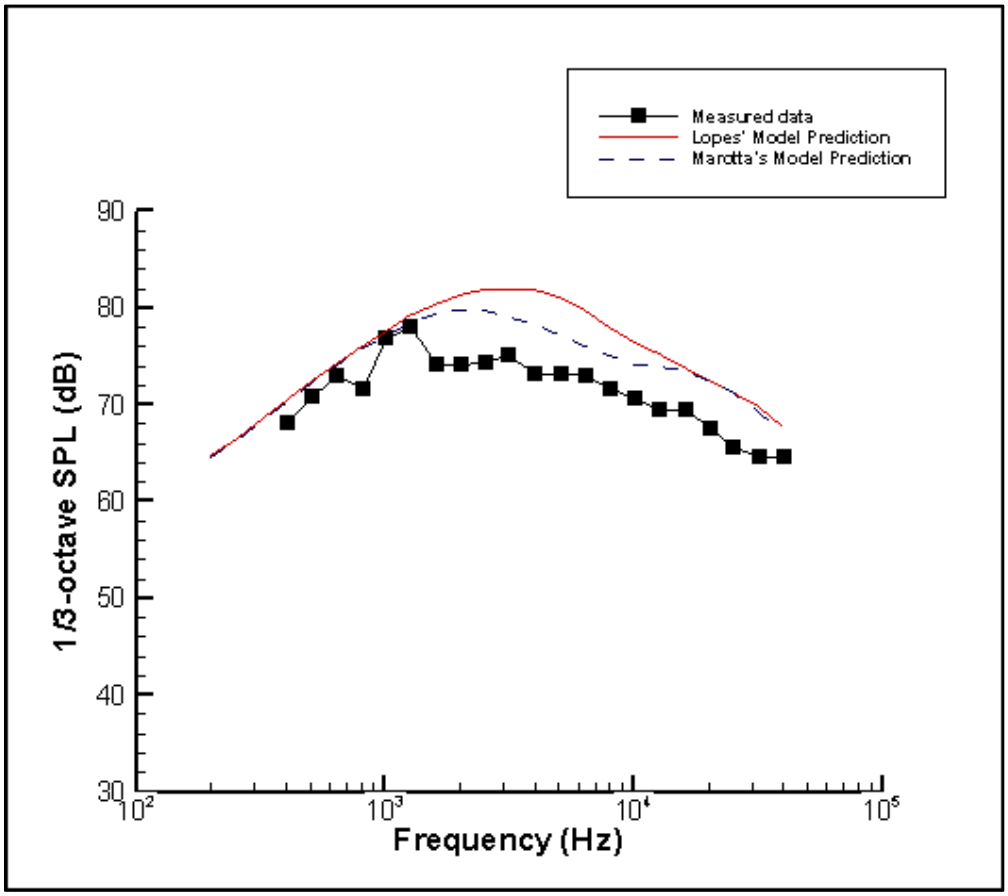

Figure 4-10. LGMAP predictions of a 6.3% scaled Boeing 777 main landing gear with an updated geometry model compared with Lope's model along with measured data. Observer position is at $\boldsymbol{\theta_e = 87.1°}$, $\boldsymbol{\phi_e = 1.0°}$ in ANOPP coordinates.

By separating the hydraulic hoses and cables along with their supports, one can see their contribution to the high frequency noise. As presented in Figure 4-11 and Figure 4-12, these components are the sole source of the high frequency noise. Observing a contour plot of the aircraft's flyover path using the observer criteria in Figure 3-24, the results presented in Figure 4-13 are less dramatic. The difference is the directivity the high fidelity components to the landing gear add to the high frequency plots. Though the prediction is higher than the experimental results in most areas, the shape of the contour is closer than that from those in Figure 3-24.

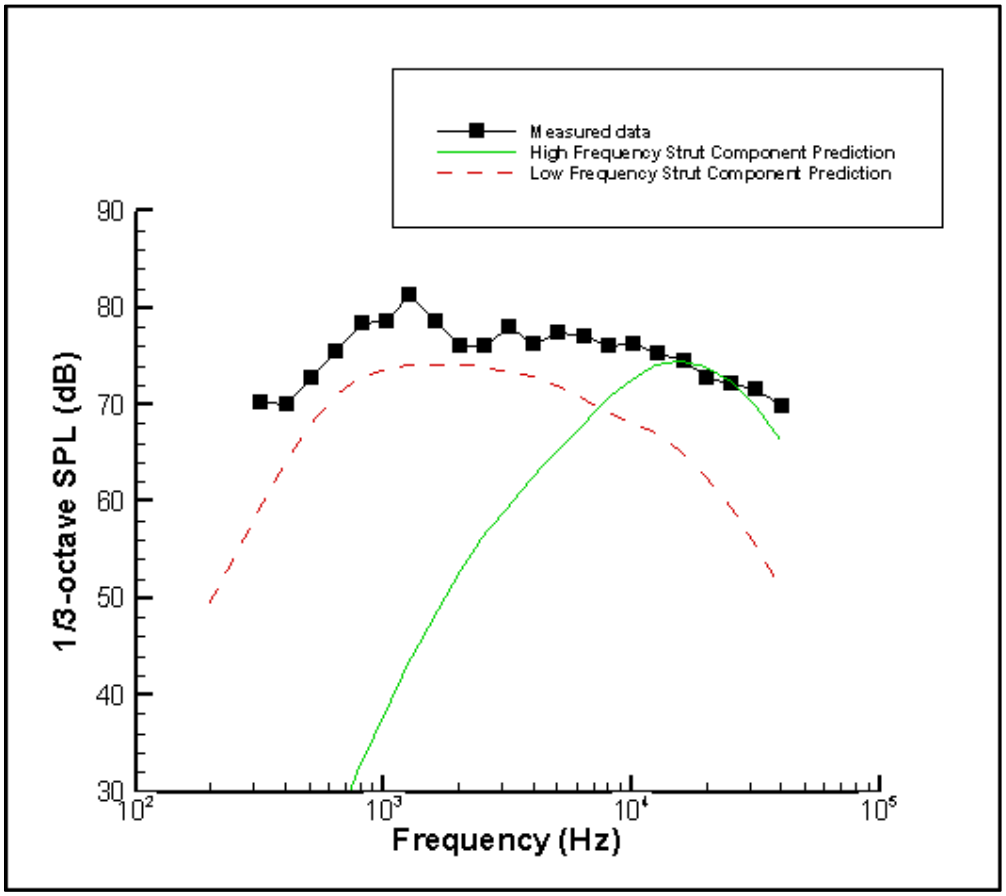

Figure 4-11. LGMAP strut predictions of a 6.3% scaled Boeing 777 main landing gear with an updated geometry model compared along with measured data. The strut is separated by low and high frequency components. Observer position is at $\boldsymbol{\theta_e = 59.3°}$, $\boldsymbol{\phi_e = 51.7°}$ in ANOPP coordinates.

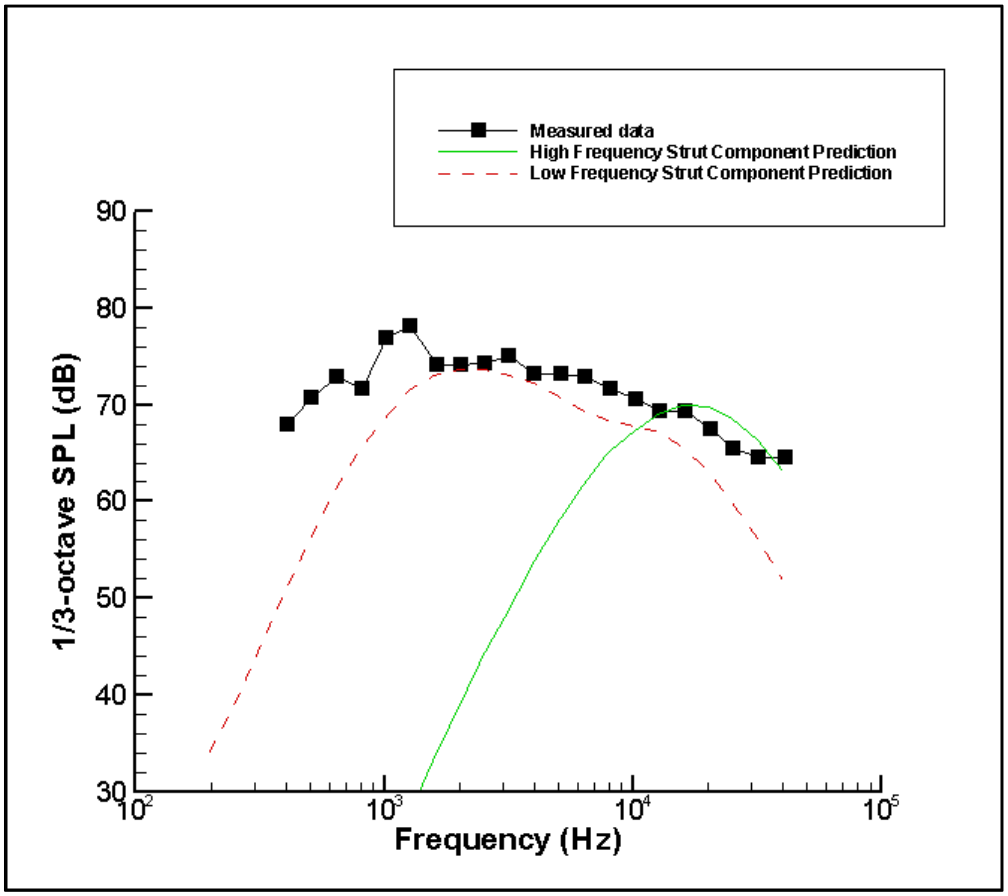

Figure 4-12. LGMAP strut predictions of a 6.3% scaled Boeing 777 main landing gear with an updated geometry model compared along with measured data. The strut is separated by low and high frequency components. Observer position is at $\boldsymbol{\theta_e = 87.1°}$, $\boldsymbol{\phi_e = 1.0°}$ in ANOPP coordinates.coordinates.

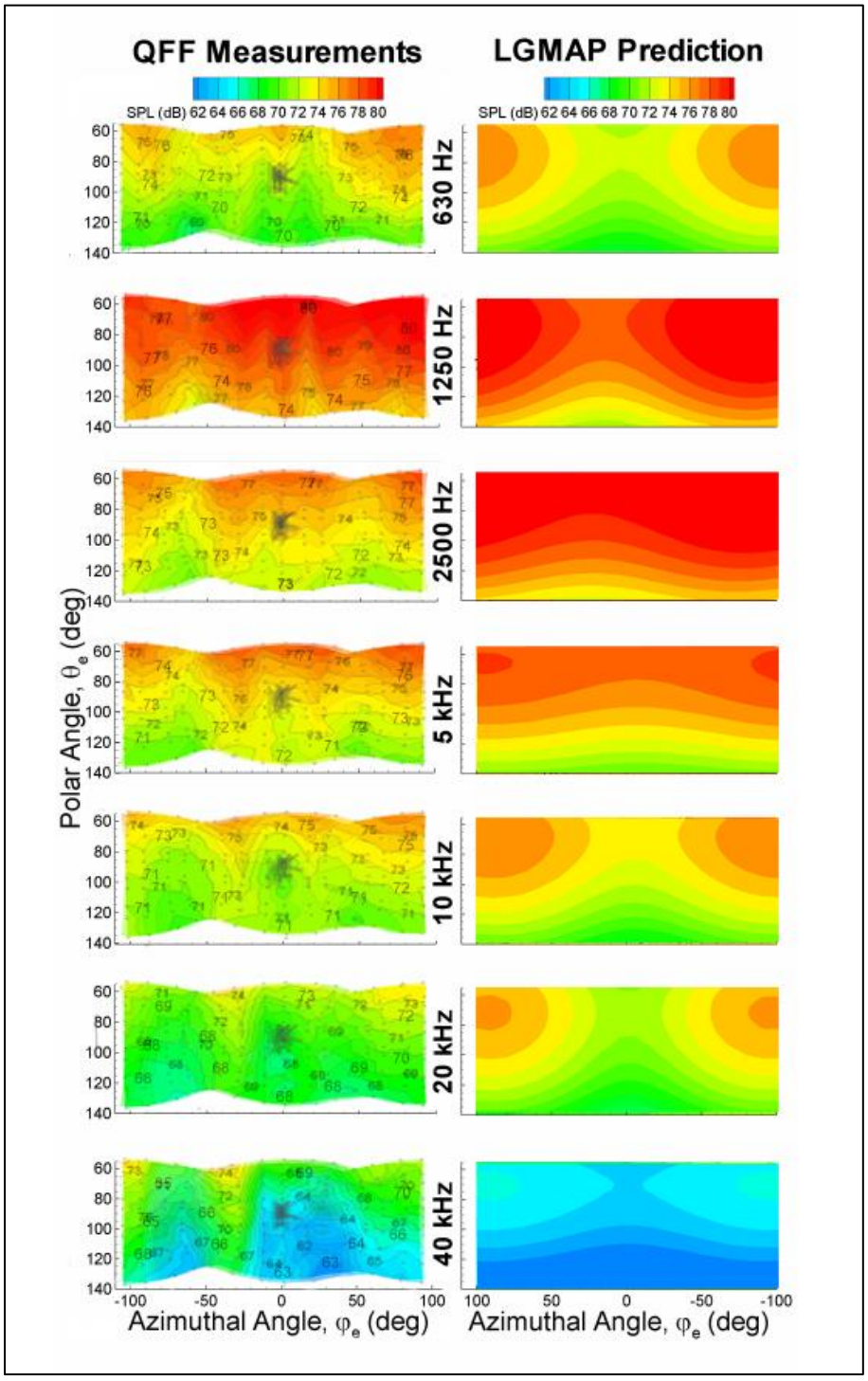

Figure 4-13. Directivity plot of LGMAP predicted noise to measurements from the QFF experiment (Ref. 20). The landing gear geometry in this prediction is of the new 777 main landing gear geometry. The angle coordinates are in the ANOPP form.

4.2 Blind Landing Gear Prediction

After LGMAP's conversion from time based calculations to frequency based, the scheme had not been validated with a landing gear case not used in the calibration. Doing a blind test will show LGMAP's capability as a landing gear prediction method. The experimental data chosen is the full scale Boeing 737 main landing gear tested at Boeing's Low Speed Aeroacoustic Facility (LSAF). The availability of data for a single point observer from several locations along with prediction made using both Fink and Guo prediction methods make this experiment a reasonable candidate to validate LGMAP's prediction method.

4.2.1 Description of experiment

A full scale Boeing 737 main landing gear's noise levels were tested at Boeing's LSAF in order to build a database that includes a range of mean flow Mach numbers and different model configurations (Ref. 6). Unlike the QFF Boeing 777 test, wires, hoses, and cables were removed in certain cases to determine their effects on generated noise. These two configurations are known as "dirty" (with wires, hoses and cables) and "clean". Most of the available results are with the "dirty" configuration. One of the goals of these experiments was to use the data gained to build the foundation of the empirical values for the Guo method. The addition and removal of high frequency noise sources allowed the formulation of the different frequency bands that the method requires for the noise spectrum buildup.

The data acquisition set up for these experiments included individual microphones and a phased array. The array was placed to the side and directly below the model. The individual

microphones were placed along the simulated flight path 117 in. below the wind tunnel centerline. Because the microphones are located very close the model, the atmospheric absorption correction is small.

4.2.2 Geometry Creation

The geometry creation for this landing gear was difficult since the geometrical description of the geometry available was much less precise than that of the 6.3% scaled Boeing 777 main landing gear. Though several images and dimensions are available in "Experimental Study on Aircraft Landing Gear Noise" (Ref. 6), the models tested included alterations to the original landing gear design. The number of and size of the wheels were altered for different test configurations. It is unclear which wheel size configuration is the representation of the real landing gear. Also from the images available, some details appear to differ from the actual landing gear. These include hydraulic hoses, cables, electrical wires, and the exclusion of the landing gear door.

Since details of the geometry of the test model are limited, a geometry based on the actual landing gear was created as a starting point. The resources used in the geometry creation included technical photos (Ref. 24) and photographs of the landing gear (Ref. 21) The information available was sufficient in creating an accurate geometry model of the real landing gear and, with that model completed, a geometry model that best represented the test model was created. This geometry is presented in Figure 4-14 with geometry coordinates given in Apendix A as Table A-5.

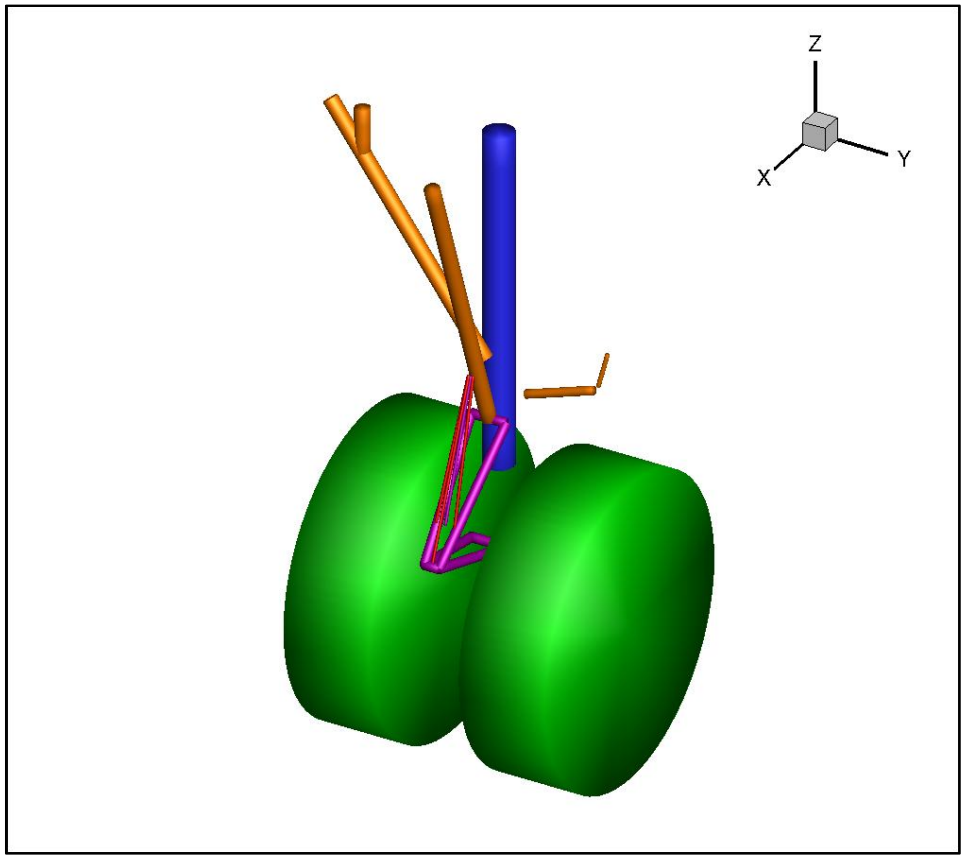

Figure 4-14. The LGMAP landing gear geometry of the Boeing 737 main landing gear. The oleo, support struts, torque arm, wheels, and hoses and wires are shown in blue, orange, purple, green, and red respectively.

4.2.3 Analysis of Results

As can be seen in Figure 4-15, Figure 4-16, and Figure 4-17, the LGMAP prediction under predicts the noise produced past 1kHz. For certain observer locations, the prediction of mid and low frequencies compared well with the experimental data. When separating the landing gear into several components, as displayed in Figure 4-18, the wheels are the dominant source for the entire frequency range.

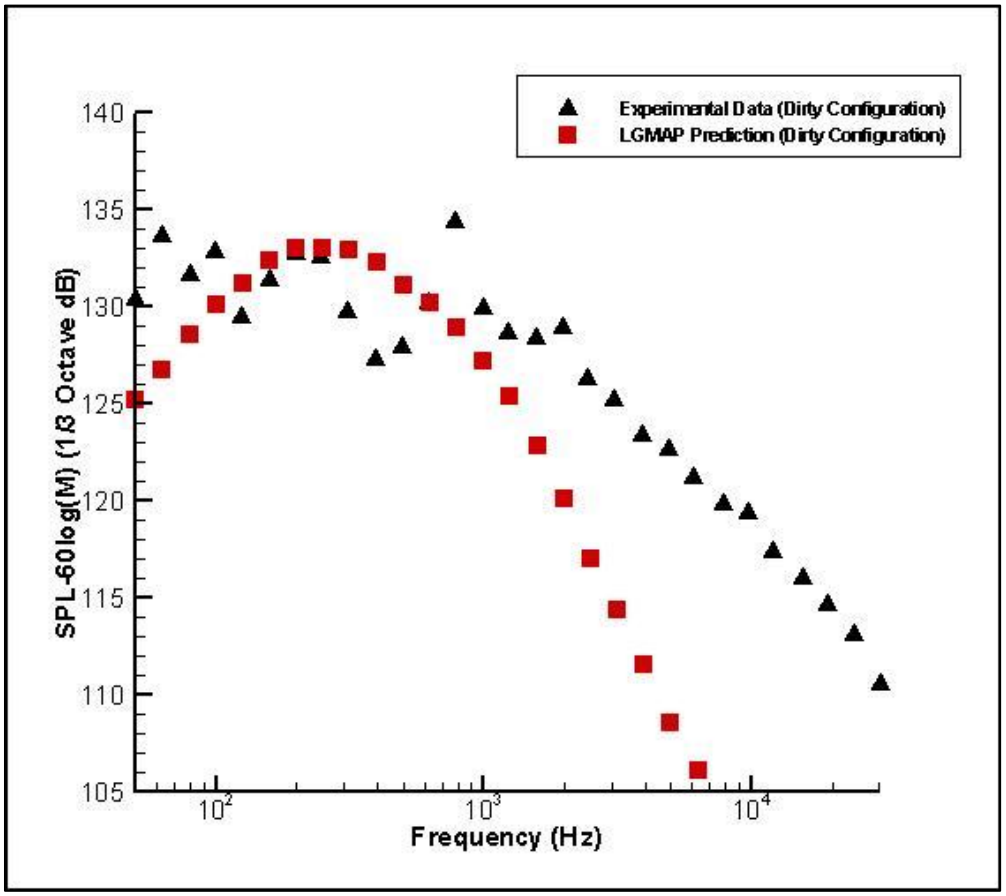

Figure 4-15. Scaled 1/3 octave prediction and experimental results of a full scaled 737 main landing gear. The observer position 30 degrees upstream from directly below the aircraft with the airspeed at Mach 0.24.

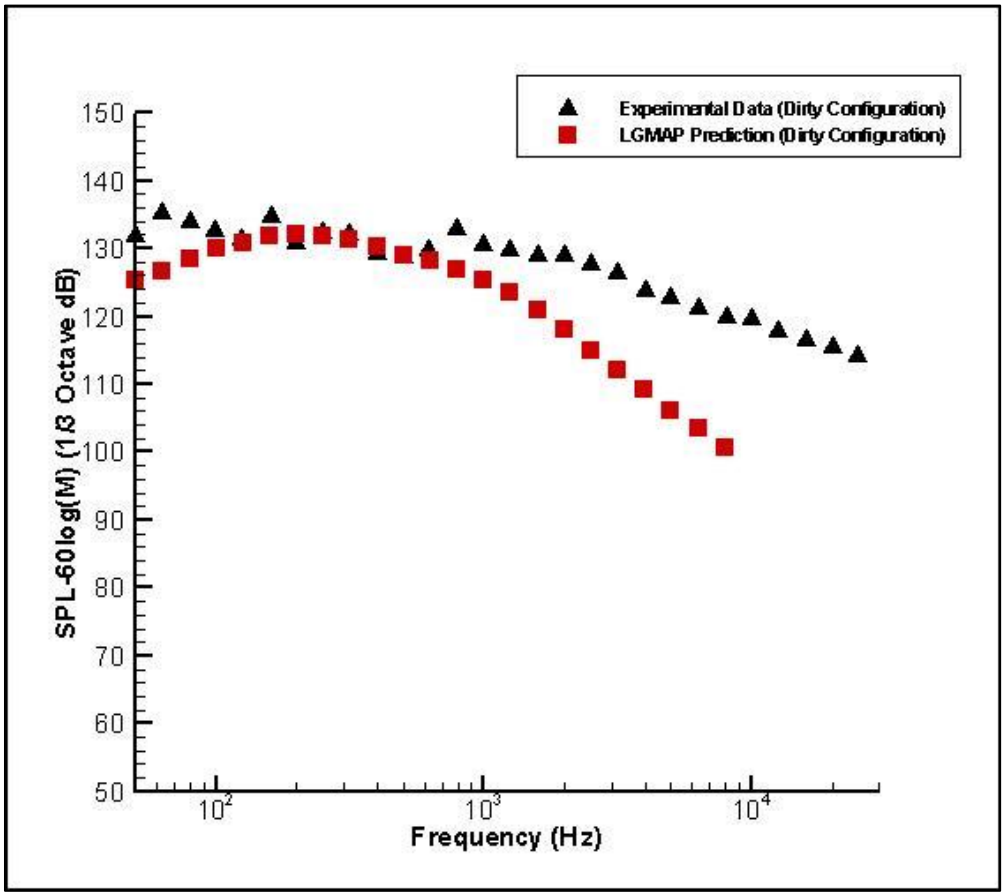

Figure 4-16. Scaled 1/3 octave prediction and experimental results of a full scaled 737 main landing gear. The observer position directly below the aircraft with the airspeed at Mach 0.24.

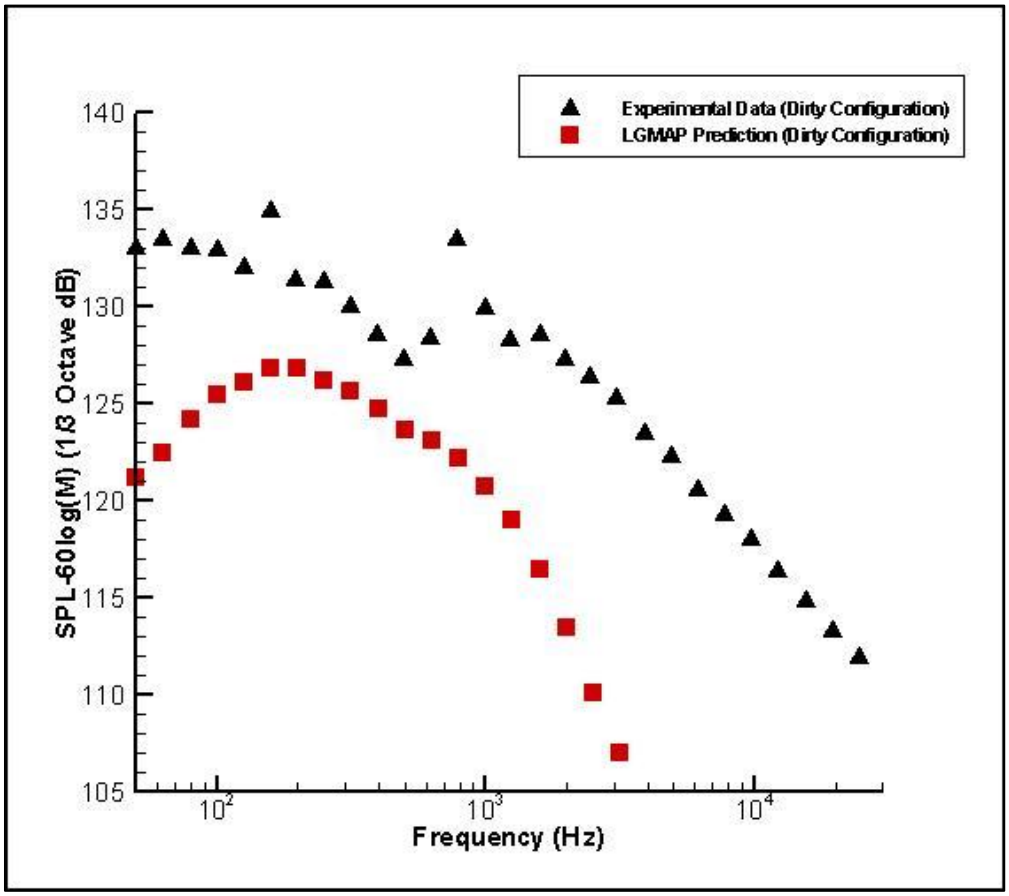

Figure 4-17. Scaled 1/3 octave prediction and experimental results of a full scaled 737 main landing gear. The observer position 30 degrees downstream from directly below the aircraft with the airspeed at Mach 0.24.

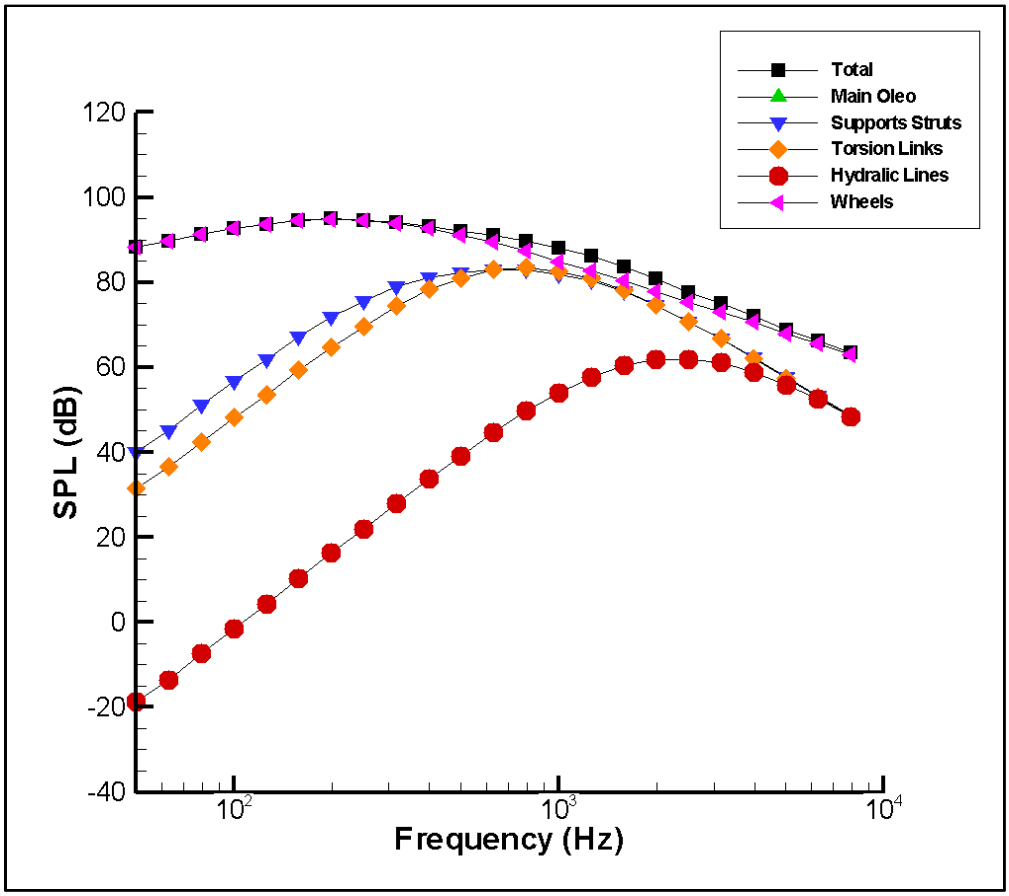

Figure 4-18. 1/3 octave prediction and experimental results of a full scaled 737 main landing gear broken down in separate components. Detail locations and names of the components can be viewed in APENDIX ??? The observer position directly below the aircraft with the airspeed at Mach 0.24.

The prediction is least accurate at 30 degrees downstream from below the aircraft. The results from the experiment, presented in Figure 4-19, do not show a decrease in OASPL from below the aircraft till the observer moves 30 degrees downstream. This is impossible for LGMAP to predict properly as the Doppler amplification factor in Equation 2-8 and Equation 3-5 reduces the noise for observers located downstream from the source for both the ABwheel and cylinder acoustic elements. The only increase of noise as the observer moves downstream would be the fluctuating drag noise component of any vertical cylinder acoustic elements. But the amplitude of this noise is overshadowed by the fluctuating lift noise components by any

horizontal cylinder acoustic elements within the landing gear geometry. The slight decrease as the observer moves upstream also contradicts the LGMAP's prediction.

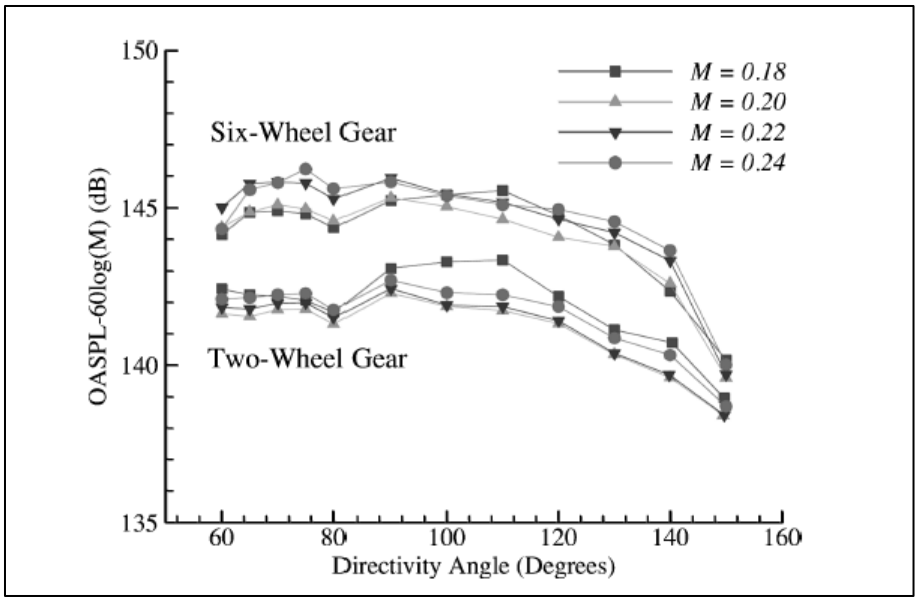

Figure 4-19. OASPL as a function of microphone angles for two gear configurations at various Mach number. 0 degrees represents the upstream direction (Ref. 6).

To fully understand LGMAP's accuracy capabilities, its prediction is compared with two others: the Guo method and Fink method. Both these methods are part of NASA's ANOPP. Before comparisons are made, it should be noted that this landing gear case was used to determine many empirical constants for the Guo method. Figure 4-20 presents both ANOPP's landing gear prediction methods and LGMAP's compared with experimental data done with the full scaled model. Guo method is the most accurate prediction, especially in the high frequency range. As explained in Section 1.1, the prediction requires matching the prediction with data. As expected, the Fink prediction underpredicts the noise when compared with LGMAP. Though LGMAP's wheel prediction is almost identical to Fink's for a two wheel bogey, the strut

prediction for Fink is zero for this observer position which is directly below the aircraft. The LGMAP acoustic cylinder's parallel to the produce noise for this observer position.

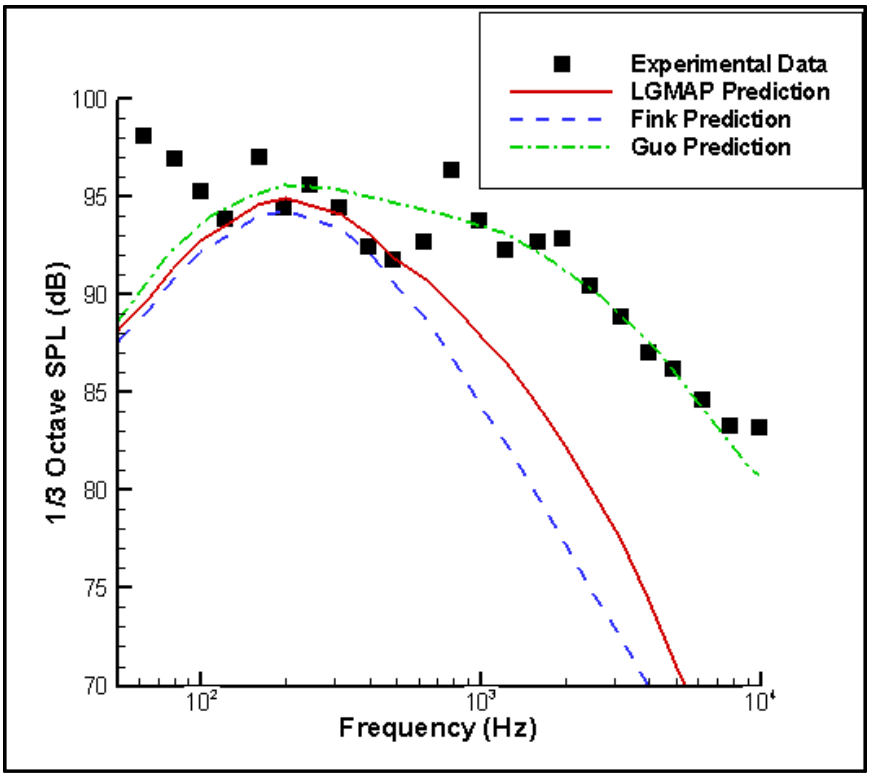

Figure 4-20. 1/3 octave prediction using LGMAP, Fink, and Guo metods and experimental results of a full scaled 737 main landing gear. The observer position directly below the aircraft with the airspeed at Mach 0.24.

LGMAP's capabilities are subpar regarding this experimental case, but there are some explanations and observations that can explain the error and possibly assist in future predictions. For one, the low frequency end of this example case cutoff for the LASF experimental chamber is 200 Hz (Ref. 6). Frequencies below 200 Hz were discarded when computing OASPL, but they are still presented in spectrum results. This explains the low frequency error for all three prediction methods.

Under closer inspection of the Boeing 737 main landing gear's strut assembly, many of the features of the support struts and locking mechanism are very complex (Figure 4-21) and the struts themselves are not circular in shape. They are rectangular cylinders which would have different noise characteristics than the circular cylinder shape that most oleo's have. The torsion links (Figure 4-22) are also very difficult to be represented as a LGMAP geometry. For the results above, the acoustic cylinders matched the larger beam like feature and not the webbing between.

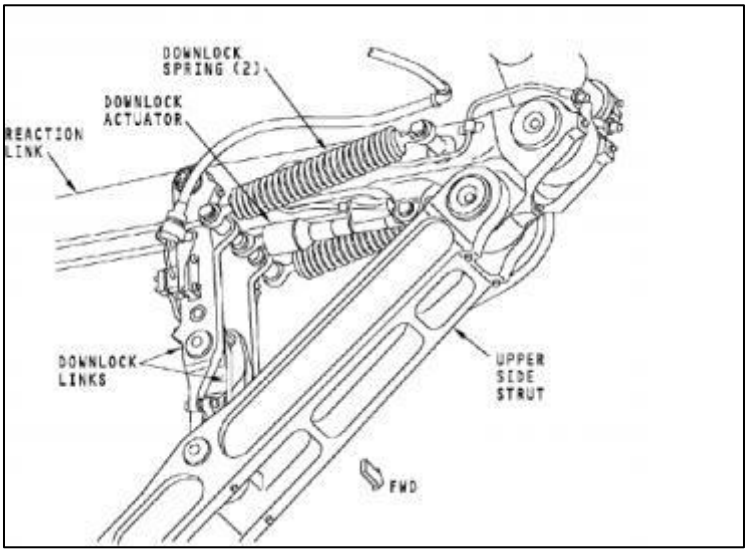

Figure 4-21. Detail image of the Boeing 737 main landing gear's struts (Ref. 24).

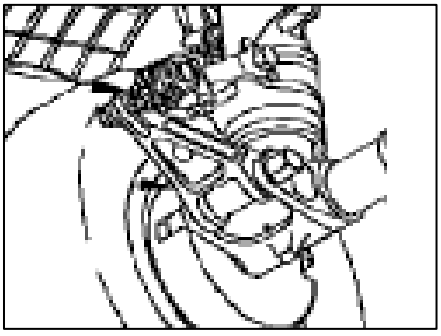

Figure 4-22. Detail image of the Boeing 737 main landing gear's torsion links (Ref. 24).

The model used in the wind tunnel tests appeared to be altered from a real 737 landing gear. For one, some if not all, of the landing gear doors appears to be removed (Figure 4-23). The landing gear's doors are separated in order to cover the wheel well during retraction, as can be viewed in Figure 4-24. If they were included in the test model, LGMAP would not have an acoustic model to represent these components. Also, upon visual inspection, not all of the wires and hoses could be accounted for. The only clear images available present the hoses near the torsion links (Figure 4-25). If a detailed reference of the model was available for the landing gear geometry constructed, it is possible that a closer prediction could be made.

Figure 4-23. The Boeing 737 main landing gear model installed in the LSAF. Note the missing landing gear doors (Ref. 6).

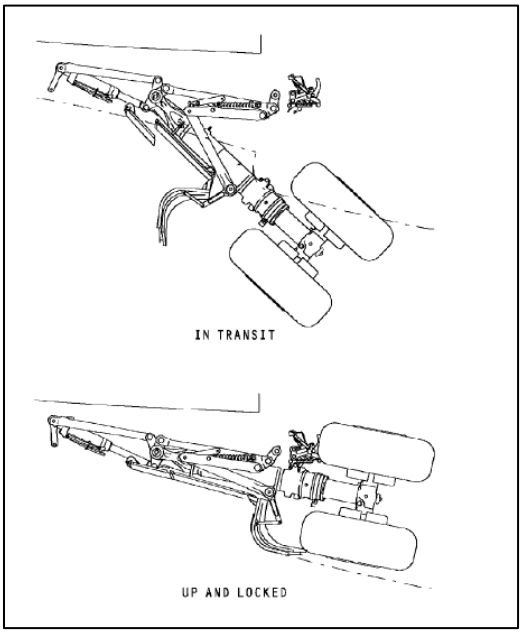

Figure 4-24. The Boeing 737 main landing during retraction. Note the several panels that make up the landing gear door (Ref. 24).

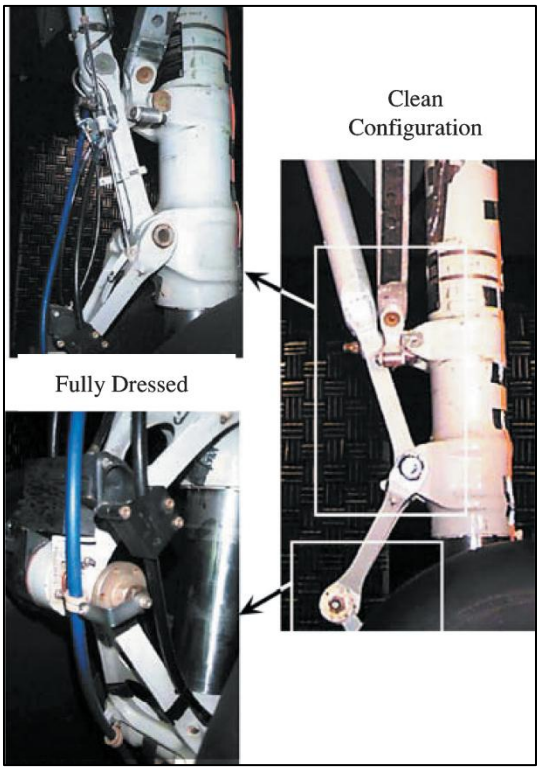

Figure 4-25 The Dirty and clean configuration of the Boeing 737 main landing gear (Ref. 6).

4.3 Noise Source Investigation

LGMAP provides the user with the ability to see the contributions of each piece of the landing gear to the total noise prediction. This is a very useful analytic tool for engineers so that they can identify features of a landing gear that will produce most at certain frequencies. Currently, there are few experimental methods that produce similar understanding of the noise characteristics of a landing gear. One of these methods incorporates the use of a phased array of microphones. By analyzing the signals picked up by the microphones, the user can virtually point at certain locations and create a noise spectrum produced by the targeted source.

To validate the usefulness of LGMAP's ability to identify sources of noise, predicted data is compared with results using phased array measurements. The landing gear experimental measurements chosen for this test is the full scale Boeing 737 main landing gear described previously and an experiment conducted on a 25% scaled Gulfstream G550 at University of Florida Aeroacoustic Flow Facility (UFAFF). A short description of the experiment is presented so that a basic understanding on the test procedure on objectives can be made.

4.3.1 Description of 25% Scaled GS550 Experiment

The 25% Gulfstream G550A nose landing gear was tested to build a database for validation of physics-based theoretical/numerical models (Refs. 19, 25). The other major goal for this experiment is to study the localization of landing gear sources using a planar acoustic array of microphones. The two algorithms employed for many of the studies available are Delay-and-Sum (DAS) and Robust Capon (RBC). The lack of extensive single point observer data limits

how LGMAP can be compared with available data. LGMAP's ability to identify noise source contributions for landing gear parts is shown against the available beamforming plots from the experimental data.

Three test configurations of the model were tested, fully-dressed cavity open, partially-dressed cavity closed, and partially dressed cavity open. Similar to the other landing gear experiments mentions in this section, the goal for these differences was to see how the high fidelity parts affect the aeroacoustic noise. The results have shown that the closed landing bay cavity has an adverse effect on the noise.

4.3.2 Geometry Creation of Gulfstream G550 Nose Gear

The Gulfstream G550 nose gear contains a feature that has not been encountered in an LGMAP prediction. The landing gear door, for this nose gear (Figure 4-26) is located at the rear and perpendicular to the flow. Other landing gears predicted with LGMAP contained doors that are parallel to the airflow and produce noise similar to a trailing edge and does not have a major input on the flow around the rest of the landing gear unlike G550. The landing gear door and brace supporting it are left out of the LGMAP geometry model. The brace is not included due to the close vicinity of the door because the vortices shed by the brace will not form properly.

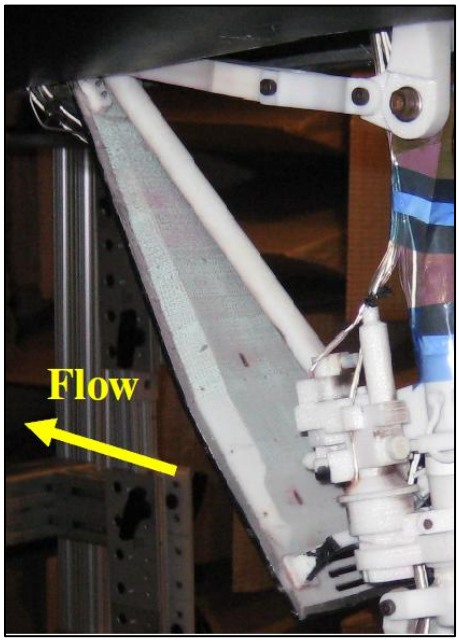

Figure 4-26. Close up of the Gulfstream G550's landing gear door (Ref. 19).

3D CAD model was available in the geometry creation process which was used to accurately measure the size of location of each landing gear feature. This model is displayed in Figure 4-27. These measurements were made using CAD software to superimpose cylinders over the model. Unlike the geometries created for LGMAP's validation, having an accurate reference of the landing gear model made it very easy to create the LGMAP geometry (Figure 4-28 and Table A-6). The CAD model was of the partially dressed configuration so hydraulic hoses and wires were not represented in the geometry model. Also, the CAD model included geometry that is located inside the landing gear cavity. This section of the oleo was removed from the LGMAP geometry.

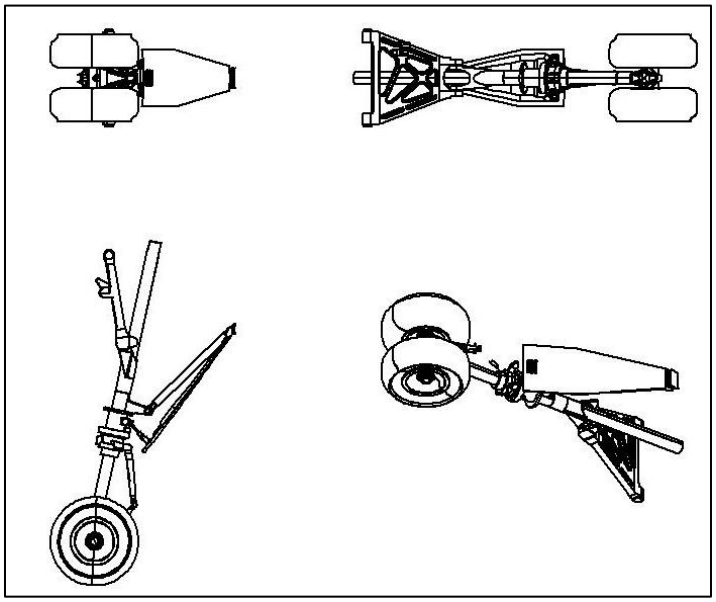

Figure 4-27. The Original CAD Drawing of the Test Model of the G550 Nose Landing Gear.

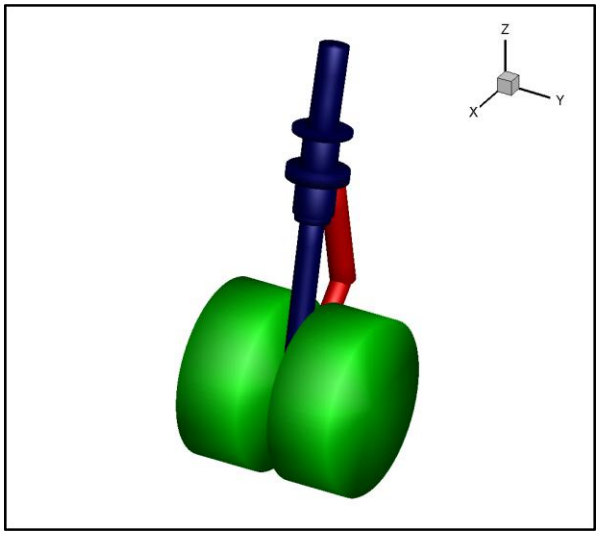

Figure 4-28. The LGMAP landing gear geometry of the Gulfstream G550 noise landing gear. The oleo, torque arm, and wheels are shown in blue, red, and green respectively.

4.3.3 LGMAP Noise Source Comparison with Phased Array Measurements

The phased array measurements taken at UFAFF, presented in Figure 4-29, display a rough interpretation of the region of dominant noise generation. At the lowest frequency of 1.25 kHz, the dominant source of noise is around the wheel bogey. As the frequency rises, the source localizes around the oleo and torque arm. The oleo at the height of the door does not produce as much noise as the lower section around the torque arm. This may be due to the flow interaction with the door. The door itself is the smallest noise contributor and possibly inessential to the noise prediction model expect for flow interactions. LGMAP includes the ability to include a local flow model which can be produced by CFD software. Using this feature may increase the accuracy of LGMAP's prediction.

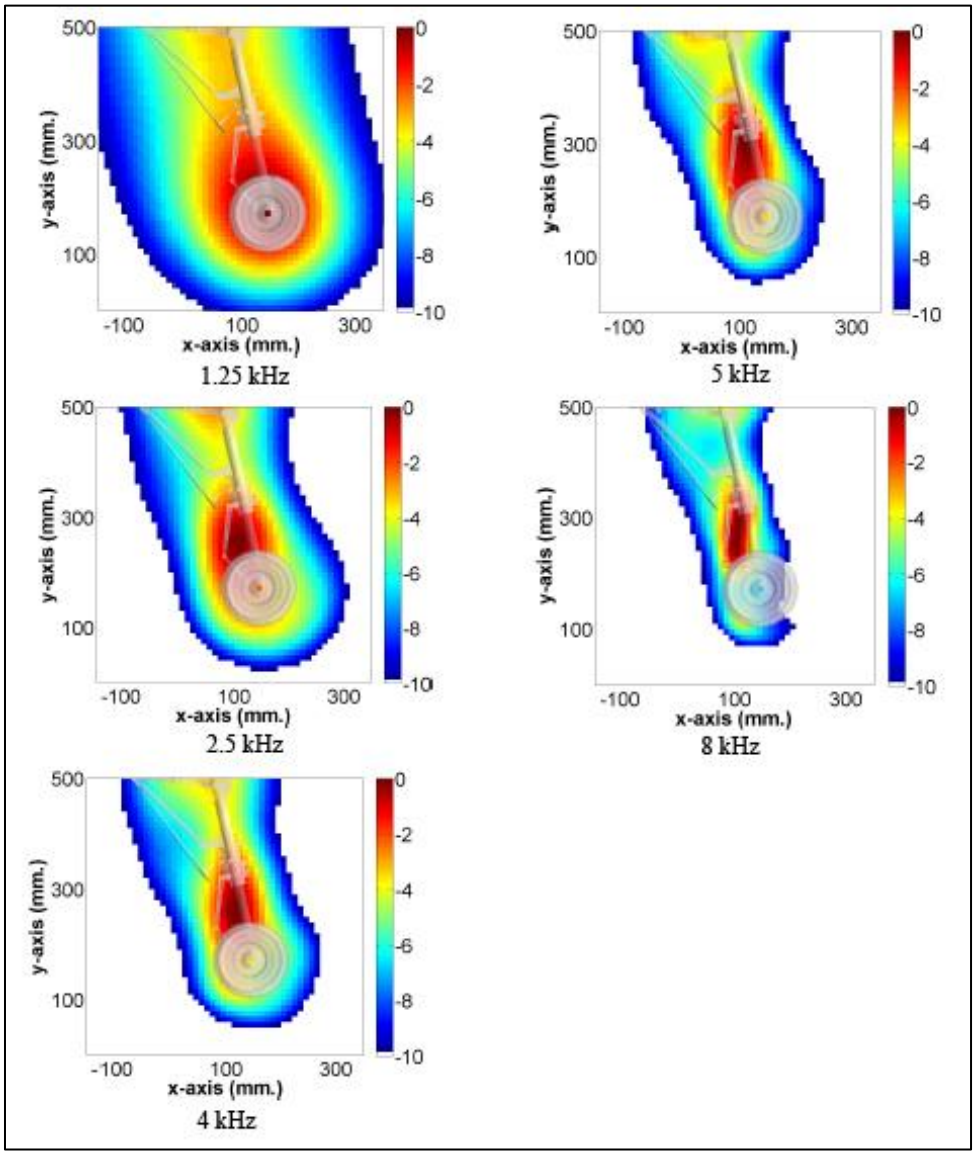

Figure 4-29. Noise source localization maps at several frequencies of the 0.25% scaled Gulfstream G550 nose landing gear model. The model is in the partially-dressed cavity open configuration. Levels are in normalized dB (Ref. 19).

LGMAP's prediction of the Gulfstream G550 is displayed in Figure 4-30. The noise is broken down to certain components of the landing gear to show the contributions of each part to the total noise. The observer is placed ten oleo lengths toward starboard to minimize the difference of observer distance between each noise source. Like the phased array measurements,

the wheel is the biggest noise contributor at low frequencies, but it remains so, though decreasing, at higher frequencies. The difference in sound pressure levels between the oleo and torque bar is minimal at 1-2 dB. The oleo noise is larger the torque bar's. If a local flow model is introduced, the oleo's noise, especially around the door would decrease. The wheel noise were the only major discrepancy between the measurement and prediction.

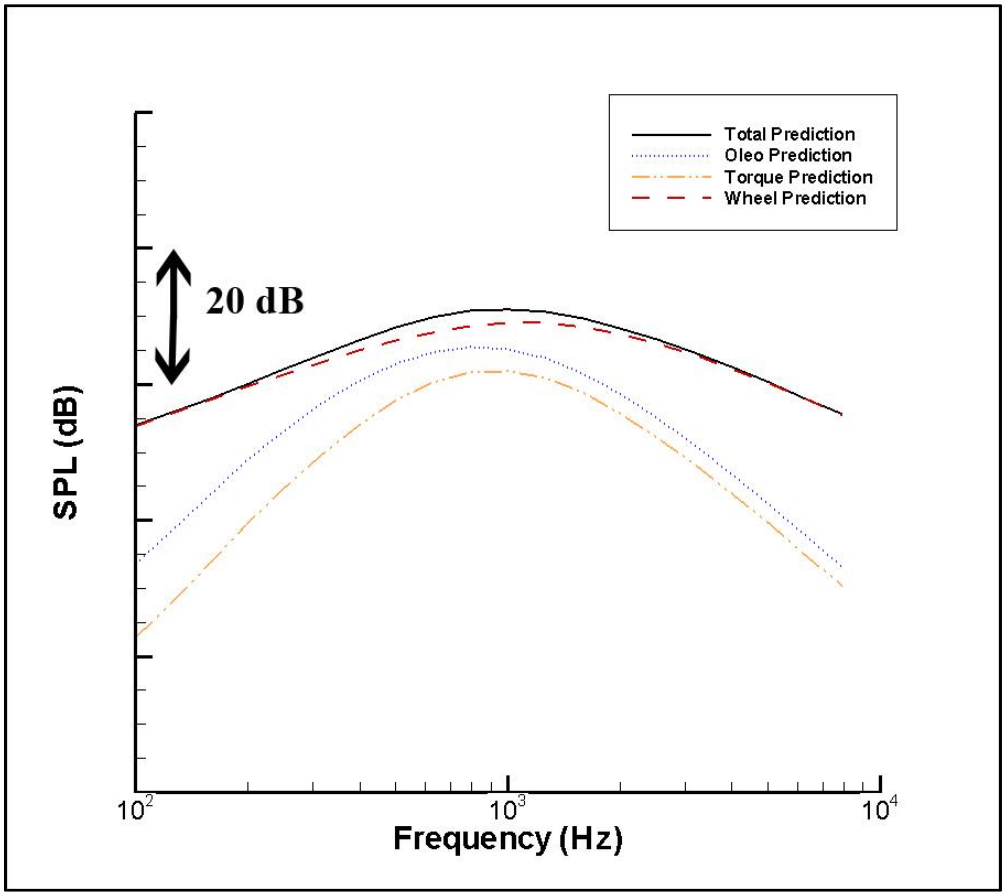

Figure 4-30. Third octave spectrum of the 25% scaled Gulfstream G550 nose landing gear model and several of its isolated features. The observer is located 10 oleo lengths toward the starboard and the flow is at Mach 0.145.

Along with single microphone measurements, phased array measurements were taken of the full scaled Boeing 737 main landing gear model at QFF. These measurements, as presented

in Figure 4-31 and Figure 4-32, are of only higher frequencies that are usually dominated by small landing gear features such as hoses and wires. These hoses and wires are located around the torque arm and forward support strut. Throughout the frequencies shown, these objects appear to be the dominant noise source. The oleo, struts, toque arm, and wheels have little to no effect on noise when compared to the hoses and wires.

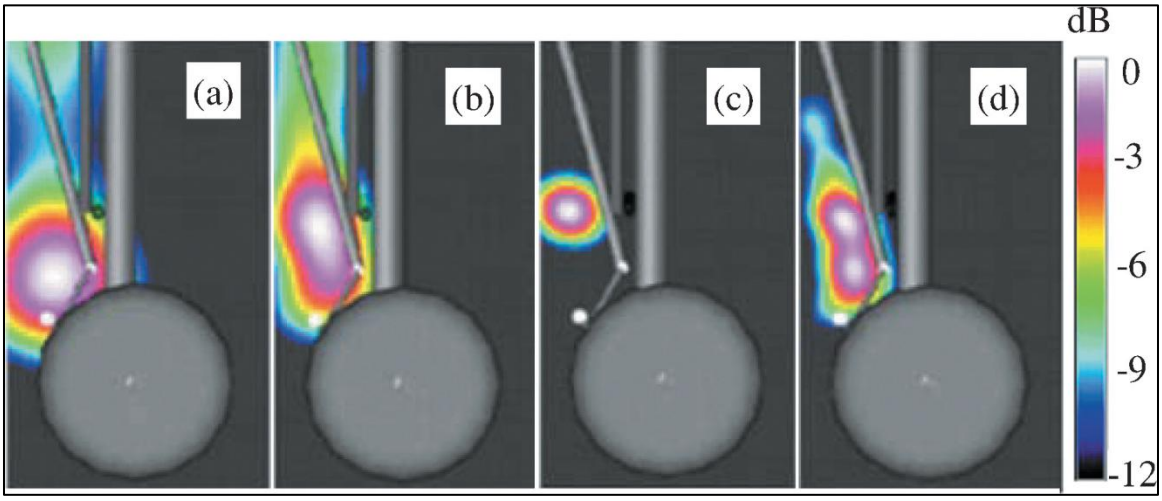

Figure 4-31. Phased array measurements of the Boeing 737 main landing gear model for frequencies: a) f = 1000 Hz, peak SPL = 94.8 dB; b) f = 1500 Hz, peak SPL = 88.9 dB; c) f = 2000 Hz, peak SPL = 96.0 dB; and d) f = 2500 Hz, peak SPL = 83.0 dB (Ref. 6).

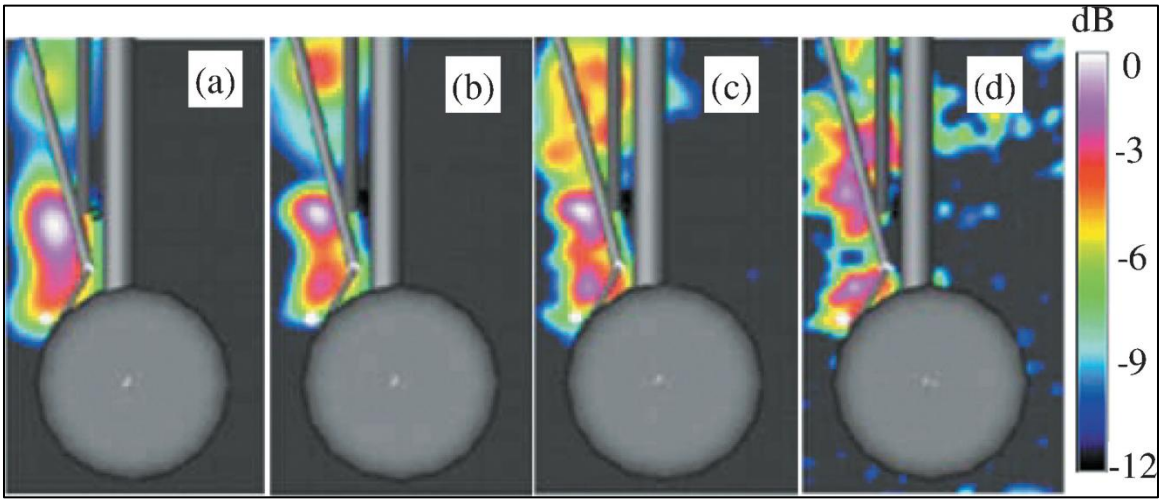

Figure 4-32. Phased array measurements of the Boeing 737 main landing gear model for frequencies: a) f = 4000 Hz, peak SPL = 78.9 dB; b) f = 6000 Hz, peak SPL = 72.0 dB; c) f = 8000 Hz, peak SPL = 64.9 dB; and d) f = 10,000 Hz, peak SPL = 59.6 dB (Ref. 6).

Similar to the Gulfstream G550 prediction, the observer location for the Boeing 737 case is located 10 oleo lengths port from the landing gear model. Like the phased array measurements, the results from this prediction, shown in Figure 4-33, also have the hoses and wires as the dominant noise source. At 1 kHz, the wheel and side (support) struts are equally noisy as the hoses and wires. This is not shown in the phased array measurements as there is no indication of noise from either of these objects. These sections of the landing gear have much less noise impact as the frequency rises. The torque arm and oleo have very little effect on the total noise generated.

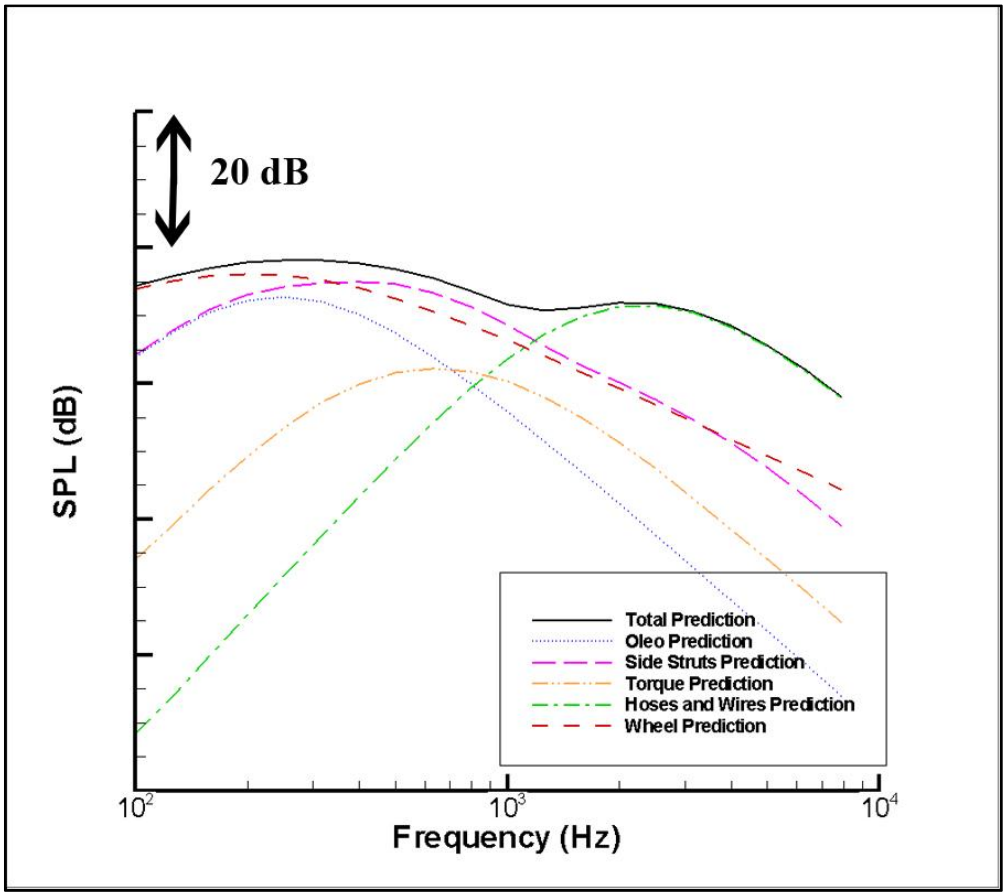

Figure 4-33. Third octave spectrum of the full scaled Boeing 737 main landing gear model and several of its isolated features. The observer is located 10 oleo lengths toward the port and the flow is at Mach 0.24.

The discrepancies between the phased array measurements and LGMAP prediction show that the directivity of the wheel model may still need to be changed. The impact of the wheel bogey prediction at high frequencies seems to be much less than what is indicated in measured results. Though the sideline measurements give little indication of noise sources for a flyover observer, accurate predictions are of some use to landing gear designers.

Chapter 5

Conclusion

The objective this research has been to validate the LGMAP method as a landing gear prediction scheme and to upgrade it when possible. The initial upgrades to LGMAP were made to correct the cylinder scaling, non dimensional spectrums, and incident velocity vectors. These changes required calibration to the coefficients of the cylinder acoustic elements. To increase the accuracy of the wheel prediction model, a new scheme was developed based on the Fink method's wheel model. Unlike the Fink wheel model, the location of each LGMAP's ABwheel is specified by the used and incorporates shielding and scattering similar to the cylinder acoustic elements.

After the upgrades were completed, the cylinder coefficients were recalibrated with the experimental data of the 6.3% scaled Boeing 777 main landing gear at NASA's QFF. The geometry model used for calibration was different from what was used previously to calibrate six wheel bogies. The new model was designed to match the model in the experiment, not the actual Boeing 777 landing gear.

One of the experiments used for validation was to compare landing gear models built by different users and the importance of an appropriate and accurate model was discovered. The new ABwheel acoustic element removes the need to build a truck and brake model in the LGMAP landing geometry. If the user were to build one, it could have a detrimental effect on the noise prediction. Also, the inclusion of high fidelity objects such as cables and hoses should be modeled accurately. Hoses and cables extremely close to large structures such as the oleo should

not be represented in the LGMAP landing gear geometry in order to prevent an overprediction in high frequency noise.

The other validation experiment was the comparison of the LGMAP prediction with experimental data and predicted data from other methods. This landing gear model was made without the help of comparison of experimental data or calibration. The results from the chosen case, a full scaled Boeing 737 main landing gear, produced underpredictions in high frequency noise and the directivity did not match that from experimental data. The experimental directivity is impossible to match with LGMAP because of the Doppler amplification factors found in the equations of the acoustic elements. The discrepancies between the experimental data and the LGMAP prediction could be the lack of resources that were used to build the landing gear geometry. The accurate location and size of the high fidelity components and inclusion of the landing gear door were unavailable during geometry construction. Also the struts of the Boeing 737 are not cylindrical and it may be difficult to model with LGMAP's current capabilities.

The Guo prediction was much more accurate than LGMAP, but this case was part of that method's calibration. Also as of this writing, the Guo method cannot make predictions without acquiring experimental data first. LGMAP showed that it was more accurate than the Fink method. Though the wheel model is very similar to Fink's, the strut model is much more complex.

The final verification experiment was to document LGMAP's capabilities as a noise source locator. The unique capability that LGMAP has is the ability to isolate specific parts of the landing gear geometry. When compared with phased array measurements, the high fidelity features of the landing gear such as hoses and wires were dominant in both prediction and measured results. LGMAP's wheel model was overpredicting for all sideline observer cases. If the phased array measurements are correct, this would require an update of the ABwheel's directivity.

5.1 Recommended Future Work.

Though this thesis provides a good representation of LGMAP's capabilities, it emphasizes the incorporation of future improvements for the prediction method. The inconsistencies of the Boeing 737 main landing gear case show that a square cylinder acoustic element could increase prediction accuracy. This would require calibration with experimental data of isolated square cylinders in flow. Improvements to the ABWheel model should also be investigated. Compared to phased array measurements, the directivity of the ABWheel is inaccurate.

The validation conducted on LGMAP did not include the trailing edge and reflective surface acoustic elements or the inclusion of shielding and scattering. The trailing edge element was validated with only one experimental case. Future work requires more cases including those with the landing gear doors modeled with the trailing edge acoustic element. The addition of the reflective surface acoustic element useful has never been explored. It should be compared with different types of landing gear cavity arrangements. Finally the effects of the scattering and shielding calculations on the ABWheels and cylinder acoustic elements should be analyzed further. Past tests have shown that there is little effect that shielding and scattering have on the landing gear prediction except extending calculation time. These tests were done before the upgrades were completed. If these questions and issues are addressed, it is possible that LGMAP could become an easy and accurate landing gear noise prediction method.

Bibliography

[1] Kipersztok, Oscar, & Sengupta, Gautam, "Flight Test of the 747-JT9D for Airframe Noise", *Journal of Aircraft*, vol. 19, no. 12, December 1982.

[2] Ravetta, Patricio A., Burdisso, Ricardo A., & Ng, Wing F., "Wind Tunnel Aeroacoustic Measurements of a 26%-scaled 777 Main Landing Gear Model," AIAA Paper No. 2004-2885, 10th AIAA/CEAS Aeroacoustics Conference, May 10-12 2004.

[3] "Landing Gear," flickr, Web, 6 Jun 2011, http://www.flickr.com/photo/blumpy/1354588824.

[4] Lopes, Leonard V., *A New Approach to Complete Aircraft Landing Gear Noise Prediction*, Dissertation, The Pennsylvania State University, University Park, Pennsylvania, December 2005.

[5] Lopes, Leonard V., *A New Model and Prediction Tool for Landing Gear Acoustics*, Master's Thesis, The Pennsylvania State University, University Park, Pennsylvania, December 2005.

[6] Guo, Yueping P. & Stoker, Robert W., "Experimental Study on Aircraft Landing Gear Noise," *Journal of Aircraft*, vol. 43, no. 2, March-April 2006, pp. 306-317.

[7] Burley, Casey L., Brooks, Thomas F., & Humphreys Jr., William M., "ANOPP Landing-Gear Noise Prediction with Comparison to Model Scale Data," *International Journal of Aeroacoustics*, vol. 8, no. 5, 2009, pp.445-476.

[8] Fink, M. R., "Component Method for Airframe Noise," Technical report, FAA-RD-77-29. Available from DTIC as AD A039 664, 1977.

[9] Fink, M. R., "Noise Component Method for Airframe Noise," *Journal of Aircraft*, vol. 16, no. 10, October 1979, pp. 659-665.

[10] Heller, H. and Dobrzynski, W., "Sound Radiation from Aircraft Wheel-Well/ Landing-Gear Configurations," *Journal of Aircraft,* vol. 14, no. 8, 1977, pp. 768-774.

[11] Cox, Jared S., Brentner, Kenneth S., & Rumsey, Christopher L., "Computation of Vortex Shedding and Radiated Sound for a Circular Cylinder: Subcritical to Transcritical Reynolds Numbers," *Theoretical and Computational Fluid Dynamics,* vol. 12, 1998, pp. 233-253.

[12] Zorumski, William .E., "Aircraft Noise Prediction Program. Theoretical Manual. Part 2," Technical report, NASA TM 83199, 1982.

[13] Guo, Yueping, Yamamoto, K. J. & Stoker, Robert W., "Component-Based Empirical Model for High-Lift System Noise Prediction," *AIAA Journal of Aircraft,* volume 40, no. 5, September-October 2003, pp. 914-922.

[14] Zdravkovich, M. M., "Flow Around Circular Cylinders. Fundamentals, Vol. 1," Oxford University Press, 1997.

[15] Farassat, Feri, "Linear Acoustic Formulas for Calculation of Rotating Blade Noise," *AIAA Journal*, colume 19, no. 9, September 1981, pp. 1122-1130.

[16] Ffowcs Williams, J. E. & Hawkings, David L., "Sound Generated by Turbulance and Surfaces in Arbitrary Motion," *Philosophical Transactions of the Royal Society*, volume A264, no 1151, 1969, pp. 321-342.

[17] Ffows William, J. E., & Hall, L. H., "Aerodynamic Sound Generation by Turbulent Flow in the Vicinity of a Scattering Half-Plane," *Journal of Fluid Mechanics*, 1970, pp. 657-670.

[18] Jaeger, S. M., Burnside, N. J., Soderman, P. T., Horne, W. C., & James, K. D., "Microphone Array Assessment of an Isolated, 26%-Scale, High-Fidelity Landing Gear", AIAA Paper No. 2002-2410, *8th AIAA/CEAS Aeroacoustics Conference & Exhibit*, Breckenridge, Colorado, June 17-19 2002

[19] Zawodny, N. S., Liu, F., Yardibi, T., Cattafesta, L., Khorrami, M. R., Neuhart, D. H., et al., "A Comparative Study of a 1/4-scale Gulfstream G550 Aircraft Nose Gear Model", AIAA-2009-3153. *15th AIAA/CEAS Aeroacoustics Conference (30th AIAA Aeroacoustics Conference)*, Miami, Florida, May 11-13 2009.

[20] Humphreys, W. M., & Brooks, T. F., "Noise Spectra and Directivity For a Scale-Model Landing Gear", AIAA Paper No. 2007-3458,. *13th AIAA/CEAS Aeroacoustic Conference (28th AIAA Aeroacoustic Conference*), Rome, Italy, May 21-23 2007.

[21] Dekkers, Daniel, Hink, Teun, Hottinga, Michel, Oostrom, Rudvan, Ori, Anjali, Peeters, Tom, Regtop, Lex, & Salim, Sipan, "Analysis Landing Gear 737-500," Amsterdam, Hogeschoolvan Amsterdam, October 2008.

[22] Tummers, Bas, Lann, Janvander,& Huyser, Kees. "DataThiefIII", November 2010.

[23] Jones, William A., "N60659 (cn. 33781/504) The Big 777 Landing Gear in Action at BFI on Friday Afternoon. Seattle, Washingtion", April 2005.

[24] *"*Aircraft Maintenance Manual Boeing 737-300/400/500*,"* Revision no. 57, Continental Airlines, July 12 2004.

[25] Keating, Anthony, Dethioux, Patrick, Satti, Rajani, Noelting, Swen, Louis, John, Van de Ven, Thomas, & Vieito, Robert, “Computational Aeroacoustics Validation and Anaylsis of a Nose Landing Gear,” AIAA Paper no. 2009-3154, Maimi, Florida,, May 11-13 2009.

Appendix

LGMAP Landing Gear Geometries

Table A-1. Original 6.3% scaled Boeing 777 main landing gear LGMAP geometry used for cylinder calibration. 6.3% scaling is done outside the landing gear geometry namelist. Units are in meters and radians.

777 Main Landing Gear							
Translation Change of Base	0.0	0.0	4.00548				
Name	**X1**	**Y1**	**Z1**	**X2**	**Y2**	**Z2**	**Diameter**
Shock Strut Assembly							
Oleo	-0.2931	0.0	0.0	-0.2931	0.0	-4.0054	0.1954
Upper Hydraulic Actuator	-0.1587	-0.3663	0.0	-0.1948	-0.3663	-0.5373	0.1954
Lower Hydraulic Actuator	-0.1948	-0.3663	-0.5373	-0.2688	-0.3663	-1.6412	0.0733
Drag Strut	1.3614	-1.8636	-0.3908	-0.1573	-0.1343	-2.3446	0.1954
Drag Strut Locking Mech.	0.3090	-0.9990	-1.3677	0.0	-0.1343	-0.6838	0.0733
Drag Strut Spacer	1.3615	-1.8636	0.0	1.3615	-1.8636	-0.3908	0.1954
Side Strut	-0.1573	-2.4234	-0.3908	-0.1573	-1.343	-2.3446	0.1954
Side Strut Locking Mech.	-0.4334	-1.2788	-1.3677	-0.3717	-0.1343	-1.1723	0.0733
Side Strut Spacer	-0.7096	-2.234	0.0	-0.7095	-2.234	-0.3908	0.1954
Name	**X**	**Y**	**Z**	**Radius**	**Treadwidth**		
Center Port Wheel	-0.2535	-0.3757	-4.019	0.6604	0.586		
Center Starboard Wheel	-0.2535	0.3757	-4.019	0.6604	0.586		
Rear Port Wheel	-1.6477	-0.3757	-4.2906	0.6604	0.586		
Rear Starboard Wheel	-1.6477	0.3757	-4.2906	0.6604	0.586		
Front Port Wheel	1.1405	-0.3757	-3.6497	0.6604	0.586		
Front Starboard Wheel	1.1405	0.3757	-3.6497	0.6604	0.586		

Table A-2. New 6.3% scaled Boeing 777 main landing gear LGMAP geometry used for cylinder calibration. 6.3% scaling is done outside the landing gear geometry namelist. Units are in meters and radians.

777 Main Landing Gear							
Translation Change of Base	0.0	0.0	4.00548				
Name	**X1**	**Y1**	**Z1**	**X2**	**Y2**	**Z2**	**Diameter**
Shock Strut Assembly							
Top Oleo	-0.2931	0.0	0.0	-0.2931	0.0	-2.7354	0.3712
Bottom Oleo	-0.2931	0.0	-2.7354	-0.2931	0.0	-.3810	0.1954
Upper Hydraulic Actuator	-0.1587	-0.3663	0.0	-0.1948	-0.3663	-0.5373	0.3050
Lower Hydraulic Actuator	-0.1948	-0.3663	-0.5373	-0.2688	-0.3663	-1.6412	0.0760
Drag Strut	1.3614	-1.8636	-0.3908	-0.1573	-0.1343	-2.3446	0.1856
Drag Strut Locking Mech.	0.3090	-0.9990	-1.3677	0.0	-0.1343	-0.6838	0.0977
Drag Strut Locking Hyd.	0.0602	-0.2208	-0.5568	0.3010	-0.5666	-0.8304	0.0315
Drag Strut Spacer	1.3615	-1.8636	0.0	1.3615	-1.8636	-0.3908	0.1856
Side Strut	-0.1573	-2.4234	-0.3908	-0.1573	-1.343	-2.3446	0.1856
Side Strut Locking Mech.	-0.4334	-1.2788	-1.3677	-0.3717	-0.1343	-1.1723	0.0977
Side Strut Locking Hyd.	-0.3779	-0.2488	-0.9965	-0.4025	-0.7066	-1.0746	0.0315
Side Strut Spacer	-0.7096	-2.234	0.0	-0.7095	-2.234	-0.3908	0.1856
Name	**X**	**Y**	**Z**	**Radius**	**Treadwidth**		
Center Port Wheel	-0.2535	-0.8	-4.019	0.6604	0.508		
Center Starboard Wheel	-0.2535	0.8	-4.019	0.6604	0.508		
Rear Port Wheel	-1.6477	-0.8	-4.2906	0.6604	0.508		
Rear Starboard Wheel	-1.6477	0.8	-4.2906	0.6604	0.508		
Front Port Wheel	1.1405	-0.8	-3.6497	0.6604	0.508		
Front Starboard Wheel	1.1405	0.8	--3.6497	0.6604	0.508		

Table A-3. Original 6.3% scaled Boeing 777 main landing gear LGMAP geometry. 6.3% scaling is done outside the landing gear geometry namelist. Units are in meters and radians.

777 Main Landing Gear							
Translation Change of Base	0.0	0.0	4.00548				
Name	**X1**	**Y1**	**Z1**	**X2**	**Y2**	**Z2**	**Diameter**
Shock Strut Assembly							
Oleo	-0.2931	0.0	0.0	-0.2931	0.0	-4.0054	0.1954
Upper Hydraulic Actuator	-0.1587	-0.3663	0.0	-0.1948	-0.3663	-0.5373	0.1954
Lower Hydraulic Actuator	-0.1948	-0.3663	-0.5373	-0.2688	-0.3663	-1.6412	0.0733
Drag Strut	1.3614	-1.8636	-0.3908	-0.1573	-0.1343	-2.3446	0.1954
Drag Strut Locking Mech.	0.3090	-0.9990	-1.3677	0.0	-0.1343	-0.6838	0.0733
Drag Strut Spacer	1.3615	-1.8636	0.0	1.3615	-1.8636	-0.3908	0.1954
Side Strut	-0.1573	-2.4234	-0.3908	-0.1573	-1.343	-2.3446	0.1954
Side Strut Locking Mech.	-0.4334	-1.2788	-1.3677	-0.3717	-0.1343	-1.1723	0.0733
Side Strut Spacer	-0.7096	-2.234	0.0	-0.7095	-2.234	-0.3908	0.1954
Aft Hydraulic Bracket							
Translation Change of Base	-1.2625	0.0	-3.9130				
Rotation Change of Base (About Y axis)	-0.2269 radians						
Translation Change of Base	-1.4149	0.0	0.0				
AHB Lower Cross	-0.1954	-0.0733	0.1465	-0.1954	-0.0733	0.1465	0.0244
AHB First Middle Cross	-0.1172	-0.0879	0.4054	-0.1172	0.0879	0.4054	0.0147
Second Middle Cross	-0.0391	0.1026	0.6643	-0.0391	-0.1026	0.6643	0.0147
AHB Top Cross	0.0	-0.1099	0.7938	0.0	0.1099	0.7938	0.0320
Starboard Side Support	-0.1954	0.0733	0.1465	0.0	0.1099	0.7938	0.0147
Port Side Support	-0.1954	-0.0733	0.1465	0.0	-0.1099	0.7938	0.0147
Aft Hydraulic Dressing							
Translation Change of Base	-1.2625	0.0	-3.9130				
Rotation Change of Base (About Y axis)	-0.2269 radians						
Translation Change of Base	-1.4149	0.0	0.0				
Hose 1 to Bracket	-0.1954	0.0879	0.1465	0.0488	0.0977	0.7938	0.0098
Hose 1 to Oleo	0.0488	0.0977	0.7938	1.6119	0.0977	1.27	0.0098
Hose 1 to Top	1.6119	0.0977	1.27	2.1737	0.0977	3.7123	0.0098
Hose 2 to Bracket	-0.1954	0.0440	0.1465	0.0488	0.0537	0.7938	0.0098
Hose 2 to Oleo	0.0488	0.0440	0.7938	1.6119	0.0537	1.27	0.0098
Hose 2 to Top	1.6119	0.0537	1.27	2.1737	0.0537	3.7123	0.0098
Hose 3 to Bracket	-0.1954	-0.0440	0.1465	0.0488	-0.0537	0.7938	0.0098
Hose 3 to Oleo	0.0488	-0.0440	0.7938	1.6119	-0.0537	1.27	0.0098
Hose 3 to Top	1.6119	-0.0537	1.27	2.1737	-0.0537	3.7123	0.0098
Hose 4 to Bracket	-0.1954	-0.0879	0.1465	0.0488	-0.0977	0.7938	0.0098
Hose 4 to Oleo	0.0488	-0.0977	0.7938	1.6119	-0.0977	1.27	0.0098
Hose 4 to Top	1.6119	-0.0977	1.27	2.1737	-0.0977	3.7123	0.0098

Continued on next page

Table A-3 continued. Original 6.3% scaled Boeing 777 main landing gear LGMAP geometry. 6.3% scaling is done outside the landing gear geometry namelist. Units are in meters and radians.

Name	X1	Y1	Z1	X2	Y2	Z2	Diameter
Forward Horizontal Hydraulic Bracket							
Translation Change of Base	-1.2625	0.0	-3.9130				
Rotation Change of Base (About Y axis)	-0.2269 radians						
Translation Change of Base	0.9469	0.0	0.0				
FHHB Starboard Supp.	0.2029	-0.1038	0.8730	-0.6068	-0.1588	1.0271	0.0488
FHHB Port Supp.	0.2029	0.1038	0.8730	-0.6068	0.1588	1.0271	0.0488
FHHB Forward Cross	0.2029	-0.1038	0.8730	0.2029	0.1038	0.8730	0.0366
FHHB First Middle Cross	0.1198	-0.1038	0.8888	0.1198	0.1038	0.8888	0.0119
FHHB Second Middle Cr.	-0.0990	-0.1038	0.9304	-0.0990	0.1038	0.9304	0.0119
FHHB Aft Cross	-0.5458	-0.1038	1.0155	-0.5458	0.1038	1.0155	0.0119
Forward Horizontal Hydraulic Dressing							
Translation Change of Base	-1.2625	0.0	-3.9130				
Rotation Change of Base (About Y axis)	-0.2269 radians						
Translation Change of Base	0.9544	0.0	0.0				
Dressing 1	0.2029	-0.0733	0.8730	-0.6068	-0.0733	1.0271	0.0098
Dressing 2	0.2029	-0.0244	0.8730	-0.6068	-0.0244	1.0271	0.0098
Dressing 3	0.2029	0.0733	0.8730	-0.6068	0.0733	1.0271	0.0098
Dressing 4	0.2029	0.0244	0.8730	-0.6068	0.0244	1.0271	0.0098
Forward Vertical Hydraulic Bracket							
Translation Change of Base	-1.2625	0.0	-3.9130				
Rotation Change of Base (About Y axis)	-0.2269 radians						
Translation Change of Base	0.9544	0.0	0.0				
FVHB Lower Starboard	0.0	-0.5651	0.0	0.1222	-0.1099	0.5182	0.0342
FVHB Lower Port	0.0	0.5651	0.0	0.1222	0.1099	0.5182	0.0342
FVHB Upper Starboard	0.1222	-0.1099	0.5182	0.2029	-0.1099	0.8730	0.0342
FVHB Upper Port	0.1222	0.1099	0.5182	0.2029	0.1099	0.8730	0.0342
FVHB Lower Cross	0.1222	-0.1099	0.5182	0.1222	0.1099	0.5182	0.0489
FVHB Upper Cross	0.1872	-0.1099	0.80312	0.1872	0.1099	0.80312	0.0391
Forward Vertical Hydraulic Dressing							
Translation Change of Base	-1.2625	0.0	-3.9130				

Continued on next page

Table A-3 continued. Original 6.3% scaled Boeing 777 main landing gear LGMAP geometry. 6.3% scaling is done outside the landing gear geometry namelist. Units are in meters and radians.

Rotation Change of Base (About Y axis)	-0.2269 radians						
Translation Change of Base	0.9544	0.0	0.0				
FVHB Hose 1	0.1222	-0.0733	0.5182	0.2029	-0.733	0.8730	0.0098
FVHB Hose 1 to Oleo	-0.6068	-0.0733	1.0271	0.0	-0.733	3.7123	0.0098
FVHB Hose 2	0.1222	-0.0244	0.5182	0.2029	-0.0244	0.8730	0.0098
FVHB Hose 2 to Oleo	-0.6068	-0.0244	1.0271	0.0	-0.0244	3.7123	0.0098
FVHB Hose 3	0.1222	0.0244	0.5182	0.2029	0.0244	0.8730	0.0098
FVHB Hose 3 to Oleo	-0.6068	0.0244	1.0271	0.0	0.0244	3.7123	0.0098
FVHB Hose 4	0.1222	0.0733	0.5182	0.2029	0.733	0.8730	0.0098
FVHB Hose 4 to Oleo	-0.6068	0.0733	1.0271	0.0	0.733	3.7123	0.0098
Name	**X**	**Y**	**Z**	**Radius**	**Treadwidth**		
Center Port Wheel	-0.2535	-0.3757	-4.019	0.6604	0.586		
Center Starboard Wheel	-0.2535	0.3757	-4.019	0.6604	0.586		
Rear Port Wheel	-1.6477	-0.3757	-4.2906	0.6604	0.586		
Rear Starboard Wheel	-1.6477	0.3757	-4.2906	0.6604	0.586		
Front Port Wheel	1.1405	-0.3757	-3.6497	0.6604	0.586		
Front Starboard Wheel	1.1405	0.3757	-3.6497	0.6604	0.586		

Table A-4. New 6.3% scaled Boeing 777 main landing gear LGMAP geometry. 6.3% scaling is done outside the landing gear geometry namelist. Units are in meters and radians.

777 Main Landing Gear							
Translation Change of Base	0.0	0.0	4.00548				
Name	**X1**	**Y1**	**Z1**	**X2**	**Y2**	**Z2**	**Diameter**
Shock Strut Assembly							
Top Oleo	-0.2931	0.0	0.0	-0.2931	0.0	-2.7354	0.3712
Bottom Oleo	-0.2931	0.0	-2.7354	-0.2931	0.0	-.3810	0.1954
Upper Hydraulic Actuator	-0.1587	-0.3663	0.0	-0.1948	-0.3663	-0.5373	0.3050
Lower Hydraulic Actuator	-0.1948	-0.3663	-0.5373	-0.2688	-0.3663	-1.6412	0.0760
Drag Strut	1.3614	-1.8636	-0.3908	-0.1573	-0.1343	-2.3446	0.1856
Drag Strut Locking Mech.	0.3090	-0.9990	-1.3677	0.0	-0.1343	-0.6838	0.0977
Drag Strut Locking Hyd.	0.0602	-0.2208	-0.5568	0.3010	-0.5666	-0.8304	0.0315
Drag Strut Spacer	1.3615	-1.8636	0.0	1.3615	-1.8636	-0.3908	0.1856
Side Strut	-0.1573	-2.4234	-0.3908	-0.1573	-1.343	-2.3446	0.1856
Side Strut Locking Mech.	-0.4334	-1.2788	-1.3677	-0.3717	-0.1343	-1.1723	0.0977
Side Strut Locking Hyd.	-0.3779	-0.2488	-0.9965	-0.4025	-0.7066	-1.0746	0.0315
Side Strut Spacer	-0.7096	-2.234	0.0	-0.7095	-2.234	-0.3908	0.1856
Torque Arm							
Top Torque Arm	-0.45	0.0	-2.598	-0.9135	0.0	-2.9	0.15
Bottom Torque Arm	-0.9135	0.0	-2.9	-0.45	0.0	-3.82	0.15
Aft Hydraulic Supports							
AHB Lower Cross	-1.6476	-0.0903	-4.2906	-1.6476	0.0903	-4.2906	0.0189
AHB First Middle Cross	-1.795	-0.0903	-3.9604	-1.795	0.0903	-3.9604	0.0189
Second Middle Cross	-1.9425	-0.0903	-3.6302	-1.9425	-0.0903	-3.6302	0.0189
AHB Top Cross	-2.09	-0.0903	-3.3	-2.09	-0.0903	-3.3	0.0189
Starboard Side Support	-2.09	0.0903	-3.3	-1.6476	0.0903	-4.2906	0.0189
Port Side Support	-2.09	-0.0903	-3.3	-1.6476	-0.0903	-4.2906	0.0189
Aft Hydraulic Bracket Dressing							
Hose 1 in Bracket	-2.09	-0.08	-3.3315	-2.308	-0.08	-3.6302	0.01889
Hose 1 to Aft	-2.308	-0.08	-3.6302	-2.35	-0.08	-3.795	0.01889
Hose 1 to Axel	-2.35	-0.08	-3.795	-1.6976	-0.4	-4.2906	0.01889
Hose 2 from Oleo	-2.09	0.0	-3.3315	-0.9135	0.0	-3.3315	0.0315
Hose 2 in Bracket	-2.09	0.0	-3.3315	-2.308	0.0	-3.6302	0.0315
Hose 2 to Aft	-2.308	0.0	-3.6302	-2.35	0.0	-3.795	0.0315
Hose 2 to Axel	-2.35	0.0	-3.795	-1.6976	-0.14	-4.2906	0.0315
Hose 3 in Bracket	-2.09	0.08	-3.3315	-2.308	0.08	-3.6302	0.01889
Hose 3 to Aft	-2.308	0.08	-3.6302	-2.35	0.08	-3.795	0.01889
Hose 3 to Axel	-2.35	0.08	-3.795	-1.6976	0.4	-4.2906	0.01889
Forward Horz. Hydraulic Bracket							
Top Starboard Support	-0.171	0.0903	-2.8	1.140	0.0903	-2.989	0.015
Top Port Support	-0.171	-0.0903	-2.8	1.140	-0.0903	-2.989	0.015
Bottom Starboard Support	0.64	0.0903	-3.45	1.140	0.0903	-2.989	0.015
Bottom Port Support	0.64	-0.0903	-3.45	1.140	-0.0903	-2.989	0.015

Continued on next page

Table A-4 continued. New 6.3% scaled Boeing 777 main landing gear LGMAP geometry. 6.3% scaling is done outside the landing gear geometry namelist. Units are in meters and radians.

Name	**X1**	**Y1**	**Z1**	**X2**	**Y2**	**Z2**	**Diameter**
Cross Support	1.140	-0.10	-2.989	1.140	0.10	-2.989	0.0315
Forward Horz. Hydraulic Dressing							
Name	**X1**	**Y1**	**Z1**	**X2**	**Y2**	**Z2**	**Diameter**
Hose 1 From Oleo 1	-0.171	0.09	-2.65	0.5	0.02	-3.1	0.0315
Hose 1 From Oleo 2	0.5	0.02	-3.1	0.8675	0.02	-2.94	0.0315
Hose 1 for Forward 1	0.8675	0.02	-2.94	1.4	0.02	-2.8	0.0252
Hose 1 for Forward 2	1.4	0.02	-2.8	1.375	0.02	-3.3	0.0252
Hose 1 End	1.375	0.02	-3.3	0.252	0.02	-3.4	0.0252
Hose 2 From Oleo 1	-0.171	0.05	-2.65	0.5	-0.02	-3.1	0.0315
Hose 2 From Oleo 2	0.5	-0.02	-3.1	0.8675	-0.02	-2.94	0.0315
Hose 2 for Forward 1	0.8675	-0.02	-2.94	1.4	-0.02	-2.8	0.0252
Hose 2 for Forward 2	1.4	-0.02	-2.8	1.375	-0.02	-3.3	0.0252
Hose 2 End	1.375	-0.02	-3.3	0.973	-0.02	-3.4	0.0252
Hose 3 From Oleo 1	-0.171	-0.09	-2.65	0.5	0.0	-3.1	0.0315
Hose 3 From Oleo 2	0.5	-0.02	-3.1	0.8675	0.02	-3.0	0.0315
Hose 3 for Forward 1	0.8675	0.02	-3.0	1.4	0.09	-2.8	0.0252
Hose 3 for Forward 2	1.4	0.09	-2.8	1.375	0.09	-3.3	0.0252
Hose 3 End	1.375	0.09	-3.3	0.973	0.08	-3.4	0.0252
Hose 4 From Oleo 1	-0.171	-0.09	-2.65	0.5	-0.02	-3.1	0.0315
Hose 4 From Oleo 2	0.5	-0.02	-3.1	0.8675	-0.02	-3.0	0.0315
Hose 4 for Forward 1	0.8675	-0.02	-3.0	1.4	-0.09	-2.8	0.0252
Hose 4 for Forward 2	1.4	-0.09	-2.8	1.375	-0.09	-3.3	0.0252
Hose 4 End	1.375	-0.09	-3.3	0.973	-0.08	-3.4	0.0252
Name	**X**	**Y**	**Z**	**Radius**	**Treadwidth**		
Center Port Wheel	-0.2535	-0.8	-4.019	0.6604	0.508		
Center Starboard Wheel	-0.2535	0.8	-4.019	0.6604	0.508		
Rear Port Wheel	-1.6477	-0.8	-4.2906	0.6604	0.508		
Rear Starboard Wheel	-1.6477	0.8	-4.2906	0.6604	0.508		
Front Port Wheel	1.1405	-0.8	-3.6497	0.6604	0.508		
Front Starboard Wheel	1.1405	0.8	--3.6497	0.6604	0.508		

Table A-5. Full scaled Boeing 737 main landing gear LGMAP geometry. Units are in meters and radians.

737 Main Landing Gear							
Translation Change of Base	0.0	0.0	-0.4284				
Name	**X1**	**Y1**	**Z1**	**X2**	**Y2**	**Z2**	**Diameter**
Main Strut Assembly							
Shock Strut	0.0	0.0	0.37	0.0	0.0	1.8	0.127
Side Strut	0.1	0.0	0.867	0.1	-0.6695	1.8	0.0635
Downlock Strut	0.1	-0.53	1.8	0.1	-0.53	1.6	0.0635
Forward Strut	0.075	0.0	0.6	0.5	0.0	1.8	0.0635
Inner Door Strut	-0.075	0.075	0.65	-0.075	0.366	0.75	0.036
Inner Door Control Rod	-0.108	-.366	-0.75	-0.108	0.526	0.75	0.018
Torque Arm							
Bottom Cross	0.075	-0.075	0.0655	0.075	0.075	0.0655	0.4
Bottom Torque Bar 1	0.075	0.075	0.0655	0.5	0.0318	0.17	0.4
Bottom Torque Bar 2	0.075	-0.075	0.0655	0.5	-0.0318	0.17	0.4
Middle Cross	0.5	0.0318	0.17	0.5	-0.0318	0.17	0.4
Top Torque Bar 1	0.5	0.0318	0.17	0.075	0.075	0.6	0.4
Top Torque Bar 2	0.5	-0.0318	0.17	0.075	-0.075	0.6	0.4
Top Cross	0.075	0.075	0.6	0.075	-0.075	0.6	0.4
Aft Hydraulic Supports							
Blue	0.225	0.0	0.86	0.5	0.0	0.17	0.0127
Black S	0.21	0.01	0.85	0.4	0.04	0.3	0.0127
Black P	0.21	-0.01	0.85	0.4	-0.04	0.3	0.0127
Black C	0.21	0.0	0.85	0.4	0.0	0.3	0.0127
Name	**X**	**Y**	**Z**	**Radius**	**Treadwidth**		
Port Wheel	0.0	-0.378	-0.2	0.635	0.3683		
Starboard Wheel	0.0	0.378	-0.2	0.635	0.3683		

Table A-6. 25% scaled Gulfstream G550 nose gear LGMAP geometry. 25% scaling is done inside the landing gear geometry namelist. Units are in meters and radians.

G550 Nose Gear							
Name	**X1**	**Y1**	**Z1**	**X2**	**Y2**	**Z2**	**Diameter**
Oleo System							
Oleo One (Top)	0.0562	0.0	0.2889	0.0384	0.0	0.2070	0.0233
Oleo Two	0.0384	0.0	0.2070	0.0376	0.0	0.2035	0.468
Oleo Three	0.0376	0.0	0.2035	0.0317	0.0	0.1762	0.0288
Oleo Four	0.0317	0.0	0.1762	0.0298	0.0	0.1674	0.0494
Oleo Five	0.0298	0.0	0.1674	0.0239	0.0	0.1402	0.032
Oleo Six	0.0239	0.0	0.1402	0.0227	0.0	0.1348	0.028
Oleo Seven Bottom	0.0227	0.0	0.1348	-0.0054	0.0	0.009	0.0191
Torque Arm							
Top	0.0530	0.0	0.1502	0.0686	0.0	0.0607	0.02
Bottom	0.0654	0.0	0.0592	0.0183	0.0	0.0108	0.016
Name	**X**	**Y**	**Z**	**Radius**	**Treadwidth**		
Port Wheel	0.0	0.3957	0.0	0.0698	0.0521		
Starboard Wheel	0.0	-0.3957	0.0	0.0698	0.0521		